SUPRAMOLECULAR ORGANIZATION OF METAL NANOPARTICLES IN SOLUTION AND OF PHENYLENEETHYNYLENES ON SURFACES

THESIS SUBMITTED TO

THE COCHIN UNIVERSITY OF SCIENCE AND TECHNOLOGY

IN PARTIAL FULFILMENT OF THE REQUIREMENTS FOR THE FOR THE
DEGREE OF DOCTOR OF PHILOSOPHY

IN CHEMISTRY

UNDER THE FACULTY OF SCIENCE

By

K. YOOSAF

UNDER THE SUPERVISION
OF
Dr. K. GEORGE THOMAS

PHOTOSCIENCES AND PHOTONICS
CHEMICAL SCIENCES AND TECHNOLOGY DIVISION
NATIONAL INSTITUTE FOR INTERDISCIPLINARY SCIENCE AND TECHNOLOGY (CSIR)
TRIVANDRUM-695019
KERALA, INDIA

JANUARY 2008

In Dedication to……

……My family……

……And Friends

STATEMENT

I hereby declare that the matter embodied in the thesis entitled, ***"Supramolecular Organization of Metal Nanoparticles in Solution and of Phenyleneethynylenes on Surfaces"*** are results of investigations carried out by me at the Photosciences and Photonics Section, Chemical Sciences and Technology Division of the National Institute for Interdisciplinary Science and Technology (CSIR), Trivandrum, under the supervision of Dr. K. George Thomas and the same has not been submitted elsewhere for a degree.

In keeping with the general practice of reporting scientific observations, due acknowledgement has been made wherever the work described is based on the findings of other investigators.

K. Yoosaf

NATIONAL INSTITUTE FOR INTERDISCIPLINARY SCIENCE AND TECHNOLOGY

(Formerly Regional Research Laboratory)
Council of Scientific & Industrial Research (CSIR)
Industrial Estate P.O.,Trivandrum – 695 019
Kerala, INDIA

ISO 9001 REGISTERED
DNV Certification B.V., The Netherlands

Dr. K. George Thomas
Scientist E II
E-mail: kgt@vsnl.com

Tel : +91-471-2515 364
Fax : +91-471-2490 186

January 24, 2008

CERTIFICATE

This is to certify that the work embodied in the thesis entitled, ***"Supramolecular Organization of Metal Nanoparticles in Solution and of Phenyleneethynylenes on Surfaces"*** has been carried out by Mr. K. Yoosaf under my supervision and the same has not been submitted elsewhere for a degree.

K. George Thomas
Thesis Supervisor

ACKNOWLEDGEMENTS

It is my great pleasure to express my deep sense of gratitude to my research supervisor, Dr. K. George Thomas, for suggesting the research problem, and his constant support and encouragement. I am also grateful for his inspiring and thought provoking guidance that lead to the successful completion of this work.

My words fail to express my heartful gratitude to Professor M. V. George for being an inspiration, his encouragement and fruitful discussions during the different stages of this work.

My sincere thanks are also due to Dr. Suresh Das, the Head, Chemical Sciences and Technology Division, for his kind availability to have fruitful discussions and suggestions during the tenure of this work.

I thank Prof. T. K. Chandrasekhar, Director, and Dr. B. C. Pai, former acting Director of the National Institute for Interdisciplinary Science and Technology (CSIR), Trivandrum, for providing necessary facilities for carrying out the work.

I also thank Dr. A. Ajayaghosh, Dr. K. R. Gopidas, Dr. D. Ramaiah and Dr. A. Srinivasan, scientists of the Photosciences and Photonics group, for all the help and support extended to me. I would like to thank Dr. G. U. Kulkarni and his group members at JNCASR, Bangalore, for their help and fruitful discussions which enabled the standardization of Scanning Tunneling Microscope.

Words are not just enough to express my sincere thanks to my beloved and respectful seniors Dr. Binil Itty Ipe and Dr. P. K. Sudeep for always being as inspiring models and their incomparable hand of help extended towards me at the earlier stages of my research life. I also record my strong and sincere gratitude to Dr. Mahesh Hariharan for consoling and raising my level of confidence at different stages of research life.

I also thank my colleagues and beloved friends Dr. P. V. James, Dr. Shibu Joseph, Mr. P. Pramod, Mr. R. Vinayakan, Mr. A. R. Ramesh, Mr. Pratheesh V Nair, Mr. Satish, Mr. Jino George and Mr. M. Shanthil for always being with me and for their invaluable help and support. I also thank Ms. Indulekha, Summer Research Fellow, JNCASR, for her appreciable help.

I also express my sincere thanks to Mr. Robert Philip and my friends in other divisions of the NIIST, Trivandrum for their help and cooperation. Also, I wish to thank Mrs. Soumini Mathew, Mrs. S. Viji, Ms.Priya A. Nair for helping in NMR, HRMS, GCMS and FTIR studies.

I take this opportunity to record my heartful gratitude to Dr. Nicola Armaroli and his group members, Ms. Raffaellae Amadio, Dr. Gianluca Accorsi, Mr. Abdelhalim Belbakra, Mr. Andrea Listorti and all other members of ISOF-CNR, Bologna, Italy for their remarkable help and support during my stay in Italy for two months.

I am deeply grateful to my parents and all the family members for their constant love, invaluable support and understanding that have been a great motivation for these efforts.

I take this opportunity to record sincere thanks to Dr. George Thoma's family who have great care and concern.

Financial assistance from the Council of Scientific and Industrial Research (CSIR), Government of India is gratefully acknowledged and DST for travel funds to Italy and back.

K. Yoosaf

CONTENTS

PREFACE

Design of organic, inorganic and hybrid nanomaterials with novel physical properties has emerged as one of the most exciting areas of research in this decade. In the size regime of 1-100 nm, metal and semiconductor nanoparticles possess unusual physical and chemical properties which are distinctly from that of bulk. The collective oscillation of electrons on the surface of metal nanoparticles, in presence of electromagnetic radiation, results in strong surface plasmon absorption. Gold and silver nanoparticles possess intense surface plasmon absorption and found to have potential applications in optical devices, spectroscopy and as chemical and biosensors. One of the objectives of the present investigation is to develop newer approaches for the synthesis of water soluble Au and Ag nanoparticles and their use in the selective sensing of toxic metal cations from aqueous medium through supramolecular organization and plasmon coupling. Another objective of the present investigation is to understand various factors affecting the supramolecular organization of a class of optically active molecules namely phenyleneethynylenes on surfaces.

The thesis consists of four chapters. The first section of chapter 1 provides an overview on nanomaterials and various approaches adopted for the synthesis and organization of metal nanoparticles. The second section of this chapter describes approaches for understanding the self-organization of molecules on surfaces using scanning tunneling microscopic (STM) studies.

Chapter 2 presents detailed investigation on the synthesis of Au and Ag nanoparticles using bifunctional biomolecules namely gallic acid and L-DOPA. Nanoparticles synthesized were characterized using various analytical, spectroscopic and microscopic techniques. The mechanism of nanoparticle formation was investigated by conducting controlled experiments using structurally similar molecules. Detailed kinetic studies indicate that the formation of nanoparticle is autocatalytic in nature. The present synthetic methodology does not involve the use of any strong reducing agent and the synthesis is carried out in aqueous medium at room temperature by mixing gallic acid/L-DOPA and the corresponding metal salts, making it useful for biological applications.

Metal cation induced supramolecular organization of Au and Ag nanoparticles were investigated by spectroscopic techniques at various pH conditions. Complexation of metal cations with the surface bound ligands on two or more Au/Ag nanoparticles, bring them close to each other, resulting in a supramolecular assembly. The close proximity of the Au/Ag nanoparticles induces coupling of their plasmon oscillations (interplasmon coupling) resulting in a bathochromic shift in their absorption band. At pH 4.5, Pb^{2+} ions can selectively induce a bathochromic shift in plasmon absorption, which resulted in a visual color change from red to blue in the case of Au nanoparticles and yellow to red in the case of Ag nanoparticles. Aggregate formation was further confirmed by Atomic Force Microscopy (AFM), Transmission Electron Microscopy (TEM) and FTIR studies. A complete reversal of plasmon absorption, on addition of EDTA, confirms the existence of the complex between Pb^{2+} ions and the surface bound ligand on Au/Ag nanoparticles. At pH 5.5, both Pb^{2+} and Fe^{3+} ions induce bathochromic shift in the plasmon absorption. The newly synthesized Au/Ag nanoparticles possess high negative zeta potential and it is difficult to bring them close to each other due to strong electrostatic repulsion. The unique coordination ability of Pb^{2+} ions allows the formation of a stable supramolecular complex resulting in a plasmon coupling and visual color change.

In the fourth chapter supramolecular organization of a series of phenyleneethynylene derivatives were investigated on surfaces. The organization of these systems can be modulated by varying the length of alkyloxy groups and introducing proper functional groups. An understanding on the factors affecting the self-organization of molecules on surfaces can help in tuning their opto-electronic properties. High resolution STM images revealed that phenyleneethynylenes possessing hexyloxy groups are arranged in a skewed 1D fashion and the distance between these wires can be varied by increasing the length of the alkyloxy group. Interestingly, phenyleneethynylene possessing a hydroxyl group at terminal positions form a linear organization in an end to end fashion, through the intermolecular hydrogen bonding.

CHAPTER 1

Nanomaterials and their Supramolecular Organizations: An overview

1.1. General Introduction to Nanoscience and Technology

Nanoscience is the study of phenomena and manipulation of materials at nanoscale (approximately between 1 to 100 nm), where the properties of matter differ significantly from those of bulk. **Nanotechnology** refers to the field of applied science and technology which involves the fabrication and application of structures, devices and systems through the control of shape and size at the nanoscale. It was Richard P. Feynman, in his classical talk of 1959,[1] introduced the concept of this new field of science and technology wherein one can design and manipulate materials atom by atom, and create nanostructures of various size and shape which possess fundamentally new properties and functions.

Miniaturization has been the key to the major technological innovations in last decades leading to a number of important scientific discoveries. The thrust to achieve controlled organization of materials with micrometer scale precision has become the primary aim of researchers working in the design of optoelectronic devices.[2,3]

With the rapid developments in the area of nanoscience and technology in this decade, the scientific world has witnessed the disappearance of barriers between different research fields, making science more interdisciplinary.[4] Nanoscale is not just another step towards miniaturization from micrometer scale to nanoscale, but a new size regime where materials behave differently from that of bulk.[5,6] In nano regime, rather than the constituting elements and their chemical composition, size and shape plays a dominant role in tuning their properties. One of the unique properties of nanomaterials is its extremely small size (1-100 nm) and correspondingly large surface-to-volume ratio, which makes them ideal candidates for various biological, catalytic and electronic applications. Nanomaterials possess size and shape dependent physical and chemical properties which are distinctly different from that of bulk. For example, bulk silicon doesn't emit light, where as nanoscale silicon showed enhanced light emission. Another example illustrating the variation of optical properties of Au and Ag nanoparticles, as a function of the size and shape,[7] is presented in Figure 1.1.

Quantum confinement: As mentioned in previous section, nanoscale materials exhibit many interesting phenomena which are different from bulk and their constituting elements (for e.g., physical, chemical, electronic and magnetic properties) and are highly dependant on the size and shape

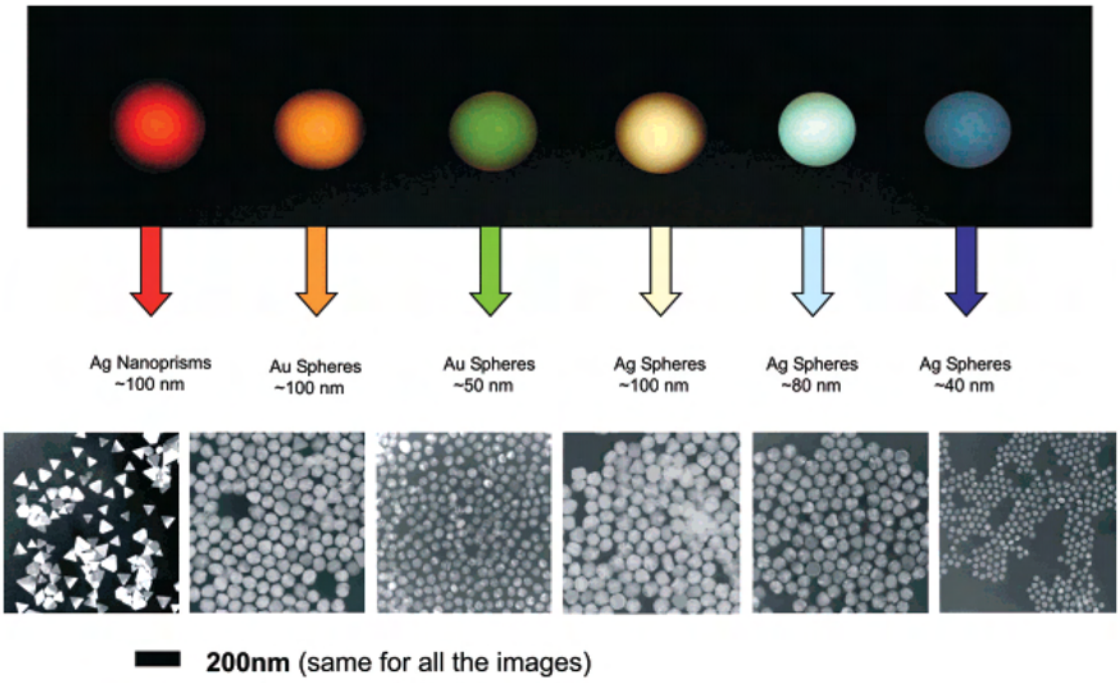

Figure 1.1. Optical properties of Au and Ag nanoparticles by varying the size and shape. (*adapted from reference 7*)

of the material. The classical laws of physics fail to explain the behavior of materials at this scale.[8] When one or more dimensions of a crystal are confined to nanoscale and as it approaches the size of an exciton in bulk crystal (often termed as Bohr exciton radius), the electrons experience a confinement of motion in space. This situation can be described in terms of particles in a box and under this condition, quantum mechanics is more suitable to explain their behavior. The boundary conditions play an important role in the confinement of electrons and the properties of matter at nanoscale are highly dependant on their size and shape. For example, quantum confinement results in discretization of energy levels in Au

nanoparticles and they exhibit metallic to semiconducting to insulator transition as their size decreases from 5 nm to 2 nm.[6] Figure 1.2 illustrates the variation of electronic states of a metal particle during its transition from a bulk to a nanocluster.[5] The bulk metal has a quasi-delocalized electronic state of overlapping valence (VB) and conductivity bands (CB). As the size of the metal particle is continuously decreased, the overlap between VB and CB becomes smaller and smaller, finally results in a band gap (transition from Figure 1.2(a) to Figure 1.2(b)). An extreme situation is illustrated in Figure 1(b) where the particle diameter '*d*' corresponds with $\lambda/2$ (λ = de Broglie wavelength) in the ground state. This energy state can be compared with the s orbital of a giant metal atom (n = 0) which can be occupied by two electrons. The first excited state (n = 1) then corresponds to an atomic p orbital. In Figure 1.2(c), bonding (MO_b) and antibonding (MO_{ab}) molecular orbitals characterize the localized bonds between a few atoms in a molecular cluster. One of the direct observations of quantum size effect in semiconductor nanocrystals is the blue shift in the absorption and emission spectra with decrease in size.

The shape of nanomaterials also has a remarkable effect on its properties: electrons experience different confinement depending upon the particle shape.[6] Depending upon the dimensionality of confinement, nanomaterials are classified as 2D, 1D or 0D structures. For 2D nanomaterials,

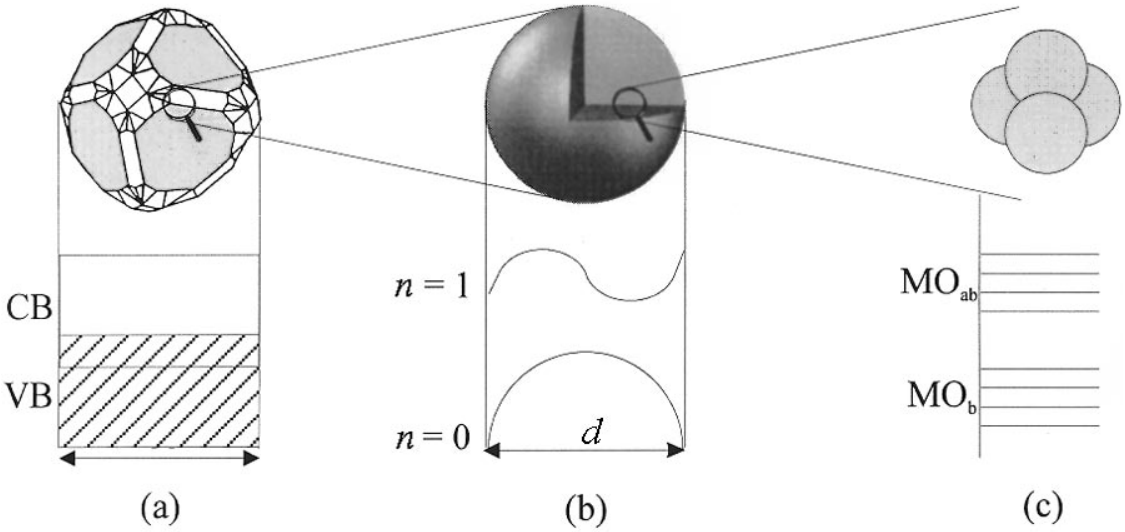

Figure 1.2. Illustration of the variation of band structure during transition of a bulk metal *via* a nanocluster to a molecule; (a) bulk (b) nanoparticle with diameter corresponds with the de Broglie wavelength and (c) molecular state. (*adapted from reference 5*)

the confinement is imposed only along one axis and the situation is best explained as in the case of quantum well. In the case of one dimensional nanomaterial, the electrons experience confinement along two dimensions. The electrons are free to move only in one dimension and best example is a nanowire. The material is termed as quantum dot when the particle experience confinement along all the three dimensions. The dimensional confinement of electrons in materials always leads to dramatic modifications in their density of states (DOS). For example, the density of states changes from continuous in the bulk, through step like in quantum wells, and to discrete states in quantum dots and the situation is illustrated in Figure 1.3.

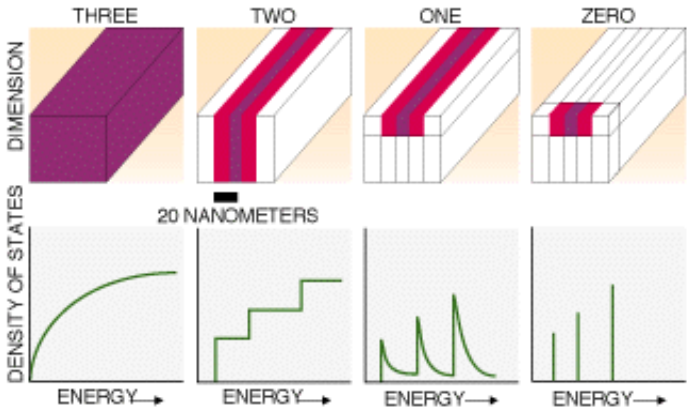

Figure 1.3. The density of electron states in selected semiconductor crystals (a) bulk semiconductor (b) quantum well (c) quantum wire and (d) quantum dot. (*adapted from reference 6*)

In addition to quantum confinement, materials in its nanoscale also exhibit enormous catalytic activity.[9-12] The enhanced activity in the nanodimension can be attributed to large percentage of surface atoms as compared to the bulk, resulting in enhanced surface area and high edge concentrations with unusual electronic properties. For example, a nanoparticle of 10 nm diameter possesses ~10 % of atoms on its surface compared to 99 % for a particle having 1 nm diameter. Despite of the fact that gold is inert in its bulk state, recent reports indicate that gold nanocluster is an efficient catalyst for a variety of environmentally and industrially important reactions.[9-11] Various reactions include oxidation of CO to CO_2,[13] reduction of NO by dihydrogen,[13] water-gas shift reaction,[14] epoxidation of propylene,[15] aqueous-phase oxidation of ethanol into acetic acid[16] and formation of vinyl acetate from ethylene and acetic acid.[17]

Nanoparticles are also proposed as potential building blocks in light emitting devices, optical transformers, photonic-switches, nanoelectronic circuits, sensors and other biological applications. It has been already demonstrated that properly designed and interconnected nanomaterials can function as rectifiers and field effect transistors (for e.g., carbon nanotube based field effect transistors).[18] Advances in the area of nanoscience may result in the miniaturization of electronic, electro-optic and optical devices. Thus, the transition from bulk semiconductor to nano scale may eventually lead to the design of devices with improved properties and resolution. Data storage devices based on nanostructures provide smaller, faster and lower power consumption systems. Nanoparticles are currently being used for the manufacture of scratchproof eye-glasses, crack-resistant paints, anti-graffiti coatings for walls, transparent sunscreens, stain-repellent fabrics, self-cleaning windows and ceramic coatings for solar cells. Nanoparticles can also contribute in the design of stronger, lighter, cleaner and smarter surfaces and systems.

1.2. Synthesis of Nanomaterials

The efficiency of any nanodevice mainly relies on our ability to fabricate functional heterostructures and interfaces with desirable characteristics. The design and construction of size controlled nanomaterials and their integration into meso and macroscopic world is one of the major

challenges and two approaches namely, 'top-down' and 'bottom-up' have been adopted for their creation.

(i) Top-down approach: This approach involves the breaking down of large pieces of materials to generate the required nanostructures. Nano-objects thus constructed does not possess any atomic-level control, however capable of creating features down to nanometer range by adopting techniques such as ball milling. Various other top-down approaches currently used to create nanostructures include lithographic techniques, writing, stamping, etching, and microcontact printing. Top-down assembly methods are currently utilized for interconnecting of electronic circuits. However, fascinating physical and chemical properties of materials arise in sub-nanometer dimensions as envisaged by Richard Feynman in his talk entitled "the plenty of room at the bottom." The top-down approach is not successful for the design of such materials.

(ii) Bottom-up approach: Materials in sub-nanometer scale are designed through the hierarchical integration of atoms or molecular components by utilizing the principles of controlled growth, self-assembly and molecular recognition. Bottom-up approach is largely the realm of nanoscience and nanotechnology as it is very powerful in creating identical structures with atomic scale precision. Among the various supramolecular approaches, self-organization of atoms and molecules has emerged as an attractive and

efficient bottom-up strategy to position and design well defined shape-persistent objects under thermodynamic control at predefined locations. A brief account of the various supramolecular approaches adopted for the organization of nanomaterials in one, two and three dimensions is illustrated below.

1.3. Supramolecular Organization of Nanoparticles

Supramolecular chemistry, the 'chemistry beyond the molecule', is the study of interactions between, rather than within, the molecules.[4,19,20] In supramolecular chemistry, molecules are used as building blocks which provide excellent possibilities for the design of complex architectures. Herein molecular building blocks are assembled together by relatively weak non-covalent interactions such as hydrogen bonding, π–π stacking, electrostatic, and hydrophilic–hydrophobic interactions and van der Waals forces.[4,19-26] In fact, nature has utilized these interactions for the creation of well defined and aesthetically appealing architectures that can perform specific functions.[27-30] Using nature as a source of inspiration, over the years, scientists have mastered the principles of supramolecular chemistry for the demonstration of many important concepts like molecular and nanomaterial self-assembly, folding, molecular recognition, host-guest chemistry, mechanically-interlocked molecular architectures, and dynamic covalent chemistry.[27,31-43] Numerous reports are available in the literature on these aspects.[27,31-43] In the following

section, we outline a breif summary of various supramolecular approches adopted for the controlled organization of nanoparticles in one, two and three dimensions and also the organization of functional organic molecules on surfaces.

Many of the synthetic schemes reported for the preparation of nanoparticles utilize supramolecular approaches involving electrostatic or covalent interactions of the capping agent which stabilizes the nanoparticles (Figure 1.4).[44] For example, the citrate capped metal nanoparticles (reported by Turkevich et al.) are stabilized by an electrical double layer of citrate and chloride ions.[45-48] The coulombic repulsions between the particles, which decay exponentially with increasing interparticle separation, further reduce agglomeration of nanoparticles. Polymer and dendrimer capped nanoparticles are stabilized through the steric interactions. The ability of thiol groups to form self-assembled monolayer on metallic surfaces have been effectively utilized for the preparation of thiolate stabilized Au/Ag nanoparticles.[11,49,50]

As described earlier, nanomaterials possess many interesting size and shape dependant physical properties which include (i) localized surface plasmon absorption of metal nanoparticles and (ii) tunable emission properties of semiconductor quantum dots. The miniaturization of

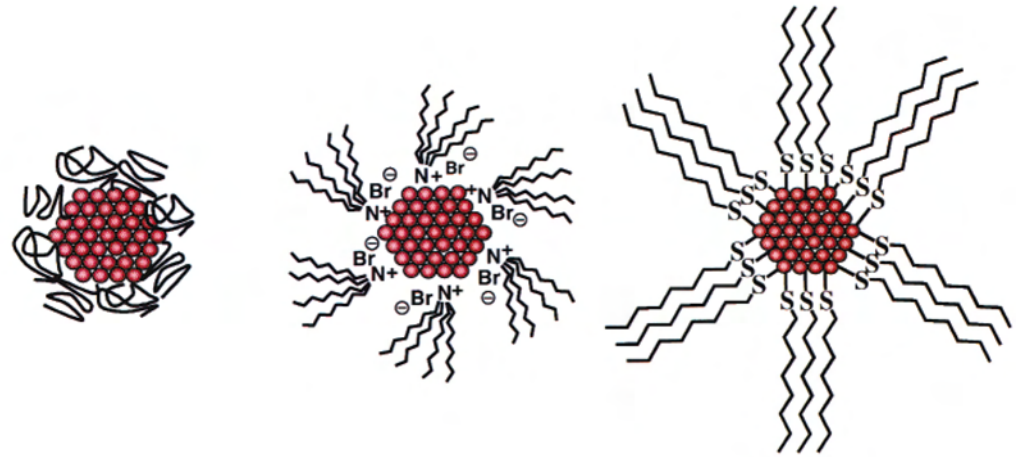

Figure 1.4. Supramolecular approaches adopted for the stabilization of metal nanoparticles through various interactions. (*adapted from reference 50*)

opto- electronic materials is often limited by the diffraction limit of light. In principle, one can overcome this problem by using surface plasmon resonance in nanostructured materials. This can be achieved by first converting light to surface plasmon, which is not diffraction limited, and propogating it to the desired locations using nanostrucutred materials and converting it back to light. More recently, Ebbesen and coworkers have developed subwavelength waveguide components (Y-splitters, interferometers and ring resonators), operating at telecom wavelengths, which can afford efficient large angle bending and splitting of radiation.[51] Another rich potential of surface plasmon has been earlier demonstrated by the same group with the discovery of enhanced light transmission through

subwavelength holes, which is attributed to the activation of surface plasmons.[52-55] The phenomenon of enhanced transmission is in contrast to the standard aperture theory which predicts that the transmission of light through a small hole is very weak. Interestingly, they have demonstrated that the transmission spectra of hole arrays can be tuned by adjusting the period and symmetry of the holes. A variety of approaches have been demonstrated for the fabrication of nanostructures on solid supports for such plasmonic applications. These includes various lithographic methods such as electron-beam lithography, nanosphere lithography and dip-pen nanolithography.[56,57]

The transport of optical energy using materials that are considerably smaller than the wavelength of light is one of the most challenging issues in the miniaturization of photonic components. Design of higher order nanostructured materials (for example, one-dimensional arrays of noble metal nanoparticles with defined particle spacing) is an essential requirement for achieving this goal. Lithographic methods such as electron beam lithography are more commonly used for the construction of higher order nanostructures and details are summarized in recent reviews.[56,57] Such nanostructures can convert photons into surface plasmons that are not diffraction limited (focused more tightly than $\lambda/2$). Within the propagation length, the surface plasmon modes can be decoupled to light and this possibility offers tremendous

opportunities in the design of nanoscale optical and photonic devices such as metal nanoparticle based plasmon waveguides. Maier et al. have recently demonstrated the transport of electromagnetic energy over a distance of 0.5 μm using plasmon waveguides consisting of closely spaced silver rods.[58] The waveguides were excited by the tip of a near-field scanning optical microscope and energy transport was probed by using fluorescent nanospheres.

Tailoring the optoelectronic properties of nanomaterials through the stepwise integration of nanoscale building blocks (nanoparticles, nanorods, nanotubes, etc.) is another major challenge in the area of nanotechnology. Recent studies have shown that it is possible to fine tune the optical properties of metallic nanoparticles by their controlled organization into periodic arrays.[56,57] Two types of interactions exist in organized metal nanoparticles: near-field coupling and far-field dipolar coupling. Near-field coupling (evanescent coupling) is observed in an ensemble of closely packed particles which nearly touch each other. In the latter case, the dipole field resulting from the plasmon oscillation of a metal nanoparticle induces an oscillation in a neighboring nanoparticle.

Surface plasmon properties of nanoparticles is influenced by interparticle spacing and the propagation of light in a defined path can be modulated by the precise control of the distance between particles. To

achieve this goal, the hierarchical integration of nanoparticles into a symmetrically and spatially well-defined 1D, 2D and 3D structures is essential.[59] Recent literature reports have shown that supramolecular approach is a potential route for assembling of nanomaterials. A brief summary of the theoretical as well as experimental investigations on the plasmon resonances in nanoparticle arrays, with emphasis on 1D organization of spherical and rod shaped Au nanoparticles, is summarized in the following section.

1.3.1. Conjugation with Organic Molecules

Gold nanoparticles are one of the most widely investigated metal nanoparticle systems owing to their chemical inertness, ease of preparation, excellent optical and electronic properties and their ability to undergo strong bonding with thiols. Supramolecular organization of thiol capped nanoparticles can be tuned by the proper choice of ligand bearing the appropriate functional moieties. Two methods have been utilized for the organization of gold nanoparticles into two- or three dimensional networks. The first method involves the use of organic dithiol as linkers and the morphology of the assembly can be controlled by choosing either rigid or flexible spacer groups.[60-63] For example, Feldheim and coworkers have demonstrated the formation of gold nanoparticle dimers and trimers using linear and branched phenylacetylene derivatives (Figure 1.5). The non-

centrosymmetric trimers showed large second-harmonic responses, compared to centrosymmetric monomers and dimers and the value of first hyperpolarizability (β) is much larger than that of molecular chromophores.[62,64]

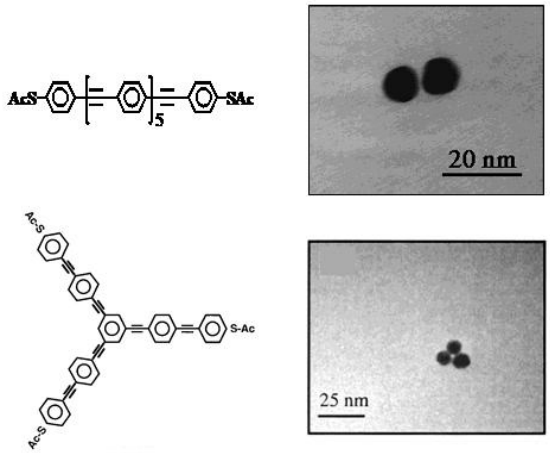

Figure 1.5. Organization of gold nanoparticles into dimers and trimers linked by rigid phenylacetylene bridges. (*adapted from reference* 64)

The second method is based on the modification of nanoparticle surface with functional ligands and assembling them through intermolecular interactions such as hydrogen bonding interactions, electrostatic interactions, antibody-antigen recognition, DNA recognition and metal ion complexation.[65] Mann, Dujrardin and coworkers have demonstrated the formation of 1D arrays of gold nanoparticles by adopting ligand exchange and hydrogen bonding strategy.[66] The citrate stabilized spherical gold nanoparticles were exchanged with a ditopic molecule namely 2-mercaptoethanol [$HS(CH_2)_2OH$; MEA]. The thiol group binds on to the nanoparticle surface and the hydrogen

bonding interaction of the OH group resulted in the formation of chain like superstructures (Figure 1.6A). In another attempt, Thomas and coworkers have demonstrated the integration of gold nanorods into one dimensional chains by using electrostatic/supramolecular/covalent approaches and modulation of their optical properties.[67-70] Interaction of various bifunctional molecules with Au nanorods was investigated using absorption studies and transmission electron microscopy (Figure 1.6B). Based on these studies a novel approach of linking Au nanorods to nanochains, using various bifunctional molecules, was reported. The new band observed in the near-infrared region results from the selective coupling of the longitudinal surface plasmon oscillations of Au nanorods in 1D-nanochains.

In a recent work, Liz-Marzan and coworkers have demonstrated the one dimensional alignment of nanorods on carbon nanotubes using layer by layer assembly in combination with electrostatic interaction.[71] A schematic representation of this methodology is presented in Figure 1.6C. Carbon nanotubes were first wrapped with negatively charged polyelectrolytes (polystyrene sulfonate, PSS), followed by electrostatic assembly of positively charged polyelectrolytes (poly(diallyldimethyl) ammonium chloride, PDDA). Gold nanorods having negative surface charges (functionalized with poly(vinylpyrrolidone) were electrostatically

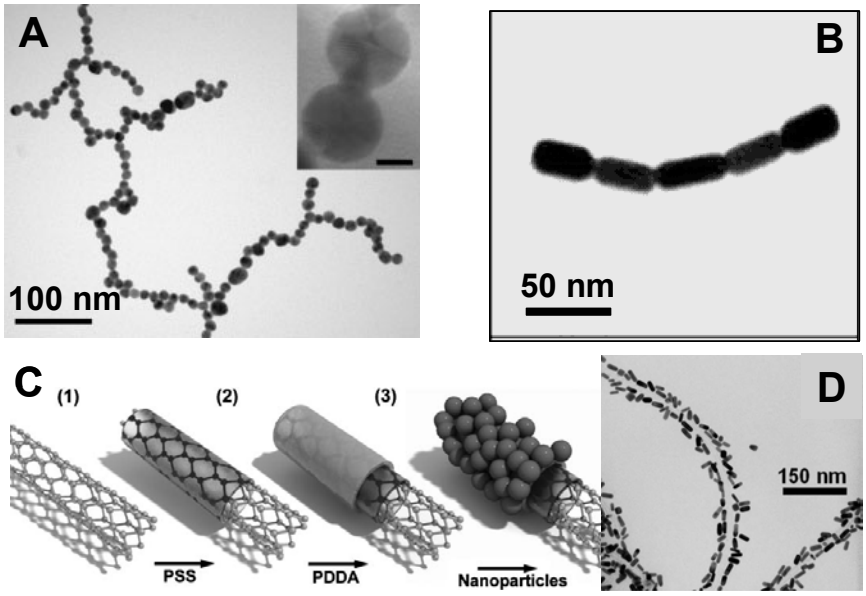

Figure 1.6. (A, B) TEM images of one dimensional superstructures of (A) gold nanoparticles produced by functionalizing with 2-mercaptoethanol (B) gold nanorods via hydrogen bonding of mercaptopropionic acid (C, D) illustration of electrostatic assembly of (C) gold nanoparticles on to polymer wrapped carbon nanotube (D) the corresponding TEM image of 1D array of nanorods. (*adapted from references 66, 67 and 71*)

assembled on positively charged carbon nanotube composite. TEM investigation of the assembly showed a high degree of one dimensional alignment of the nanorods in the form of stripes on opposite sides of the carbon nanotubes, rather than uniformly covering the surface (Figure 1.6D). It has been shown more recently that the potential decays more rapidly in areas with larger curvature (near the tips) for nanorods. This allows an end to end organization of nanorods rather than side-wise, resulting in a string-like conformation. Such supramolecular architectures can assist the near field

coupling of plasmon oscillations which enables the confinement and propagation of light waves in nanometric dimensions.

Further, the supramolecular approaches have been effectively utilized for the preparation of supracrystals of nanoparticles. Grzybowski and coworkers could successfully functionalize the surface of nanoparticles with various ligands bearing positive and negative charges.[72,73] The assembly of nanoparticles is driven by the electrostatic attraction between nanoparticles bearing opposite surface charges (Figure 1.7A). Authors have demonstrated the light induced isomerization of surface bound ligands resulting in a dipole change which was utilized for the self-assembly of nanoparticles. Nanoparticles were functionalized with azobenzene, a photo-isomerizable chromophore which possess a high dipole moment of 4.4 debye in the *cis* conformation compared to its *trans* form (0 debye).[72] Light induced *trans* to *cis* isomerization of azobenzene moiety results in the formation of molecular dipoles on the surface of nanoparticles. The electrostatic interaction between the dipoles drives the aggregation of nanoparticles resulting in the formation of supraspheres (Figure 1.7B). The assembly of nanoparticles into supraspheres and their disassembly can be modulated by using light of different wavelengths. Furthermore, authors have also reported that such materials possess plastic and moldable properties, along with good electrical conductivity.[73]

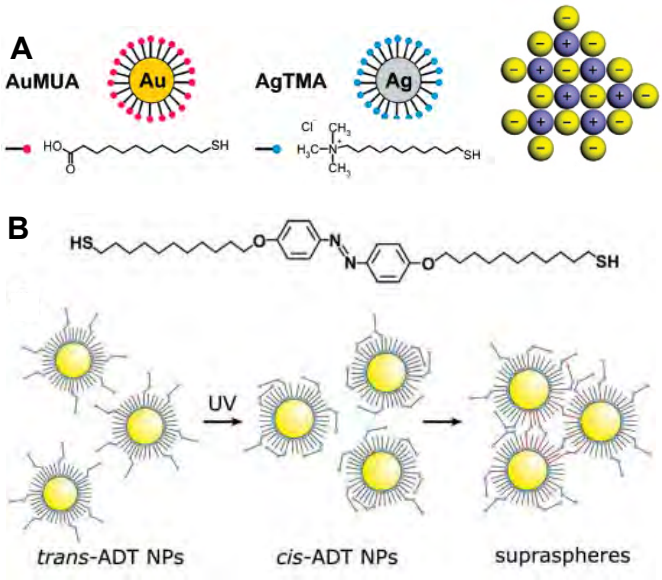

Figure 1.7. Schematic representation of the supracrystal formation of nanoparticles through (A) electrostatic assembly and (B) light induced changes in the dipoles of azobenzene. (*adapted from references 72 and 73*)

1.3.2. Conjugation with Biomolecules

Biomolecules possess well defined length, unique base pair recognition capabilities and possibility of functionalization. These properties enable precise positioning of biomolecules on nanomaterials and provide excellent opportunity for designing suprastructures through self-organization.[74] Various groups have extensively investigated the unique possibility of integration of nanoparticles with biomolecules and the development of functional devices. The first practical utility of nanoparticles in biomolecular recognition was illustrated by Mirkin and coworkers by combining the sequence specific DNA pairing and interparticle plasmon

coupling of Au nanoparticle.[7,75-77] Authors have demonstrated that the oligonucleotide functionalized gold nanoparticles can be used for the one-pot colorimetric detection of even single base-pair mismatches (Figure 1.8). In this approach, nanoparticles were functionalized with 3'- and 5'-(alkanethiol)oligonucleotides which act as the probe. The hybridization of the probe oligonucleotide with a 24-base polynucleotide target results in the formation of an extended polymeric Au nanoparticle/polynucleotide aggregate. A schematic representation of the formation of nanoparticle bio-conjugate assembly is presented in Figure 1.8A. The interplasmon coupling arising from the supramolecular assembly results in a color change of the solution from red to purple (Figure 1.8B). The supramolecular assembly exhibits exceptionally sharp "melting transitions" (Figure 1.8C) and this system is a very powerful analytical tool: it can distinguish a target sequence that has even only one base pair mismatch from the fully complementary target. The bio-conjugation of metal nanoparticles with various biomolecules was further extended by several groups for analytical and diagnostic applications.[7,78] These include DNA functionalized gold nanoparticles for the colorimetric detection of Pb^{2+} ions, Hg^{2+} ions[79] and DNAs,[80,81] real time colorimetric endonuclease-inhibition assay[82] and nanomechanical devices.[83,84]

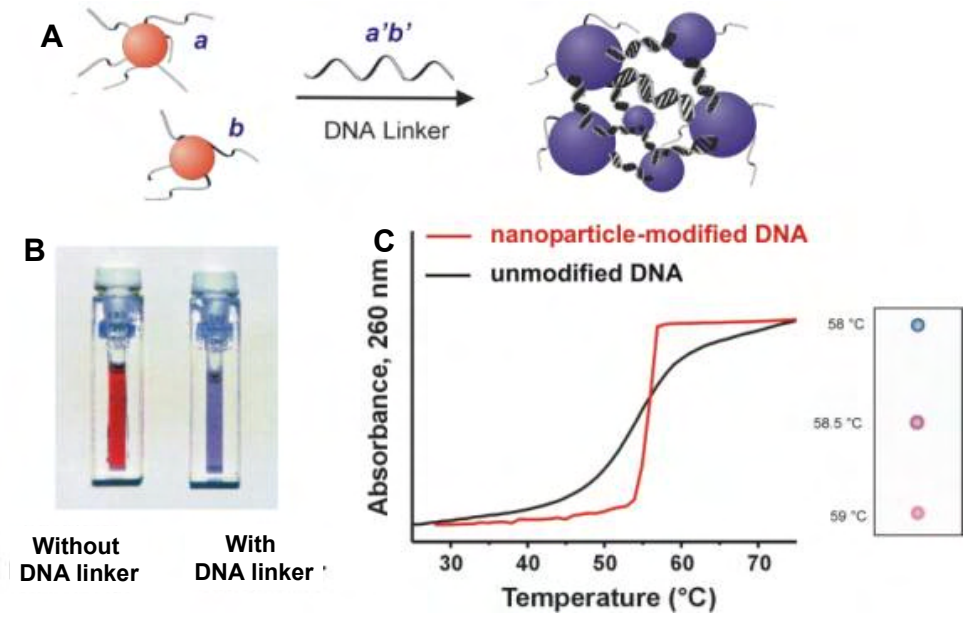

Figure 1.8. (A) Schematic representation illustrating the formation of supramolecular assembly of nanoparticles through DNA base pairing (B) color photographs of nanoparticle solution in the absence and presence of DNA cross linker (C) melting curve of the DNA assembly. (*adapted from references 7 and 77*)

Besides these, biocojnugation of metal nanoparticles were extensively utilized for creating nanoarchitectures that find potential applications in various optoelectronic devices. For example, Li, et al. have demonstrated the use of strong biotin–streptavidin interaction, together with the specific nucleic acid hybridization capabilities of DNA, for the controlled assembly of 5 nm Au particles along linear arrays of DNA triple cross-over molecules (TX).[85] The selected TX molecule was derived from DNA motifs consisting of seven oligonucleotides and has two protruding stem loops, one each from the upper and the lower helices. In order to template the assembly of 5 nm

nanoparticles, streptavidin molecules were selectively bound to biotin groups, which are incorporated into the hairpin loops. In the next step, Au nanoparticles were conjugated to the streptavidin, resulting in a periodic sequence of uniform particles along the linear TX DNA. Formation of single-layer or double-layer nanoparticle linear arrays was achieved by controlling the biotin modification either on one or both the stem loops (Figures 1.9A,B). Design of such DNA nanoparticle arrays was first demonstrated by Kretschmer and Fritsche for device fabrication.[86] Authors have combined both the top-down and bottom-up approaches for the integration of DNA templated Au nanoparticle arrays into gaps of microelectrode (Figure 1.9C).

The microelectrodes were prepared by employing standard photolithographic technique, and the assembly of Au nanoparticle strings into the microelectrode gap was achieved by dielectrophoresis. The electrical measurements conducted on this nanodevice showed promising ohmic behavior indicating that such systems can be further extended for sensing applications by making use of conductivity measurements (Figure 1.9D).

Creation of heteronanostructures with novel properties is another major challenge in the area of nanoscience. This is usually achieved by the asymmetric functionalization of nanoparticles with various functional molecules. The major challenges in the design of such materials are the

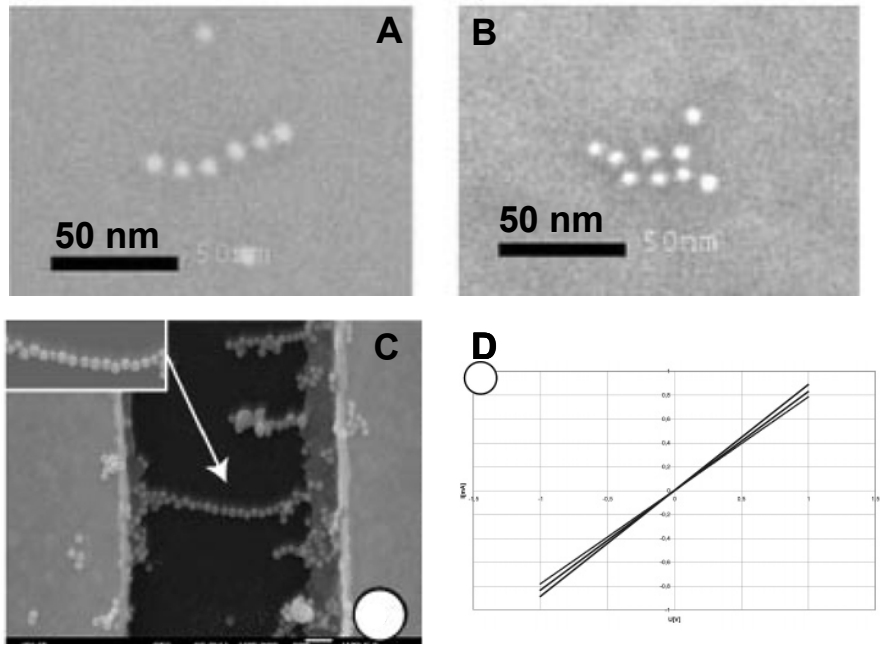

Figure 1.9. TEM images of (A) single and (B) double arrays of nanoparticles prepared through binding with DNA triple cross-over molecule (C) SEM image of microelectrode fabricated through DNA templated 1D assembly of gold nanoparticles and (D) the corresponding I-V characteristics of the assembly. (*adapted from references 85 and 86*)

selective placement of different molecules at specific locations on the particle and their hierarchical assembly. Compared to usual organic molecules, biomolecular functionalized nanoparticles provide excellent possibilities for developing such novel nanostructures. For example, it has been shown that controlled spatial organization of gold nanoparticles into satellite structures can be achieved by linking them with DNAs (Figure 1.10).[87,88]

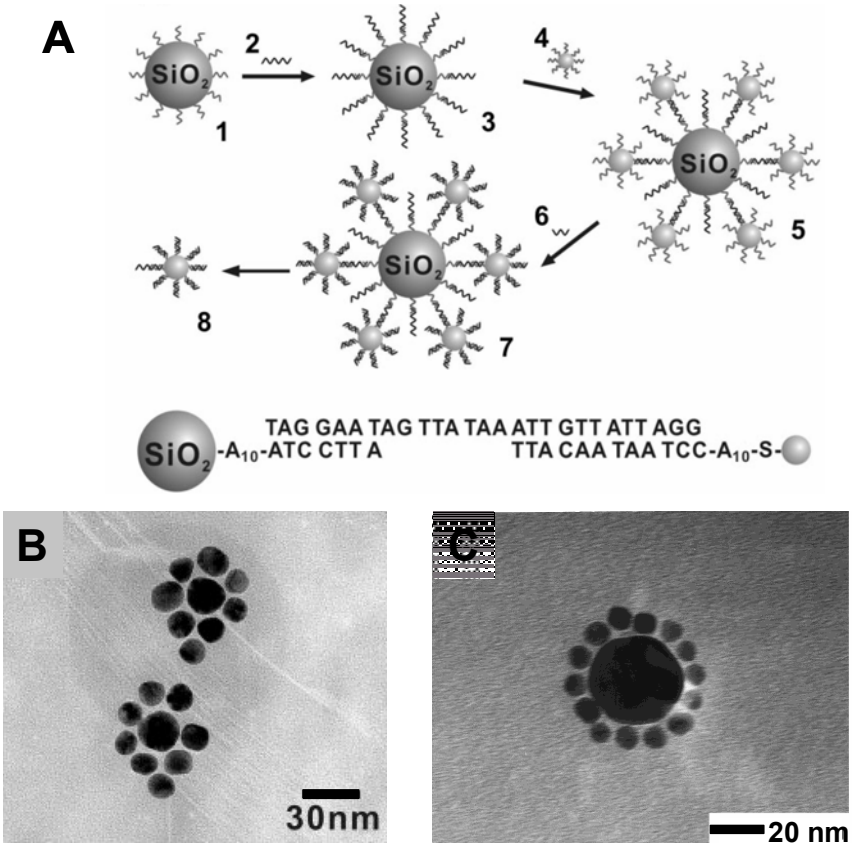

Figure 10. (A) Schematic representation of asymmetric functionlization of nanoparticles and their controlled organization and (B,C) TEM images of satellite nanostructures created by controlled spatial organization of nanoparticles using DNA linkers. (*adapted from references 87 and 88*)

1.4. Self-organization of Organic Molecules on Surfaces

Even though notable progress has been made in the synthesis of metal or semiconductor nanomaterials and understanding their functional properties, devices derived out of these systems are still under development. In contrast, organic molecules have already become an integral part of many optoelectronic devices such as organic light emitting

diodes (OLEDs), dye sensitized solar cells (DSSC) and thin-film transistors (OTFTs). Understanding the self-assembly of organic molecules on surface and the formation of nanostructures is of great interest from device fabrication and performance point of view.

It was Ratner and Aviram in mid 1970's, put forward the idea of using organic molecules as a functional substitute for semiconductor devices in electronic equipments to perform various functions such as rectification, amplification and storage.[3,89-91] They have shown that a molecule containing both donor and acceptor moieties behave like a diode. Later in 1999, Tour and coworkers have reported that phenyleneethynylene derivatives with amino and nitro groups show pronounced negative differential resistance (NDR) activity:[92,93] an initial rise in current, followed by a steep decrease when the voltage is progressively increased. Various investigations clearly suggest the potential application of organic molecules in electronic devices, however there are some major challenges in this area. These include the (i) precise positioning of organic molecules at predefined locations and the creation of well defined structures and (ii) interconnecting various functional devices and further integrating into the macroscopic world.

Controlled organization of molecules on surfaces is one of the prerequisite for the fabrication of devices. The characterization of these molecular assemblies on surfaces, with atomic or molecular resolutions, remained as a major challenge for several years. With the invention of newer instrumental techniques such as scanning probe microscopes, it is now possible to real time image and study molecular assemblies on surfaces with atomic scale precision both under vacuum and ambient conditions. More recently, attempts have been made to characterize molecular assemblies on surfaces using scanning tunneling microscopy and a brief description on these aspects is provided.

1.4.1. Self-assembled Monolayers

The chemisorption of surfactants, with electron rich head groups (e.g., S, O, N), on transition metals such as copper and gold is one of the widely used method for organizing molecules on surfaces.[94,95] The assembly is formed through the polar covalent or ionic bond interactions between the surfaces and head group. The assembly is further strengthened through favorable lateral interactions between adjacent molecules. The chemisorption of thiol groups on Au(111) surface is the most widely investigated system due to its strong coordinating ability with the metal. A schematic representation of self-assembled monolayer (SAM) of n-alkanethiolate molecules chemisorbed to a gold surface is shown in Figure 1.11. SAMs are of prime technological

interest: the presence of molecules chemically bound to the surface renders modified interfacial properties (wetting, conductivity, adhesion, and chemistry) which are distinctly different from those of the bare substrate. For example, the surface properties can be easily tuned by adsorbing organo-sulfur ligands with proper terminal functionality (i.e., alkyl, carboxylic acids, quinones, amines, anhydrides).[95]

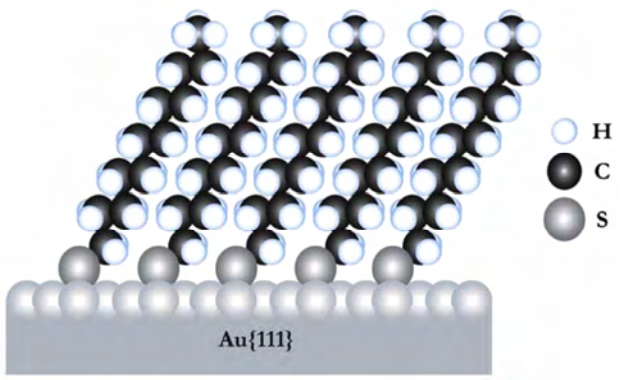

Figure 1.11. Schematic representation of an n-dodecanethiolate monolayer, self-assembled on an atomically flat gold substrate (*adapted from reference 95*)

Scanning tunneling microscopy can be employed for the direct determination of molecular conductivity of SAM. The molecular conductivity of the SAM can be easily tuned by varying the nature of molecules (alkyl, aromatic etc.) and by the incorporation of functional moieties such as chromophores, electroactive groups, or host molecules (that can complex with analytes). Such systems are useful as sensors and electron transfer devices.

1.4.2. Patterned Organic Monolayers

Physisorption of molecules on surfaces can also lead to patterned monolayers through self-assembly.[96] Molecules are adsorbed onto the surface through relatively weak van der Waals interactions and probable electronic interactions of the adsorbate with the surface. The overall structure and stability of the molecular assembly is determined by various intermolecular interactions such as hydrogen bonding, coordinate bonding, host-guest interactions and alkyl chain interdigitations.[36,96] Due to its high selectivity and directionality, hydrogen bond plays an important role in molecular self-assembly and is widely used for the construction of various supramolecular nanostructures.[97] For example, trimesic acid and structurally related compounds form hexagonal networks (rosette structures) through hydrogen-bonding on Cu(111)[98] and graphite surfaces[99] (Figure 1.12A). Similarly 4-[trans-2-(pyrid-4-yl-vinyl)]benzoic acid forms molecular wires through the head to tail hydrogen bonding between pyridyl and benzoic acid moieties (Figure 1.12B).[100]

Compared to hydrogen bonding, interaction of metal ion centres with organic ligands (Lewis bases) results in stronger, directional and selective bonding and are widely used for the preparation of coordination polymers and network structures. This methodology provides an excellent way of organizing metal ions on surfaces. Metal ions possess smaller size (< 1

nm) and their properties can be tailored by the type and geometrical arrangement of the ligands. The local distribution of electron density around the respective metal ion can form structural and functional base in

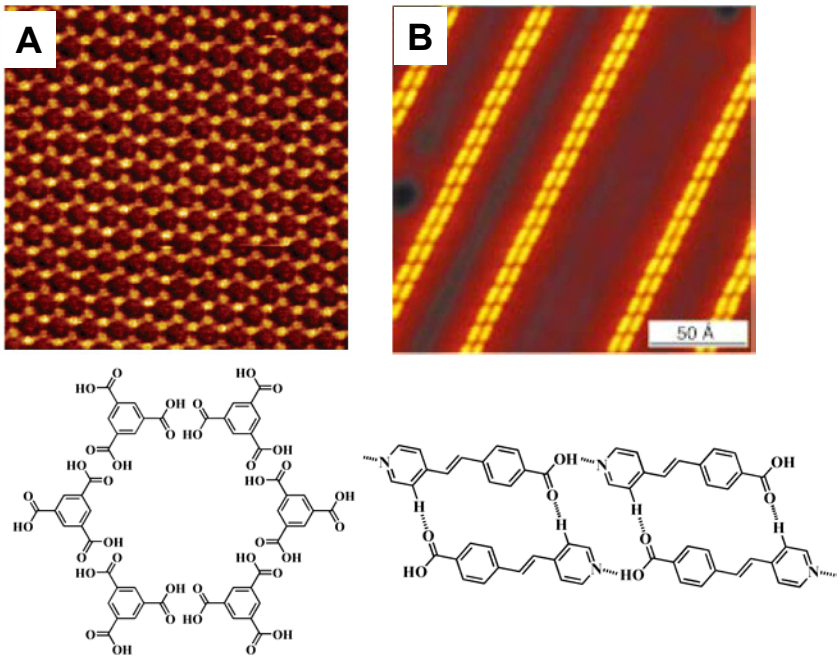

Figure 1.12. STM images of (A) hexagonal close network of trimesic acid on HOPG and (B) molecular wires of 4-[trans-2-(pyrid-4-yl-vinyl)]benzoic acid on Ag(111) surface. (*adapted from references 99 and 100*)

the design of molecular devices. The inherent properties of the coordinated metal ions such as redox, electronic or spin states can be used for multistate digital information storage and processing (for example, spintronics). Barth and coworkers have demonstrated the controlled spacing between Fe atoms through metal-organic coordination networks with the proper choice of the ligands (Figure 1.13).[101]

In the absence of strong intermolecular interactions, various other factors such as geometry of the molecule and the interdigitation of alkyl chains play a critical role in the formation of molecular assembly on surface. For example, Tobe, De Feyter and coworkers have reported that the self-organization of dehydrobenzo[12]annulene derivatives are highly dependant on their geometry.[102] Interestingly, this class of molecules lacks any hydrogen bonding moieties and assembly is formed through the

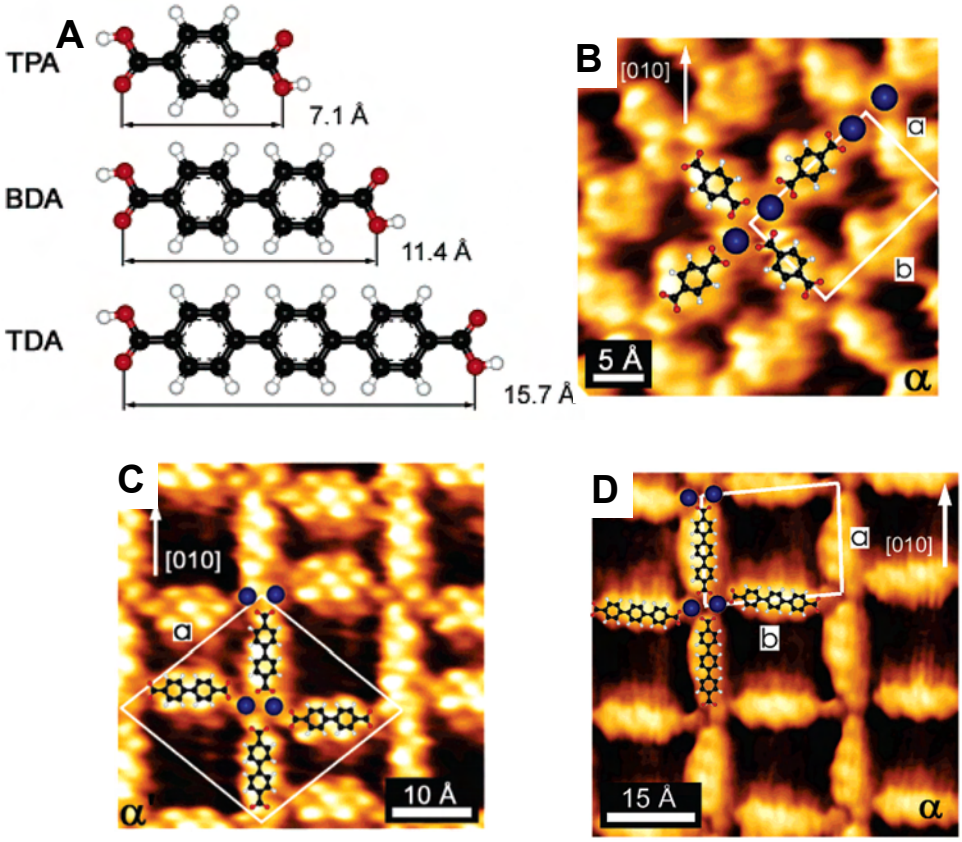

Figure 1.13. STM images illustrating the control of the spacing between iron atoms using dicarboxylic acid derivates of proper lengths. (*adapted from reference 101*)

interdigitation of alkyl chains. The authors observed that dehydrobenzo[12]annulene derivative with rhombic geometry self-organizes into Kagome structures whereas molecule with triangular geometry forms honey comb network structures (Figure 1.14).[102]

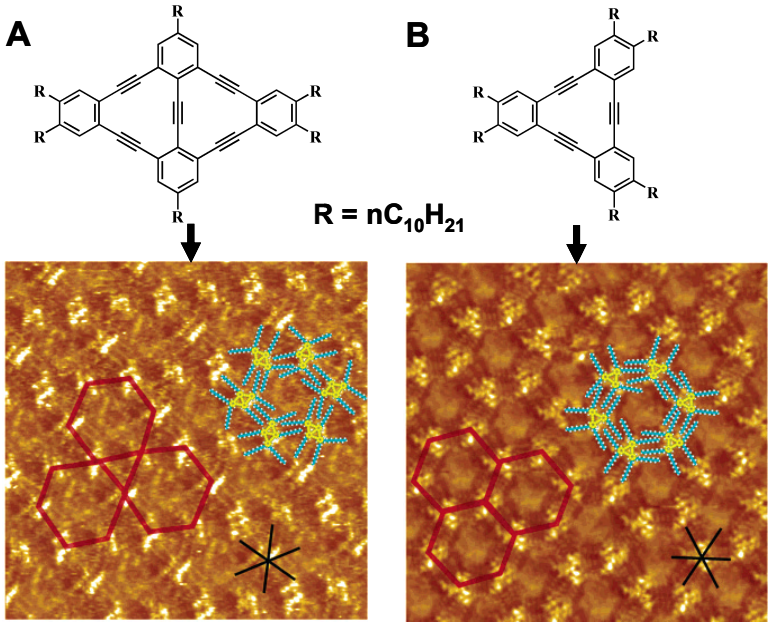

Figure 1.14. STM images illustrating the effect of geometry on the self-organization of dehydrobenzo[12]annulene derivatives: (A) rhombic geometry forms Kagome and (B) triangular geometry forms honey comb network structures. (*adapted from reference 102*)

1.4.3. Chiral Organization on Surface

Chirality, the property of an object being nonsuperimposable on its mirror image, affects the performance of many chemical, biochemical and physical systems. Adsorption of molecular systems on surfaces often display pronounced stereochemical effects which is of great practical interest in

producing surfaces with chiral signature. Chirality is often preserved when two-dimensional (2D) crystals are formed through the adsorption of a chiral molecule on surface. An excellent example of this aspect was provided by Meijer and coworkers, in which authors have shown that a chiral oligo-(p-phenylenevinylene) molecule self organizes on 2D surfaces into enantiomeric pure domains (Figure 1.15 A).[103]

More interestingly, recent research reports have shown that, adsorption of achiral or prochiral molecules on surfaces lead to enantiomeric domains. The observation of spontaneous symmetry breaking is of fundamental interest as induction of chirality is among the most intriguing and inspiring phenomenon in nature. Recent investigations have revealed that chirality of 2D molecular assemblies of achiral molecules originate if the adsorption destroys the reflection symmetry planes of the underlying surface. This induces asymmetries in lateral intermolecular interactions allowing the growth along the non-symmetry axes. However, due to the inherent non-chirality of the initial molecule, there is equal probability of nucleating reflectional chiral domains. As a result, these systems always consist of coexisting mirror chiral domains, leading to a racemic surface. Various groups have investigated this aspect and a representative example of the self-organization of a prochiral molecule into coexisting enantiomeric domains is presented in Figure 1.15B[104]

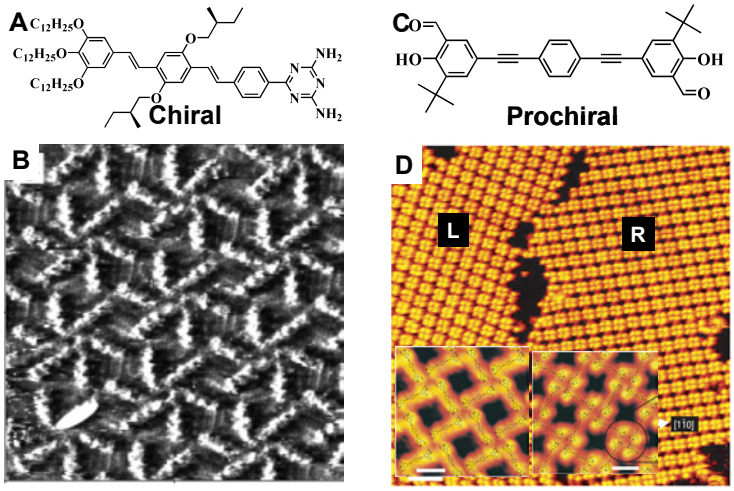

Figure 1.15. STM images of (A) chiral organization formed through the self assembly of chiral molecule (B) L and R enantiomeric domains formed from a prochiral molecule. (*adapted from references 103 and 104*)

1.5. Objectives of the Present Work

Most of the procedures reported for the synthesis of metal nanoparticles involve the use of strong reducing agents or elevated temperatures. This limits the possibility of developing metal nanoparticle based sensors for the *in situ* detection of analytes. One of the objectives of the present investigations is to (i) develop newer methodologies for the synthesis of metal nanoparticles in aqueous medium at ambient conditions and (ii) their use in the detection of metal cations by taking advantage of the unique coordination ability. Ideally, biocompatible molecules which possess both the reducing and stabilizing groups are desirable for such applications. Formation of stable supramolecular assembly, by bringing

metal nanoparticles close to each other, results in plasmon coupling and this strategy can be effectively utilized for the development of metal nanoparticle based sensors.

Another objective of the present study is to understand the supramolecular organization of molecules on surfaces. Various noncovalent interactions between the molecules and with surface play a decisive role in their organizations. An in-depth understanding of these interactions is essential for device fabrications. Recent photophysical studies have revealed that phenyleneethynylene based molecular systems are ideal for device application. The second objective of the thesis focuses on understanding the (i) organization of phenyleneethynylenes on highly oriented pyrolytic graphite (HOPG) surface with atomic level precision and (ii) weak intermolecular interactions which drive their organization.

1.6. References

1. Feynman, R. P., *Eng. Sci.* **1960,** *23*, 22-36.
2. Barth, J. V.; Costantini, G.; Kern, K., *Nature* **2005,** *437*, 671-679.
3. Joachim, C.; Gimzewski, J. K.; Aviram, A., *Nature* **2000,** *408*, 541-548.
4. Lehn, J.-M., *Science* **2002,** *295*, 2400-2403.
5. Schmid, G.; Bäumle, M.; Geerkens, M.; Heim, I.; Osemann, C.; Sawitowski, T., *Chem. Soc. Rev.* **1999,** *28*, 179-185.
6. Alivisatos, A. P., *J. Phys. Chem.* **1996,** *100*, 13226-13239.
7. Rosi, N. L.; Mirkin, C. A., *Chem. Rev.* **2005,** *105*, 1547-1562.
8. Schmid, G.; Corain, B., *Eur. J. Inorg. Chem.* **2003**, 3081-3098.

9. Lewis, L. N., *Chem. Rev.* **1993,** *93*, 2693-2730.
10. Edwards, P. P.; Thomas, J. M., *Angew. Chem. Int. Ed.* **2007,** *46*, 5480-5486.
11. Daniel, M. C.; Astruc, D., *Chem. Rev.* **2004,** *104*, 293-346.
12. Gopidas, K. R.; Whitesell, J. K.; Fox, M. A., *Nano Lett.* **2003,** *3*, 1757-1760.
13. Cha, D. Y.; Parravano, G., *J. Catal.* **1970,** *18*, 200-211.
14. Andreeva, D.; Tabakova, T.; Idakiev, V.; Christov, P.; Giovanoli, R., *Appl. Catal. A: Gen.* **1998,** *169*, 9-14.
15. Sinha, A. K.; Seelan, S.; Tsubota, S.; Haruta, M., *Top. Catal.* **2004,** *29*, 95-102.
16. Christensen, C. H.; Jørgensen, B.; Rass-Hansen, J.; Egeblad, K.; Madsen, R.; Klitgaard, S. K.; Hansen, S. M.; Hansen, M. R.; Andersen, H. C.; Riisager, A., *Angew. Chem. Int. Ed.* **2006,** *45*, 4648-4651.
17. Han, P.; Axnanda, S.; Lyubinetsky, I.; Goodman, D. W., *J. Am. Chem. Soc.* **2007,** *129*, 14355-14361.
18. Byon, H. R.; Choi, H. C., *J. Am. Chem. Soc.* **2006,** *128*, 2188-2189.
19. Lehn, J.-M., *Supramolecular Chemistry: Concepts and Perspectives: A Personal Account*. VCH: New York, 1995.
20. Lehn, J.-M., *Angew. Chem. Int. Ed.* **1988,** *27*, 89-112.
21. Mulder, A.; Huskens, J.; Reinhoudt, D. N., *Org. Biomol. Chem.* **2004,** *2*, 3409-3424.
22. Hoeben, F. J. M.; Jonkheijm, P.; Meijer, E. W.; Schenning, A. P. H. J., *Chem. Rev.* **2005,** *105*, 1491-1546.
23. Gianneschi, N. C.; Masar, M. S.; Mirkin, C. A., *Acc. Chem. Res.* **2005,** *38*, 825-837.
24. Schenning, A. P. H. J.; Meijer, E. W., *Chem. Commun.* **2005**, 3245 - 3258.
25. Oshovsky, G. V.; Reinhoudt, D. N.; Verboom, W., *Angew. Chem. Int. Ed.* **2007,** *46*, 2366-2393.
26. Ajayaghosh, A.; Praveen, V. K., *Acc. Chem. Res.* **2007,** *40*, 644-656.

27. Fialkowski, M.; Bishop, K. J. M.; Klajn, R.; Smoukov, S. K.; Campbell, C. J.; Grzybowski, B. A., *J. Phys. Chem. B* **2006,** *110*, 2482-2496.
28. LeDuc, P. R.; Robinson, D. N., *Adv. Mater.* **2007,** *19*, 3761-3770.
29. Sarikaya, M., *Proc. Natl. Acad. Sci. U. S. A.* **1999,** *96*, 14183-14185.
30. Meyers, M. A.; Chen, P.-Y.; Lin, A. Y.-M.; Seki, Y., *Prog. Mater Sci.* **2008,** *53*, 1-206.
31. Lehn, J.-M., *Angew. Chem. Int. Ed.* **1988,** *27*, 89-112.
32. Niemeyer, C. M.; Adler, M.; Lenhert, S.; Gao, S.; Fuchs, H. Chi, L., *ChemBioChem* **2001,** *2*, 260-264.
33. Mamdouh, W.; Dong, M.; Xu, S.; Rauls, E.; Besenbacher, F., *J. Am. Chem. Soc.* **2006,** *128*, 13305-13311.
34. Guillot-Nieckowski, M.; Joester, D.; Stohr, M.; Losson, M.; Adrian, M.; Wagner, B.; Kansy, M.; Heinzelmann, H.; Pugin, R.; Diederich, F.; Gallani, J. L., *Langmuir* **2007,** *23*, 737-746.
35. Klymchenko, A. S.; Furukawa, S.; Mullen, K.; VanderAuweraer, M.; De Feyter, S., *Nano Lett.* **2007,** *7*, 791-795.
36. Hermann, B. A.; Scherer, L. J.; Housecroft, C. E.; Constable, E. C., *Adv. Funct. Mater.* **2006,** *16*, 221-235.
37. Chen, C.; Daniel, M. C.; Quinkert, Z. T.; De, M.; Stein, B.; Bowman, V. D.; Chipman, P. R.; Rotello, V. M.; Kao, C. C.; Dragnea, B., *Nano Lett.* **2006,** *6*, 611-615.
38. Wasielewski, M. R., *J. Org. Chem.* **2006,** *71*, 5051-5066.
39. Otero, R.; Schöck, M.; Molina, L. M.; Lægsgaard, E.; Stensgaard, I.; Hammer, B.; Besenbacher, F., *Angew. Chem. Int. Ed.* **2005,** *44*, 2270-2275.
40. Lutzen, A., *Angew. Chem. Int. Ed.* **2005,** *44*, 1000-1002.
41. Gromov, S. P.; Vedernikov, A. I.; Ushakov, E. N.; Lobova, N. A.; Botsmanova, A. A.; Kuzmina, L. G.; Churakov, A. V.; Strelenko, Y. A.;

Alfimov, M. V.; Howard, J. A. K.; Johnels, D.; Edlund, U. G., *New J. Chem.* **2005,** *29*, 881-894.

42. Schuster, D. I.; Li, K.; Guldi, D. M.; Ramey, J., *Org. Lett.* **2004,** *6*, 1919-1922.
43. Cavallini, M.; Biscarini, F.; Massi, M.; Farran-Morales, A.; Leigh, D. A.; Zerbetto, F., *Nano Lett.* **2002,** *2*, 635-639.
44. Fendler, J. H., *Chem. Mater.* **2001,** *13*, 3196-3210.
45. Pillai, Z. S.; Kamat, P. V., *J. Phys. Chem. B* **2004,** *108*, 945-951.
46. Henglein, A.; Giersig, M., *J. Phys. Chem. B* **1999,** *103*, 9533-9539.
47. Turkevich, J.; Stevenson, P. C.; Hillier, J., *Discuss. Faraday Soc.* **1951,** *11*, 55-75.
48. Enüstün, B. V.; Turkevich, J., *J. Am. Chem. Soc.* **1963,** *85*, 3317-3328.
49. Brust, M.; Walker, M.; Bethell, D.; Schiffrin, D. J.; Whyman, R., *J. Chem. Soc., Chem. Commun.* **1994**, 801-802.
50. Thomas, K. G.; Kamat, P. V., *Acc. Chem. Res.* **2003,** *36*, 888-898.
51. Bozhevolnyi, S. I.; Volkov, V. S.; Devaux, E. s.; Laluet, J.-Y.; Ebbesen, T. W., *Nature* **2006,** *440*, 508-511.
52. Barnes, W. L.; Dereux, A.; Ebbesen, T. W., *Nature* **2003,** *424,* 824-830.
53. Barnes, W. L.; Murray, W. A.; Dintinger, J.; Devaux, E.; Ebbesen, T. W., *Phys. Rev. Lett.* **2004,** *92*, 107401-1-4.
54. Ebbesen, T. W.; Lezec, H. J.; Ghaemi, H. F.; Thio, T.; Wolff, P. A., *Nature* **1998,** *391*, 667-669.
55. Dintinger, J.; Degiron, A.; Ebbesen, T. W., *MRS Bull.* **2005,** *30*, 381-384.
56. Hutter, E.; Fendler, J. H., *Adv. Mater.* **2004,** *16*, 1685-1706.
57. Girard, C.; Dujardin, E., *J. Opt. A: Pure Appl. Opt.* **2006,** *8*, S73-S86.
58. Maier, S. A.; Kik, P. G.; Atwater, H. A.; Meltzer, S.; Harel, E.; Koel, B. E.; Requicha, A. A. G., *Nat. Mater.* **2003,** *2*, 229-232.
59. Mayer, C. R.; Neveu, S.; Cabuil, V., *Adv. Mater.* **2002,** *14*, 595-597.

60. Brust, M.; Schiffrin, D. J.; Bethell, D.; Kiely, C. J., *Adv. Mater.* **1995,** *7*, 795-797.

61. Brousseau III, L. C.; Novak, J. P.; Marinakos, S. M.; Feldheim, D. L., *Adv. Mater.* **1999,** *11*, 447-449.

62. Novak, J. P.; Brousseau, I., L. C.; Vance, F. W.; Johnson, R. C.; Lemon, B. I.; Hupp, J. T.; Feldheim, D. L., *J. Am. Chem. Soc.* **2000,** *122*, 12029-12030.

63. Novak, J. P.; Feldheim, D. L., *J. Am. Chem. Soc.* **2000,** *122*, 3979-3980.

64. McConnell, W. P.; Novak, J. P.; Brousseau, L. C.; Fuierer, R. R.; Tenent, R. C.; Feldheim, D. L., *J. Phys. Chem. B* **2000,** *104*, 8925-8930.

65. Shenton, W.; Davis, S. A.; Mann, S., *Adv. Mater.* **1999,** *11*, 449-452.

66. Lin, S.; Li, M.; Dujardin, E.; Girard, C.; Mann, S., *Adv. Mater,* **2005,** *17*, 2553-2559.

67. Thomas, K. G.; Barazzouk, S.; Ipe, B. I.; Joseph, S. T. S.; Kamat, P. V., *J. Phys. Chem. B* **2004,** *108*, 13066-13068.

68. Sudeep, P. K.; Joseph, S. T. S.; Thomas, K. G., *J. Am. Chem. Soc.* **2005,** *127*, 6516-6517.

69. Joseph, S. T. S.; Ipe, B. I.; Pramod, P.; Thomas, K. G., *J. Phys. Chem. B* **2006,** *110*, 150-157.

70. Pramod, P.; Joseph, S. T. S.; Thomas, K. G., *J. Am. Chem. Soc.* **2007,** *129*, 6712-6713.

71. Correa-Duarte, M. A.; Liz-Marzán, L. M., *J. Mater. Chem.* **2006,** *16*, 22-25.

72. Klajn, R.; Bishop, K. J. M.; Grzybowski, B. A., *Proc. Natl. Acad. Sci. U. S. A.* **2007,** *104*, 10305-10309.

73. Klajn, R.; Bishop, K. J. M.; Fialkowski, M.; Paszewski, M.; Campbell, C. J.; Gray, T. P.; Grzybowski, B. A., *Science* **2007,** *316*, 261-264.

74. Koyfman, A. Y.; Braun, G.; Magonov, S.; Chworos, A.; Reich, N. O.; Jaeger, L., *J. Am. Chem. Soc.* **2005,** *127*, 11886-11887.

75. Elghanian, R.; Storhoff, J. J.; Mucic, R. C.; Letsinger, R. L.; Mirkin, C. A., *Science* **1997,** *277*, 1078-1080.

76. Storhoff, J. J.; Elghanian, R.; Mucic, R. C.; Mirkin, C. A.; Letsinger, R. L., *J. Am. Chem. Soc.* **1998,** *120*, 1959-1964.

77. Thaxton, C. S.; Georganopoulou, D. G.; Mirkin, C. A., *Clin. Chim. Acta* **2006,** *363*, 120-126.

78. Cheng, M. M. C.; Cuda, G.; Bunimovich, Y. L.; Gaspari, M.; Heath, J. R.; Hill, H. D.; Mirkin, C. A.; Nijdam, A. J.; Terracciano, R.; Thundat, T.; Ferrari, M., *Curr. Opin. Chem. Biol.* **2006,** *10*, 11-19s.

79. Lee, J.-S.; Han, M. S.; Mirkin, C. A., *Angew. Chem. Int. Ed.* **2007,** *46*, 4093-4096.

80. Xu, X.; Georganopoulou, D. G.; Hill, H. D.; Mirkin, C. A., *Anal. Chem.* **2007,** *79*, 6650-6654.

81. Stoeva, S. I.; Lee, J.-S.; Thaxton, C. S.; Mirkin, C. A., *Angew. Chem. Int. Ed.* **2006,** *45*, 3303-3306.

82. Xu, X.; Han, M. S.; Mirkin, C. A., *Angew. Chem. Int. Ed.* **2007,** *46*, 3468-3470.

83. Niemeyer, C. M.; Adler, A., *Angew. Chem. Int. Ed.* **2002,** *41*, 3779-3783.

84. Niemeyer, C. M.; Simon, U., *Eur. J. Inorg. Chem.* **2005**, 3641-3655.

85. Li, H.; Park, S. H.; Reif, J. H.; LaBean, T. H.; Yan, H., *J. Am. Chem. Soc.* **2004,** *126*, 418-419.

86. Kretschmer, R.; Fritzsche, W., *Langmuir* **2004,** *20*, 11797-11801.

87. Mirkin, C. A., *Inorg. Chem.* **2000,** *39*, 2258-2272.

88. Huo, F.; Lytton-Jean, A. K. R.; Mirkin, C. A., *Adv. Mater,* **2006,** *18*, 2304-2306.

89. Aviram, A.; Ratner, M. A., *Chem. Phys. Lett.* **1974,** *29*, 277-83.

90. Martin, A. S.; Sambles, J. R.; Ashwell, G. J., *Phys. Rev. Lett.* **1993,** *70*, 218-221.

91. Nitzan, A.; Ratner, M. A., *Science* **2003,** *300*, 1384-1389.
92. Chen, J.; Reed, M. A.; Rawlett, A. M.; Tour, J. M., *Science* **1999,** *286*, 1550-1552.
93. Seminario, J. M.; Zacarias, A. G.; Tour, J. M., *J. Am. Chem. Soc.* **2000,** *122*, 3015-3020.
94. Poirier, G., *Chem. Rev.* **1997,** *97*, 1117-1128.
95. Smith, R. K.; Lewis, P. A.; Weiss, P. S., *Prog. Surf. Sci.* **2004,** *75*, 1-68.
96. Plass, K. E.; Grzesiak, A. L.; Matzger, A. J., *Acc. Chem. Res.* **2007,** *40*, 287-293.
97. Yang, Y.; Deng, K.; Zeng, Q.; Wang, C., *Surf. Interface Anal.* **2006,** *38*, 1039-1046.
98. Dmitriev, A.; Lin, N.; Weckesser, J.; Barth, J. V.; Kern, K., *J. Phys. Chem. B* **2002,** *106*, 6907-6912.
99. Lackinger, M.; Griessl, S.; Heckl, W. M.; Hietschold, M.; Flynn, G. W., *Langmuir* **2005,** *21*, 4984-4988.
100. Barth, J. V.; Weckesser, J.; Cai, C.; Günter, P.; Bürgi, L.; Jeandupeux, O.; Kern, K., *Angew. Chem. Int. Ed.* **2000,** *39*, 1230-1234.
101. Stepanow, S.; Lin, N.; Barth, J. V.; Kern, K., *J. Phys. Chem. B* **2006,** *110*, 23472-23477.
102. Furukawa, S.; Uji-i, H.; Tahara, K.; Ichikawa, T.; Sonoda, M.; De Schryver, F. C.; Tobe, Y.; De Feyter, S., *J. Am. Chem. Soc.* **2006,** *128*, 3502-3503.
103. Jonkheijm, P.; Miura, A.; Zdanowska, M.; Hoeben, F. J. M.; De Feyter, S.; Schenning, A. P. H. J.; De Schryver, F. C.; Meijer, E. W., *Angew. Chem. Int. Ed.* **2004,** *43*, 74-78.
104. Weigelt, S.; Busse, C.; Petersen, L.; Rauls, E.; Hammer, B.; Gothelf, K. V.; Besenbacher, F.; Linderoth, T. R., *Nat. Mater.* **2006,** *5*, 112-117.

CHAPTER 2

In Situ Synthesis of Gold and Silver Nanoparticles using Gallic acid and L-DOPA

2.1. Abstract

Synthesis of water soluble nanoparticles of gold and silver were reported in a single step using two naturally occurring molecules namely gallic acid and L-DOPA. Synthesis is carried out by mixing corresponding metal salt with gallic acid/L-DOPA in aqueous medium at room temperature and does not require any external reducing agent. Due to high negative zeta potential (-45 mV), nanoparticles are found to be highly stable for several months and hence useful for a variety of biological/sensing applications. Mechanistic details of nanoparticle formation in the presence of gallic acid were elucidated by following the reaction of metal salt with a variety of model compounds and by varying the pH of the medium. These studies clearly indicate that the hydroxyl groups assist the reduction of metal cations and the carboxylic acid serve as the stabilizing agent. Kinetics of the formation of nanoparticles was found to be autocatalytic in nature involving three stages namely, nucleation, growth and saturation. The newly synthesized nanoparticles were characterized by spectroscopic (UV-Vis, FTIR) and microscopic (AFM, TEM) techniques and these aspects are discussed in detail.

2.2. Introduction

2.2.1. Historic Overview

Metal particles in its colloidal state have attracted mankind even centuries ago due to their fascinating colors and medicinal value.[1-3] Colloidal gold has a long therapeutic history which is well rooted in Eastern traditions particularly in Indian subcontinent.[4,5] The 'elixir of life' (water of life) which was believed to provide eternal life or eternal youth was known to Indians under the name 'Amrita Rasa' or 'Amrita'. The medicinal value of colloidal gold is well documented in the books of ancient Indian ayurveda like 'Charaka Samhita' and 'Vedas'. Since Vedic era, gold was used as a medicine in India to enhance strength, potency and to promote longevity. In India, the procedure for the preparation of Swarna Bhasma (red colloidal gold) is still in use, and is usually prescribed by Ayurvedic physicians for rejuvenation and revitalization in old age.[4] 'Swarna Bhasma' is also used for the treatment of diseases such as heart and venereal problems, dysentery, epilepsy, tumors and for the diagnosis of syphilis.[5,6] Another example is the use of red colloidal gold as the alchemical drug of longevity by ancient Chinese.

Brilliant colors of noble metal particles have long fascinated scientists and have been used as pigments for coloring art wares (glass and ceramics) by Romans in the 4th and 5th century A.D. The most notable one is the

Roman Lycurgus cup of 4th century A. D. which is now preserved in British Museum. Lycurgus cup is a fascinating art ware; it appears green when viewed in reflected light and when light is transmitted through the glass it is seen as red (Figure 2.1A). Recent transmission electron microscopic analysis indicates that the glass consists of alloy of gold and silver (3:7) having a size of ~70 nm.[7,8] In the middle ages, colloidal metals were extensively used for coloring glass windows in the cathedrals and palaces of Europe (Figure 2.1B). The famous "Purple of Cassius", discovered by Andreus Cassius in 1685 (A. D.) by reacting gold, stannous and stannic chlorides with alkali have been extensively used for coloring glass and chinaware in 17th century.[9] Around 1897 (A. D.), after almost 250 years of its discovery, Richard Zsigmondy of Schott Glass works in Jena showed that Purple of Cassius consisted of colloidal gold and stannic acid. Interestingly, the principle techniques involved in producing red ruby glass are still based on this discovery.

Along with the renaissance of colloidal and cluster chemistry, there were several attempts to provide a scientific rationale for their enchanting optical properties. In 1818 (A. D.) Jermias Benjamine Richter suggested that purple color of drinkable gold results from gold particles of finest degree of subdivision whereas yellow color originates from the aggregation of fine particles. It was Michael Faraday in 1857 (A. D.) first succeeded in preparing

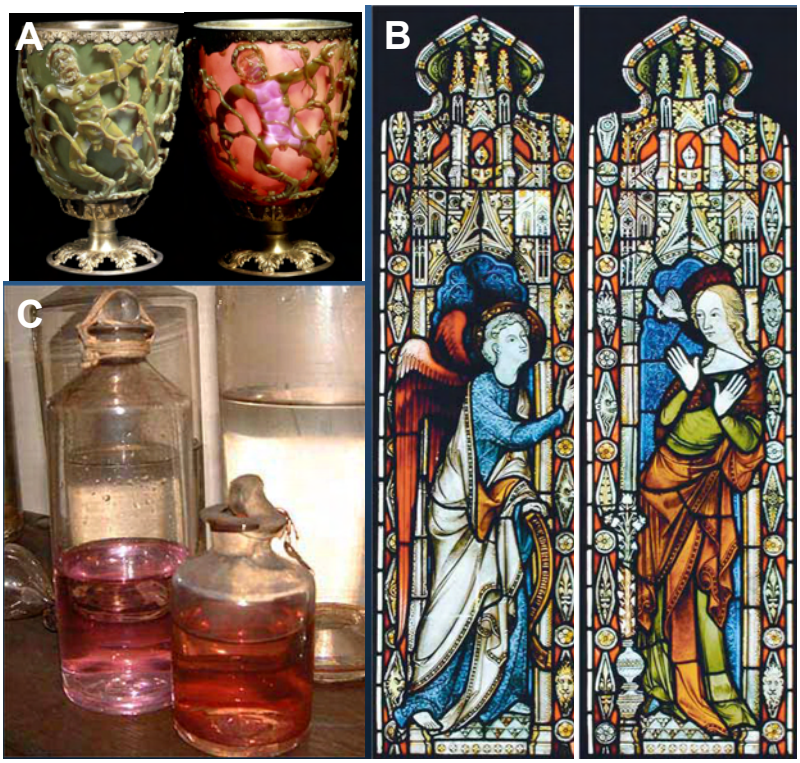

Figure 2.1. (A) Lycurgus cup showing two different colors in reflected light (green) and transmitted light (red)(*adapted from the web site of The British Museum*) (B) Stained glass windows of an old cathedral (C) Colloidal solution prepared by Michael Faraday displayed at the Museum of Royal Society, London (*adapted from the website of The Royal Institution of Great Britain*).

gold sols in laboratory by reducing $HAuCl_4$ with phosphorus in carbon disulfide. He recognized that the color of the metal colloids originates due to the presence of exceedingly fine metal particles in solution and he called them as 'divided metals'.[10,11] These colloidal gold solutions prepared by Faraday are highly stable and are still on display at the museum of the Royal Institution in London (Figure 2.1C).

Later it was recognized that metal nanoparticles having various size and shape possess attractive electronic,[2,6] optical,[12] thermal[13] and catalytic[6] properties and have potential applications in the fields of physics, chemistry, biology, medicine, material science and their interdisciplinary fields. This has initiated a plethora of activities, particularly on the synthesis of metal nanoparticles of varying size and shape and the investigations of their optical properties. Various methods adopted for the synthesis of metal nanoparticles involve chemical, biochemical, electrochemical and photochemical methods, both in aqueous as well as non aqueous media.[6] Extensive reviews are available on these aspects[2,6,14,15] and herein we report a brief summary on (i) the origin of the optical properties of metal nanoparticles (Section 2.2.2) and a few chemical and biochemical methods adopted for the synthesis of isotropic water soluble Au nanoparticles (Section 2.2.3).

2.2.2. Optical Properties

One of the most attractive features of metal nanoparticles is their intense absorption in the visible region which is of four to five orders of magnitude higher than that of organic chromophores.[16] Interestingly, the absorption maximum of metal (as well as semiconductor) nanomaterials can be tuned from visible to NIR and further to IR region by controlling their size, shape and composition.[11,12,15] Right from its discovery, numerous attempts have been made to provide a scientific rationale for their intense absorption.

Quantitative description for the resonance was first provided by Gustay Mie in 1908 by solving Maxwell's equations for spherical particles with appropriate boundary conditions.[3,11,17] According to Mie theory, the total cross section consists of both scattering and absorption (often termed as extinction) and given as summation over all electric and magnetic oscillations.[6]

The light absorption in metal nanoparticles originate from an interesting phenomena called Localized Surface Plasmon Resonance (LSPR).[12,18] A brief description on the origin of the plasmon absorption is presented below. According to the Drude-Lorentz model, the atoms in metals exist in a plasma state which is having a core of positively charged nuclei surrounded by a pool of negatively charged electrons and hence named as "plasma electrons". In the presence of an electromagnetic radiation, the free electrons get displaced by the electric vector and the columbic electrostatic interaction between the nuclei and electrons will restore them to the original position. As a result of the oscillating nature of the electric field of light, the electron clouds coherently oscillate over the surface with a frequency.[19] A schematic representation of the oscillation of the electron cloud in presence of an applied electromagnetic radiation is presented in Figure 2.2. When the frequency of this oscillation matches with that of incident radiation, a resonance condition is established which results in the intense absorption in the electronic spectra, often termed as plasmon

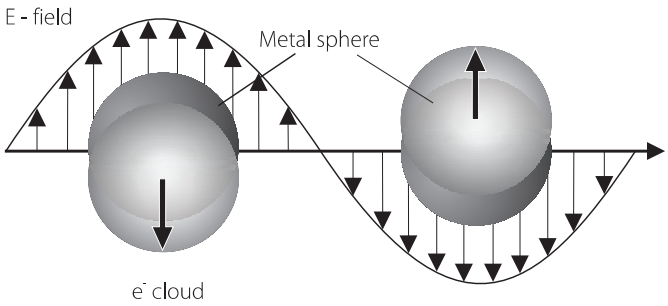

Figure 2.2. Schematic representation of the oscillation of the electron cloud in presence of an electromagnetic radiation. (*adapted from reference 19*)

absorption or more precisely surface plasmon resonance (SPR). For a bulk metal with infinite dimension in all the three directions, the resonance frequency of plasma (ω_p) can be expressed as

$$\omega_p = (Ne^2/\varepsilon_0 m_e)^{½} \qquad (1)$$

where N is the number density of the electrons, ε_0 is the permittivity of vacuum, and e and m_e are the charge and effective mass of the electron, respectively. In contrast to the bulk metal, the electron plasma in nanoparticles is confined in a finite volume which is smaller than the wavelength of light and different boundary conditions can be imposed. Hence, the frequency of oscillation of metal nanoparticles is determined mainly by four parameters: number density of electrons, effective mass of the electron and the shape and size distribution of the charge. This allows the tuning of the optical properties of noble metal nanoparticles by varying the

size, shape and dielectric environment.[12,19] For example, the plasmon absorption of smaller (~5-10 nm) silver nanoparticles peaks at 400 nm and that of gold at 520 nm. Further, it has been demonstrated that an increase in the diameter of spherical gold nanoparticles (20 to 80 nm) results in a bathochromic shift (520 to 550 nm) in their absorption maximum. More interestingly, plasmon resonance in rod shaped anisotropic nanomaterials splits into two distinct bands: a shorter wavelength originating from the transverse absorption and one at a longer wavelength from the longitudinal mode of plasmon oscillation. It has been also reported that the alloys of gold and silver nanomaterials show intermediate plasmon absorption.

2.2.3. Synthesis of Metal Nanoparticles

2.2.3.1. Chemical Methods

Among the various chemical approaches, the simplest and by far the most commonly followed method for the preparation of nanoparticles involve the reduction of metal salts (for e.g., $H[AuCl_4]$, $AgNO_3$, $H_2[PdCl_4]$ and $H_2[PtCl_6]$) by sodium citrate,[6,20,21] sodium borohydride or even alcohols in presence of a stabilizer.[6,22-25] By using appropriate stabilizing groups, it is possible to prepare optically transparent metal nanoparticles either in aqueous or organic medium.[22,26] Two classic examples are the preparation of citrate reduced nanoparticles in water[20,21] and thiolate stabilized nanoparticles which are soluble in organic solvents (two phase reduction

method).[6,22,25] The two-phase preparation of colloidal metals was first introduced by Faraday,[10] in which he reduced an aqueous gold salt with phosphorus in carbon disulfide and obtained a ruby colored aqueous solution of dispersed gold particles. Later in 1994, Schiffrin, Brust and coworkers reported a two-phase extraction procedure for the preparation of metal nanoparticles, soluble in organic solvents, by successfully combining approaches of ion extraction and monolayer self-assembly.[22] Gold ions were extracted to organic medium using a phase transfer reagent namely tetraoctylammonium bromide which was reduced using sodium borohydride in presence of alkanethiols producing monolayer protected nanoparticles. Interestingly, the size of the nanoparticle can be controlled by varying the ratio of reagents and various groups have extensively utilized this approach, with minor modifications, for designing nanoparticles possessing electro- and photoactive molecules.[6,25] Such organic-inorganic hybrid nanomaterials exhibit a unique combination of properties namely, the size and shape dependent optoelectronic properties of nanomaterials and functional properties of the organic molecules such as self-assembly and switching. The use of such hybrid materials in sensing,[27-31] targeting and controlled release,[32-36] bio-imaging,[34,37,38] therapeutics,[13,39,40] and photoelectrochemical applications[16,41-44] have been demonstrated over the years.

2.2.3.2. Biochemical Methods

Even though metal nanoparticles soluble in organic solvents are more monodisperse, easy to purify and functionalize, from an analytical point of view, water soluble systems are rather promising due to their wide range of biological applications (sensing, imaging and therapeutics such as photothermal destruction of malignant cells).[13,16] Ideally, for biological applications, preparative methods involving nontoxic reagents (biocompatible molecules such as citric acid,[20,21] starch[45,46] and sugars[47]) are desirable. Not the least, from an environmental point of view, it is appropriate to follow a green approach for their synthesis.[45] However, there are only a few methods reported in literature for the synthesis of water soluble nanoparticles using green reagents. One of the very old but still followed methods for the preparation of water soluble nanoparticles is the classical approach reported by Turkevich et al.[20] Using this procedure one can synthesize nanoparticles of gold, palladium, and silver in which citrate anions are used as both the reducing agent and stabilizer of the particles formed. Another approach is the use of sugar derivatized dendrimers for the preparation of metal nanoparticles.[47] In this case, the sugar reduces the metal cations resulting in the formation of nanoparticles which are stabilized by the dendrimer. A variety of plant products have been used by Sastry and coworkers for the synthesis of isotropic and

anisotropic metal nanoparticles, for example, reduction of Au^{3+} ions using lemon grass extract resulting in the formation of gold triangles.[48] More recently, Wallen and coworkers reported a green synthesis of silver nanoparticles using β-D glucose as reducing agent and starch as protecting agent.[45]

As mentioned in Section 2.2.2., the high optical cross-section of the surface plasmon band (typically 4-5 orders of magnitude higher compared to conventional dyes) is one of the exciting features of metal nanoparticles which provide excellent opportunities in biomedical field for diagnosis, imaging and photothermal treatment of cancer cells.[13,16] Ideally, biocompatible molecules which possess multifunctions such as the ability to reduce metal ions and stabilize them, and selectively bind with analytes are useful for sensing application. On analysis of various systems we have found that two biologically important molecules namely gallic acid and L-DOPA can perform these functions. In this chapter, detailed investigations on the one pot synthesis of water soluble gold and silver nanoparticles using these molecules are presented.

2.3. Experimental Section

2.3.1. Materials and Methods: Hydrogentetrachloraurate(III)trihydrate, was purchased from Sigma Aldrich. Silver nitrate, gallic acid, L-DOPA, various phenolic compounds listed in Chart 2.1, sodium hydroxide, and

hydrochloric acid were obtained from sd fine chemicals (analar grade) and used as received. Stock solutions of all the reagents were prepared in doubly distilled water. For adjusting the pH, use of buffer solutions was intentionally excluded to avoid further complications arising from the interaction of nanoparticle surface and the buffering material. In the present study, the pH of the medium was varied by either the addition of sodium hydroxide or hydrochloric acid. IR spectra of aqueous solution were recorded on an infrared spectrophotometer (IRPrestige-21, SHIMADZU) using ATR technique. The electronic absorption spectra were recorded on a UV-Vis-NIR scanning spectrophotometer (Shimadzu Model UV-3101). For TEM studies, a drop (~75 μL) of colloidal gold solution was placed on a formvar coated Cu grid and the solvent was allowed to evaporate. Specimens were examined on a Hitachi H600 transmission electron microscope (operating at an acceleration voltage of 75 kV). Samples for AFM studies were prepared by drop casting the solution (~75 μL) on a freshly cleaved mica surface. Specimens were imaged on a multimode scanning probe microscope (Nanoscope IV controller, digital instruments) using the tapping mode technique at ambient conditions. Zeta potentials of nanoparticles at different pH values and the particle size analysis through light scattering experiments were recorded using Malvern Zetasizer 3000HSA.

2.4. Results and Discussion

2.4.1. *In Situ* Synthesis of Au Nanoparticle using Gallic acid (Au-GA)

Gallic acid belongs to the class of secondary plant metabolites commonly termed as plant phenols. It is usually present in all fruits, vegetables including apples, coffee beans, grapes, potatoes, prunes, and green tea leaves.[49,50] Structurally gallic acid is a trihydroxy benzoic acid; a phenolic acid having three hydroxyl groups and one carboxylic acid moiety (Figure 2.3A). Phenolic acids are well known for their antioxidant activity and are involved in the defense of plants against invading pathogens, including insects, bacteria, fungi, and viruses (antimicrobial) and hence they play multiple roles in medicine and food sciences. Due to the antioxidant behavior, they are widely used as anticarcinogenic, antimutagenic, and antibacterial agents. For example, gallic acid scavenges the biologically toxic free radicals namely reactive oxygen and sulfur species, hydroxyl, azide, and superoxide radicals.[51] Gallic acid also scavenges hypochlorous acid at a rate sufficient to protect α-1-antiproteinase against inactivation.[52] In France, the consumption of a diet, high in saturated fat coupled with low incidence of coronary heart disease has been associated with the consumption of red wine (referred to as the "French Paradox").

The absorption spectrum of gallic acid, recorded in doubly distilled water, is presented in Figure 2.3B and characterized by peaks at 213 nm

and 263 nm. The pK_as of gallic acid were reported by Fink and coworkers:[53] the ionization of carboxylic acid at 4.28 (pK_{a1}) and the ionization of phenolic hydroxyl groups at 8.62 (pK_{a2}) and 11.9 (pK_{a3}).

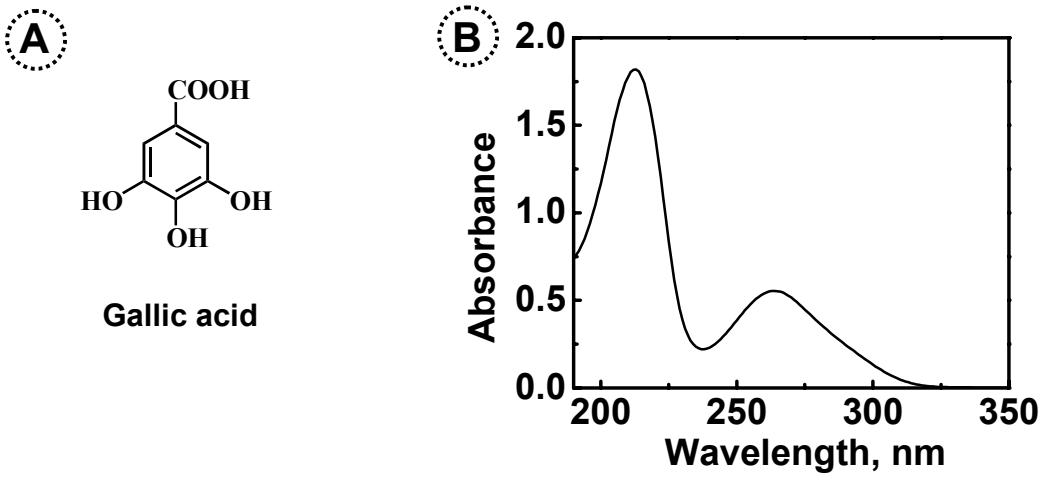

Figure 2.3. (A) Structure of gallic acid and (B) absorption spectrum of gallic acid in water.

The rationale behind the selection of this bifunctional molecule is based on the fact that it possesses both reducing and stabilizing groups, so that *in situ* synthesis is possible. Several naturally occurring biomolecules such as tannins having large percentage of phenolic moiety are known to reduce precious metal ions and have been used for their extraction from industrial affluent water.[54] In the present case, the redox potentials of gallic acid, Ag^+ and Au^{3+} ions are 0.5, 0.8 and 1.4 V, respectively[55,56] and hence the reduction of metal ions is thermodynamically favorable at room temperature (for example, ΔG for the

formation of Au^0 is -567 kJ mol^{-1}). The carboxylic acid moiety present in the capping agent can interact with nanoparticle surface and assist the stabilization.

The possibility of formation of Au nanoparticles was investigated by adding microlitre amounts of 0.5 % gallic acid (29 mM) to 3 mL of $HAuCl_4$ solution (0.2 mM) at room temperature for five minutes. Interestingly, it has been observed that, color of the solution changed slowly during the course of the reaction. After five minutes, depending upon the concentration of gallic acid used, each of the solution developed a characteristic color ranging from blue to red (Figure 2.4A). For example, the $HAuCl_4$ solution stirred with 5 μL of gallic acid (44 μM) developed a bluish red color whereas a grey color for the solution containing 10 μL of gallic acid (88 μM). With increase in concentration of gallic acid to 20 μL (180 μM) solution showed a deep red color. A bluish green color was observed on further increasing the concentration of gallic acid (> 260 μM). The absorption spectra of corresponding solutions are presented in Figure 2.4B. All the solutions under investigation possess an intense absorption in the visible region and the absorption maximum and the spectral features are highly dependant on the relative concentration of the gallic acid used. At lower concentrations of gallic acid (44 μM, trace 'a' in Figure 2.4B), solution possess an intense band at 535 nm with a broad absorption at

around 700 nm. Absorption band at 535 nm become more intense and sharp on increasing the gallic acid concentration (88 μM) and further under went a bathochromic shift (572 nm for 180 μM of gallic acid).

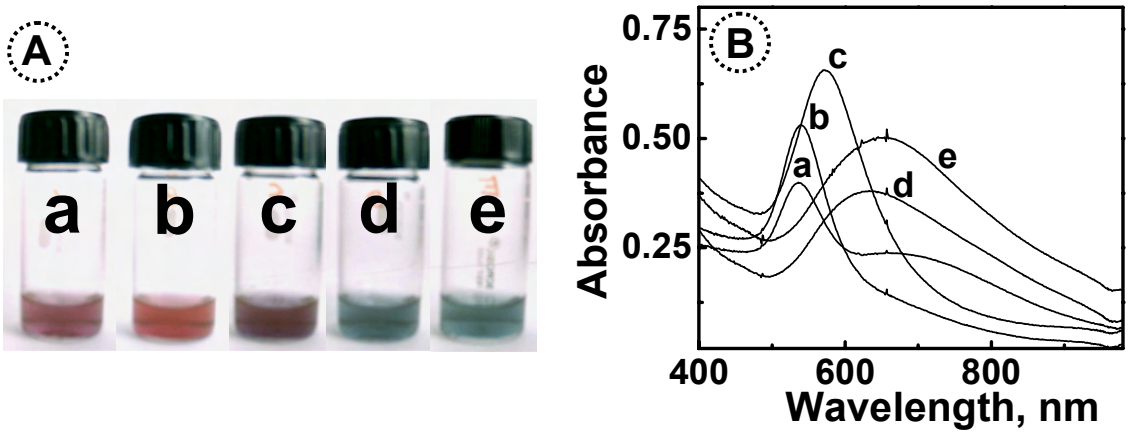

Figure 2.4. (A) Color photograph of $HAuCl_4$ (0.2 mM) solution after the addition of different amounts of gallic acid (a) 44, (b) 88, (c) 180, (d) 260 and (e) 350 μM and the (B) corresponding absorption spectra.

It has been well established that the noble metal nanoparticles exhibit intense absorption in the visible range which originate from the collective plasmon oscillation of their surface electrons (plasmon absorption, *vide supra*). Recent experimental and theoretical investigations have shown that the spectral features of plasmon absorption depend on the size, shape and dielectric environment.[19] It is also well established in the literature that the plasmon absorption of an aqueous solution of non aggregated gold nanoparticles having size ~5 nm possesses a narrow absorption at around 530 nm. Based on the concentration dependent

studies presented above we have optimized the experimental conditions for obtaining stable Au nanoparticles from gallic acid. An aqueous solution of gallic acid (180 μM) was added to 3 mL $HAuCl_4$ solution (0.2 mM) with gentle shaking and the solution was kept undisturbed for five minutes. The formation of nanoparticle was indicated by the gradual appearance of reddish wine color. The color photograph and the absorption spectrum of the nanoparticle solution are presented in Figure 2.5. Nanoparticles were further characterized using various spectroscopic and microscopic techniques (*vide infra*).

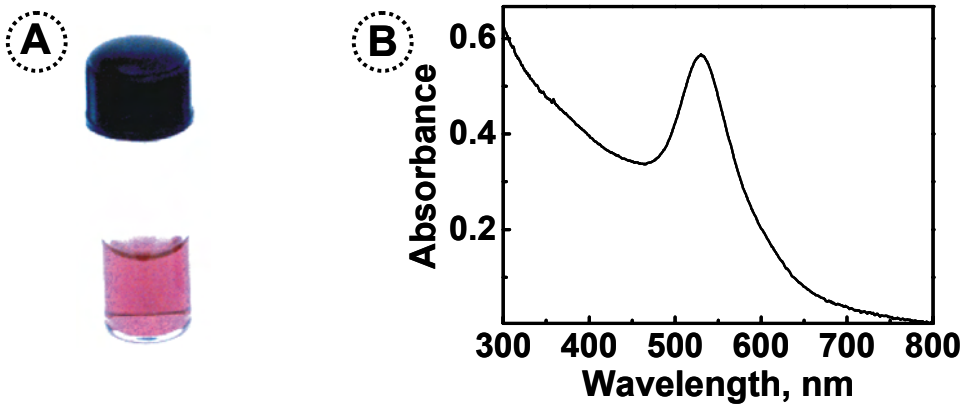

Figure 2.5. (A) Color photograph of the gold nanoparticle solution prepared by adding gallic acid (180 μM) to 3 mL of $HAuCl_4$ solution (0.2 mM) and (B) the corresponding absorption spectrum of the gold nanoparticles.

2.4.2. *In Situ* Synthesis of Ag Nanoparticle using Gallic acid (Ag-GA)

Further we have investigated the possibility of synthesizing silver nanoparticles using gallic acid. Even though the reduction of Ag^+ ion

(E_{redox}= 0.8 V) with gallic acid (E_{redox} = 0.5 V) is thermodynamically favorable (ΔG = -58 kJ mol^{-1}), the formation of silver nanoparticle was not observed by mixing gallic acid with silver nitrate at room temperature or by boiling at 100 ^{o}C. Interestingly, upon addition of micromolar quantities of sodium hydroxide, the solution turned yellow, characteristic of the formation of Ag nanoparticles. It is earlier reported that small amounts of sodium hydroxide is essential for the synthesis of silver nanoparticles using biomolecules like citrate or sugars, however the exact role of base is unclear.

Further, we have optimized the experimental conditions for obtaining stable Ag nanoparticles from gallic acid. An aqueous solution of gallic acid (10 μM) was added, with gentle shaking, to $AgNO_3$ solution (3 mL, 74 μM) containing sodium hydroxide (740 μM) and the solution was kept undisturbed for 30 min. The formation of nanoparticle was indicated by the gradual appearance of a yellow color (Figure 2.6A). The corresponding electronic spectrum showed an intense and narrow absorption with maximum at around 405 nm (Figure 2.6B) characteristic of the plasmon absorption of silver nanoparticles. The nanoparticles were further characterized by various microscopic techniques (*vide infra*).

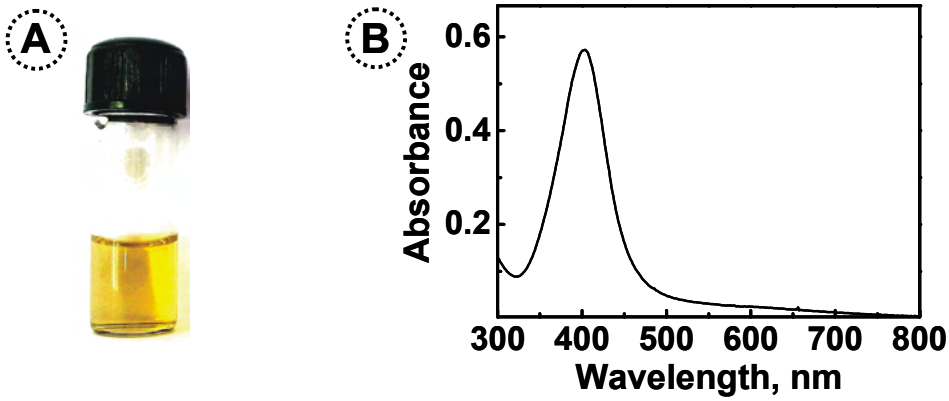

Figure 2.6. (A) Color photograph of silver nanoparticles prepared by mixing gallic acid (10 μM) and $AgNO_3$ (74 μM) containing NaOH (740 μM) and (B) the corresponding absorption spectrum.

2.4.3. *In Situ* Synthesis of Au Nanoparticle using L-DOPA (Au-DOPA)

3,4-Dihydroxy-L-phenylalanine (L-DOPA), also called as Levodopa, is another bioactive polyphenolic compound produced as an intermediate in the biosynthesis of dopamine. Therapeutically, Levodopa is used as a prodrug for the treatment of Parkinson's disease,[57] a degenerative disorder of the central nervous system that often impairs the motor skills and speech of the patient. Normally, Parkinson's disease is caused by the insufficient formation and action of dopamine, which is produced in the dopaminergic neurons of the brain. Dopamine cannot be supplimented, since it cannot cross the blood-brain barrier, whereas L-DOPA can overcome this barrier. Once L-DOPA enter the central nervous system (CNS), it gets metabolized to dopamine by aromatic L-amino acid

decarboxylase. The most common plant source of L-DOPA is a tropical legume, Mucuna pruriens, also known as "Velvet Bean". Both levodopa and the related amino acid L-tyrosine are the precursors to the biological pigment melanin.

The ability of different bioactive *o*-hydroquinones to reduce noble metal cations have been reported by Willner and coworkers.[58] The authors have observed that the addition of neurotransmitters such as dopamine, 3,4-dihydroxy-L-phenylalanine (L-DOPA), adrenaline, or noradrenaline to a $AuCl_4^-$ solution containing cetyltrimethylammonium chloride (CTAC) stabilizer resulted in the formation of gold nanoparticles. The color originating from the intense plasmon absorption of the nanoparticles enabled the colorimetric detection and quantitative analysis of different neurotransmitters in the micromolar concentrations.[58,59]

The focus of the present study is to synthesize stable Au/Ag nanoparticles by exploiting the bifunctional activity of L-DOPA. Gold nanoparticles were synthesized by adding L-DOPA (80 μL, 10 mM) to $HAuCl_4$ solution (30 mL, 0.2 mM) in water with gentle shaking and the solution was kept undisturbed for 30 min. at room temperature. The formation of nanoparticles was indicated by the gradual appearance of reddish wine color. The color photograph of the gold nanoparticle solution and the corresponding absorption spectrum are presented in Figure 2.7.

The absorption maximum of **Au-DOPA** system was observed at 540 nm which is ~10 nm red-shifted compared to **Au-GA** system indicating the formation of larger particles. Nanoparticles were further characterized using various microscopic and light scattering methods (*vide infra*).

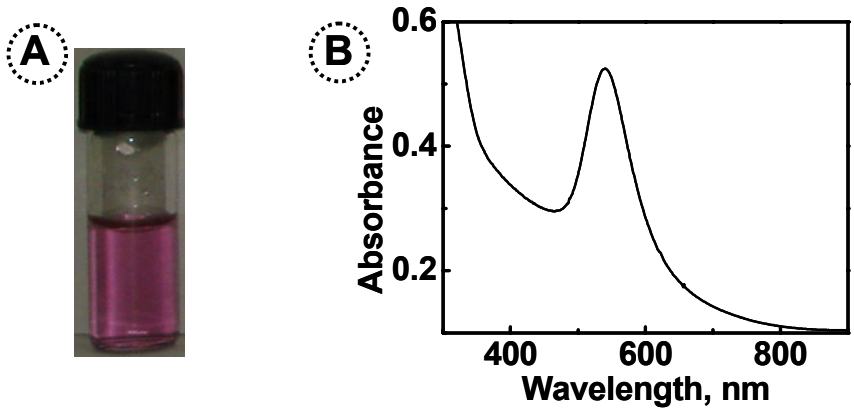

Figure 2.7. (A) Color photograph of gold nanoparticle solution prepared by mixing $HAuCl_4$ solution (30 mL, 0.2 mM) and L-DOPA (80 μL, 10 mM) and (B) the corresponding absorption spectrum.

2.4.2.3. *In situ* synthesis of Ag nanoparticle using L-DOPA (Ag-DOPA)

The synthesis of Ag nanoparticles is also thermodynamically favorable, however presence of a base is essential. Silver nanoparticles were synthesized by adding L-DOPA (10 μL, 10 mM) to $AgNO_3$ solution (30 mL, 0.67 mM) containing sodium hydroxide (25 μL, 165 mM) with gentle shaking. The solution was kept undisturbed for 30 min. at room temperature. The formation of silver nanoparticles was indicated by the slow formation of yellow color. The color photograph and the

corresponding electronic spectrum of silver nanoparticles obtained by mixing silver nitrate and L-DOPA are presented in Figure 2.8. In the present case, the plasmon absorption of silver nanoparticles peaks at ~418 nm.

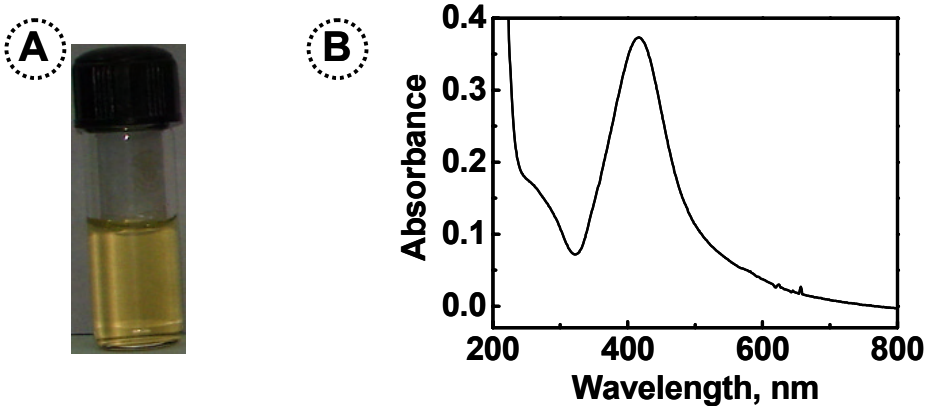

Figure 2.8. (A) Color photograph of silver nanoparticle solution prepared by mixing L-DOPA (10 μL, 10 mM) and $AgNO_3$ (30 mL, 0.67 mM) containing NaOH (25 μL 165 mM) and (B) the corresponding electronic spectrum.

2.4.3. Particle Size Analysis of Nanoparticles

Various methods adopted for the characterization of gold nanoparticles have been reviewed recently by Murray and co-workers.[14] Particle size characterization of Au/Ag nanoparticles were carried out using various microscopic techniques such as Transmission Electron Microscopy (TEM) and Atomic force microscopy (AFM).

Au-GA nanoparticles: TEM images of gold nanoparticles obtained by mixing gallic acid (180 μM) to 3 mL of $HAuCl_4$ solution (0.2 mM) at room

temperature is presented in Figure 2.9A,B. Samples were prepared by drop casting ~75 μL of the solution onto a formvar coated copper grid. It has been observed that nanoparticles are randomly distributed all over the grid and having an average size of ~45 nm. The nanoparticles were further characterized by recording tapping mode AFM images (Figure 2.9C). Samples were prepared by drop casting the solution on to a freshly cleaved mica surface. Bright spots having size in the range ~40-50 nm were observed through out. The AFM images were further analyzed

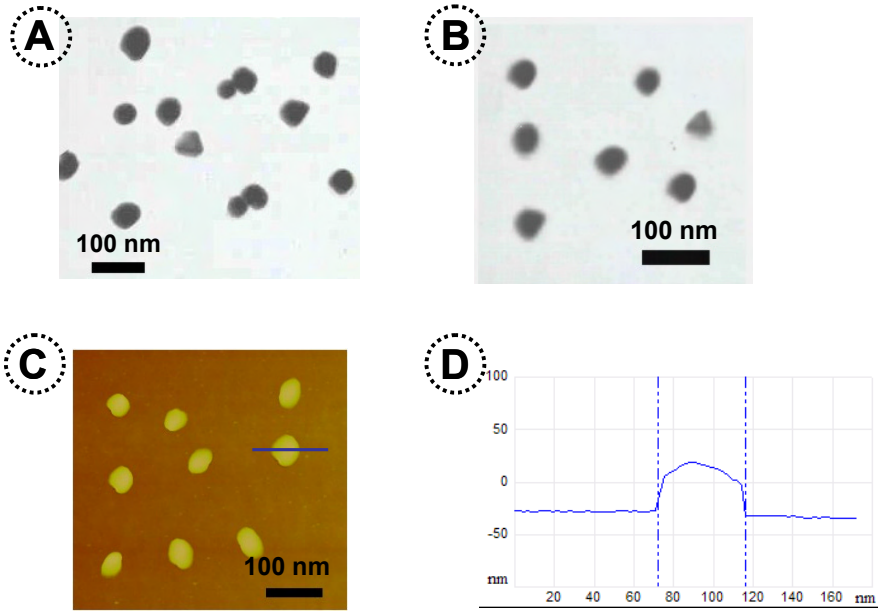

Figure 2.9. (A,B) TEM, (C) tapping mode AFM images of **Au-GA** nanoparticles and (D) the cross sectional analysis of the nanoparticle along the line in the image showing the profile of AFM tip. Samples for TEM were prepared by drop casting the solution on to a formvar coated copper grid and AFM studies by drop casting on to freshly cleaved mica surface.

through cross sectional analysis. The profile of the AFM tip over the nanoparticle (Figure 2.9D), along the line shown in Figure 2.9C indicates that most of the nanoparticles are spherical in shape.

Ag-GA nanoparticles: Representative TEM and tapping mode AFM images of silver nanoparticles prepared by reacting gallic acid (10 μM) with $AgNO_3$ solution (3 mL, 74 μM) containing sodium hydroxide (740 μM) is presented in Figure 2.10. Detailed analysis of these images indicated that the Ag nanoparticles are more or less spherical in shape having an average diameter of ~ 32 nm.

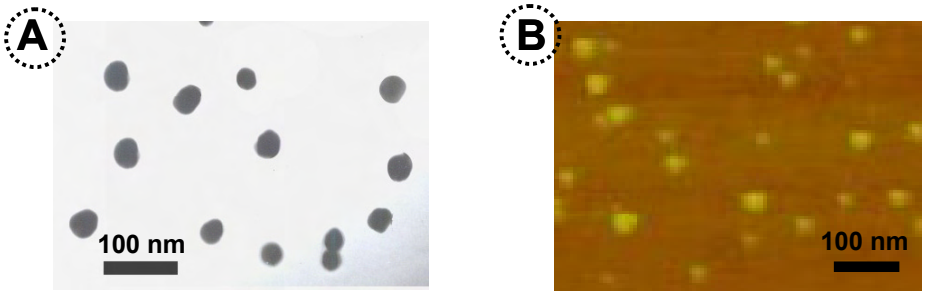

Figure 2.10. (**A**) TEM and (**B**) tapping mode AFM images of **Ag-GA** nanoparticles. Samples for TEM were prepared by drop casting the solution on to a formvar coated copper grid and AFM studies by drop casting on to freshly cleaved mica surface.

Au-DOPA nanoparticles: Tapping mode AFM images of nanoparticles synthesized by mixing L-DOPA (80 μL, 10 mM) with $HAuCl_4$ solution (30 mL, 0.2 mM) at room temperature is shown in Figure 2.11A,B. From the 3D plot (Figure 2.11B) of the AFM image, it is clear that majority of the

nanoparticles are spherical in shape having an average particle size of ~80 nm (based on section analysis). Thus, **Au-DOPA** nanoparticles are bigger in size compared to **Au-GA** nanoparticles (~45 nm) which is in accordance with the plasmon absorption maximum (540 nm for **Au-DOPA** nanoparticles and 530 nm for **Au-GA** nanoparticles). **Au-DOPA** nanoparticles were further characterized using light scattering experiments and Figure 2.11C shows the size distribution curve. It is clear that the

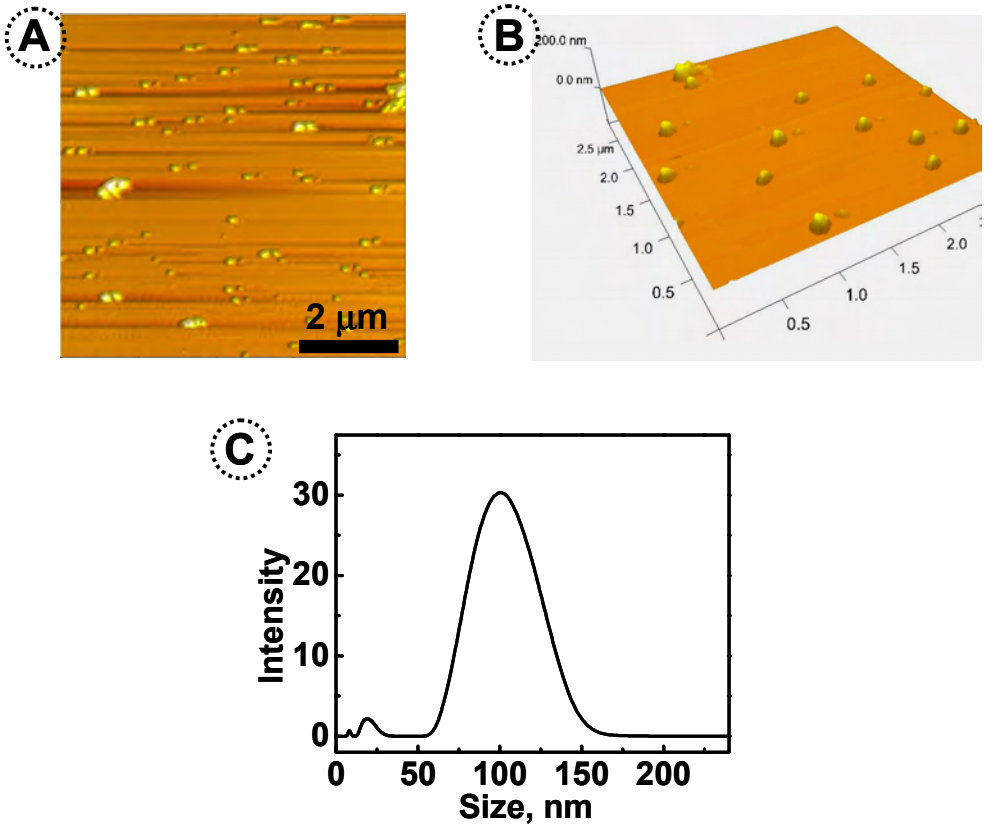

Figure 2.11. (A,B) Tapping mode AFM images of **Au-DOPA** nanoparticles (A) height image and (B) 3D plot. (C) Size distribution curve from light scattering experiments. Samples for AFM studies were prepared by drop casting the solution on to a freshly cleaved mica surface.

solution contains two types of nanoparticles: a minor fraction (less than 2 %) having size in the range of 10-20 nm and a major fraction having size in the range of 80-120 nm.

Ag-DOPA nanoparticles: Silver nanoparticles were synthesized by adding L-DOPA (10 μL, 10 mM) to $AgNO_3$ solution (30 mL, 0.67 mM) containing sodium hydroxide (25 μL, 165 mM) and were characterized through AFM and light scattering experiments. Representative AFM images of the nanoparticles are presented in Figure 2.12A and the 3D plot clearly indicates that the nanoparticles are spherical in shape. The size distribution curve obtained using light scattering technique is presented in Figure 2.12B. Based on microscopic and light scattering studies, it is concluded that the solution contains a minor fraction of smaller particles in

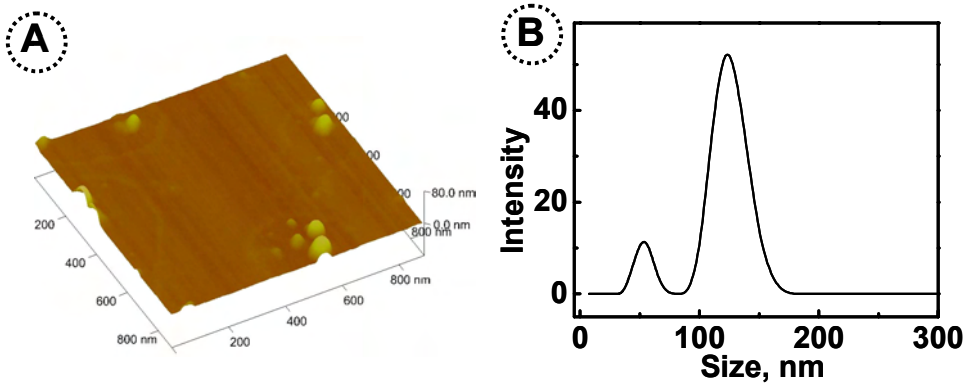

Figure 2.12. (A) Tapping mode AFM images of **Ag-DOPA** nanoparticles (3D plot) and (B) the size distribution curve from light scattering experiments. Samples for AFM studies were prepared by drop casting the solution on to a freshly cleaved mica surface.

the size range of 40-70 nm and a major fraction of bigger particles in the size range of 100-160 nm. The kinetics of the formation of larger nanoparticles is very fast (growth process) and a minor fraction of smaller nanoparticles formed in the nucleation step may be left out in the solution.

2.4.4. Zeta Potential and Stability of Nanoparticles

One of the promising features of the present system is the high stability of Au/Ag nanoparticles; the newly synthesized nanoparticles are found to be highly stable for several months in water. To have a better understanding on the stability, zeta potentials (ζ) of nanoparticle solutions were measured (Table 2.1). It is well understood that colloids having ζ value higher than +30 mV or lower than -30 mV are generally stable due to the strong electrostatic repulsion between the particles which prevent them from aggregation.[29,60] As the magnitude of zeta potential increases, the nanoparticle experiences greater interparticle repulsion and remains isolated in solution; higher the magnitude of zeta potential, greater the stability of nanoparticle system. In the present case, gold and silver nanoparticles prepared using gallic acid showed the higher zeta potential values of -45 and -36 mV, respectively and found to be highly stable in water for several months. In contrast, nanoparticle systems having lower zeta potential values such as **Au-DOPA** (-24 mV) underwent slow precipitation over a period of time.

Table 2.1. Zeta potentials of different nanoparticles.

Nanoparticle	Zeta potential ζ (mV)
Au-GA	-45
Ag-GA	-36
Au-DOPA	-24
Ag-DOPA	-28

2.4.5. Kinetics of Formation of Nanoparticles

Kinetics of the formation of nanoparticles was investigated by following the absorption spectral changes of the reaction mixture at different time intervals (Figure 2.13-16). An aqueous solution of gallic acid (180 μM) was added to 3 mL $HAuCl_4$ solution (0.2 mM) and the spectral changes observed are presented in Figure 2.13A. Gallic acid possesses two absorption bands at 213 nm and 263 nm and the spectral changes above 250 nm were followed. A decrease in the intensity of the gallic acid absorption was observed with time along with the concomitant formation of a new band at around 530 nm, through an isosbestic point, indicating the formation of Au nanoparticles. The absorption spectral changes illustrating the formation of silver nanoparticles by reacting gallic acid (10 μM) and $AgNO_3$ solution (3 mL, 74 μM) containing sodium hydroxide (740 μM) are presented in Figure 2.14A. A decrease in the gallic acid absorption with the

concomitant formation of a new band at 423 nm, corresponding to the plasmon absorption of Ag nanoparticles, was observed. Careful analysis of the absorption spectrum at the end of the reaction, in both cases, clearly indicates the presence of unreacted gallic acid. Similar absorption spectral changes were observed on addition of L-DOPA into $HAuCl_4/AgNO_3$ solutions (Figures 2.15,2.16). The evolution of absorption bands at 540 nm and 418 nm indicate the formation of the Au and Ag nanoparticles, respectively.

The evolution of plasmon absorption of Au/Ag nanoparticles in the presence of gallic acid/DOPA were monitored as a function of time and presented in Figures 2.13 to 2.16. The sigmoidal nature of the curves indicates that the formation of nanoparticle is autocatalytic in nature[47,61] which involves at least three stages namely nucleation, growth and saturation. In the initial nucleation period, gallic acid/L-DOPA reduces the metal cations (Au^{3+} ions to Au^0 and Ag^+ to Ag^0) resulting in the formation of small nuclei. In the growth stage, individual metal clusters agglomerates to form nanoparticles having intense plasmon absorption. The nanoparticles are stabilized through the electrostatic interaction between charged particles and the capping agent. The complete reduction of metal ions and the equilibration of the nanoparticles formed occur during the saturation period.

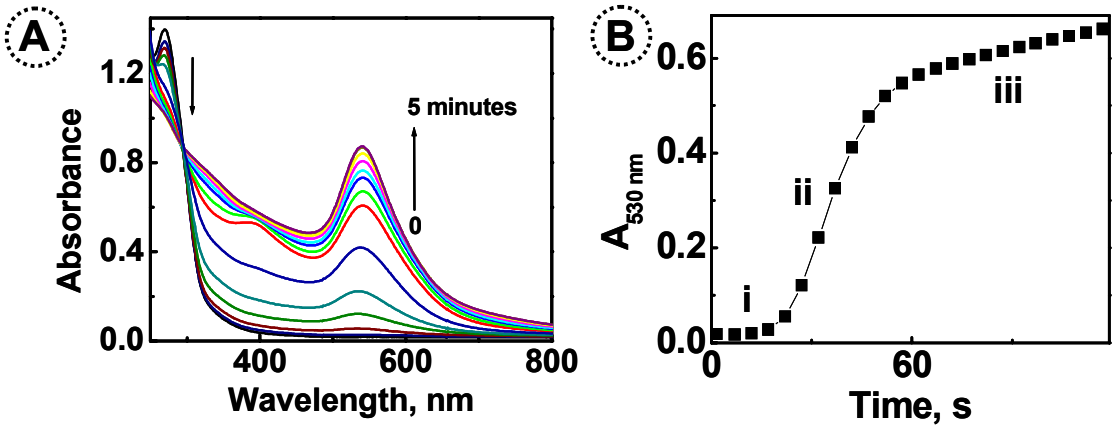

Figure 2.13. (A) Absorption spectral changes (0 to 5 min) illustrating the nanoparticle formation by mixing gallic acid (180 μM) and $HAuCl_4$ solution (3mL, 0.2 mM) at room temperature and (B) the absorption-time plot at 530 nm showing the evolution of the plasmon band.

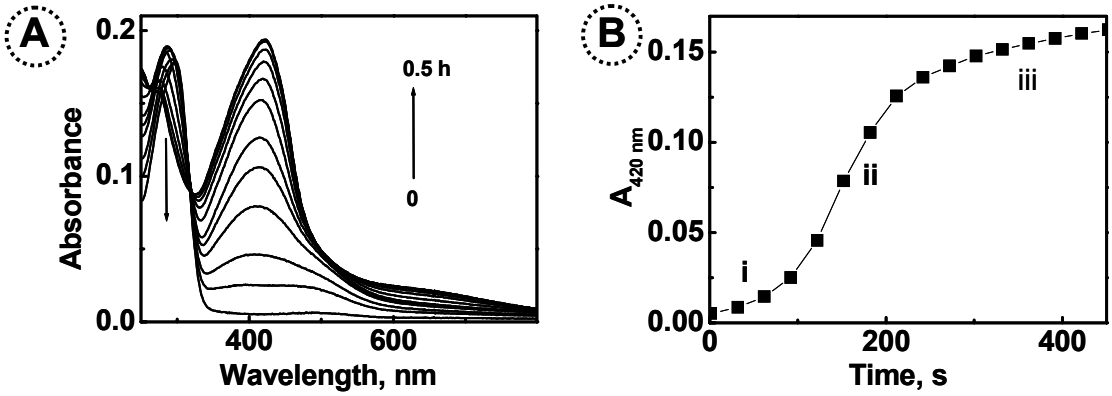

Figure 2.14. A) Absorption spectral changes (0-30 min) illustrating the nanoparticle formation by mixing gallic acid (180 μM) and $AgNO_3$ (3 mL, 74 μM) containing NaOH (740 μM) at room temperature and (B) the absorption-time plot at 420 nm showing the evolution of the plasmon band.

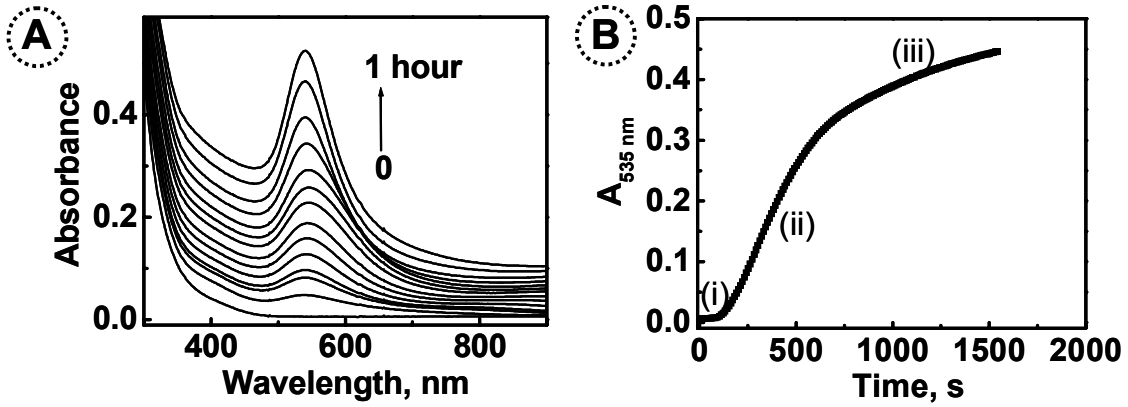

Figure 2.15. (A) Absorption spectral changes (0 to 1 h) illustrating the nanoparticle formation by mixing L-DOPA (80 μL,10 mM) to $HAuCl_4$ solution (30 mL, 0.2 mM) at room temperature and (B) the absorption-time plot at 535 nm showing the evolution of the plasmon band.

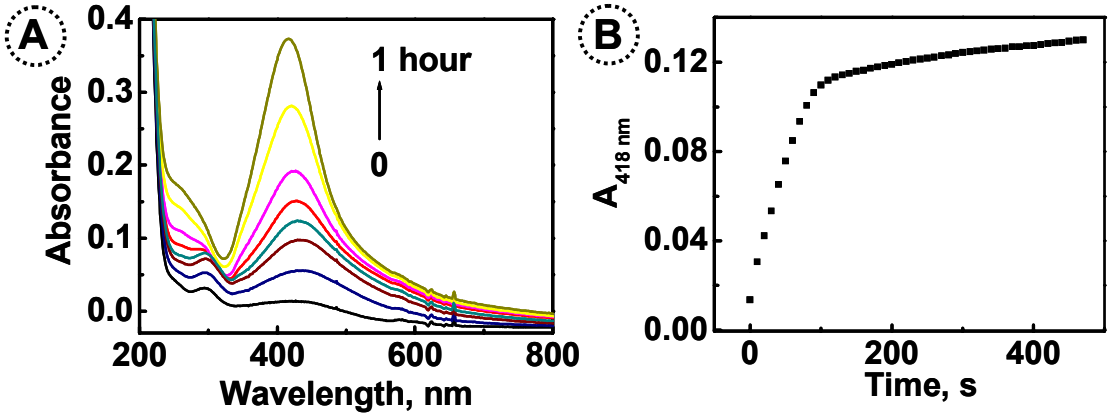

Figure 2.16. (A) Absorption spectral changes (0-30 min) illustrating the nanoparticle formation by mixing L-DOPA (10 μL,10 mM) to $AgNO_3$ (30 mL, 0.67 mM) containing sodium hydroxide (25 μL 165 mM) at room temperature and (B) the absorption-time plot at 415 nm showing the evolution of the plasmon band.

2.4.6. Mechanism of Formation of Nanoparticle

As mentioned earlier, gallic acid and L-DOPA possesses two types of functional groups; hydroxyl as well as carboxylic acid moieties. The role of these functional groups in the formation of nanoparticles was investigated by following the reactions of Au^{3+} ions with a series of phenolic acid derivatives (**2**-**10)** listed in Chart 2.1.

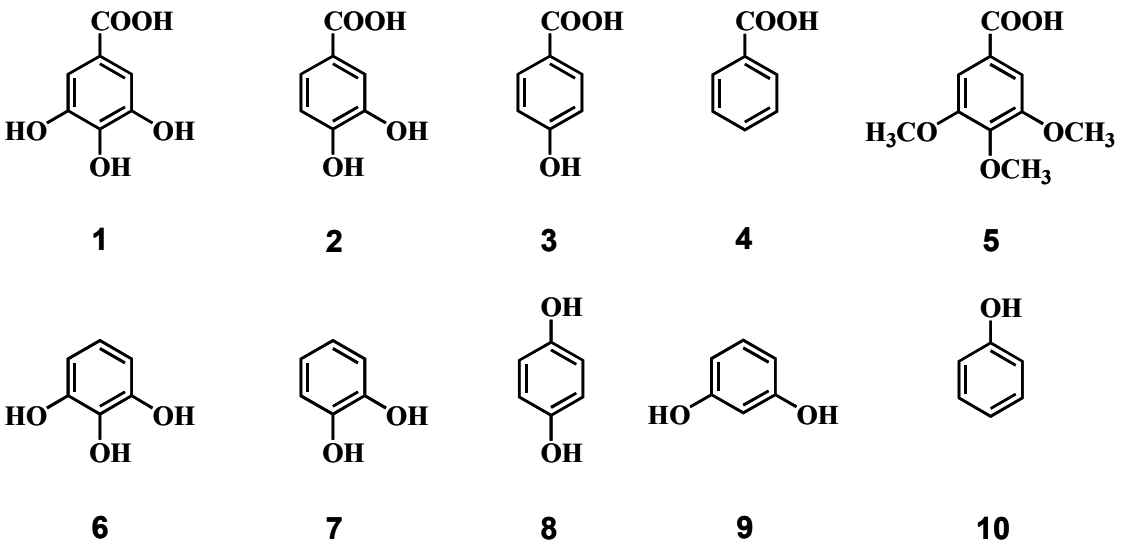

Chart 2.1. Molecular systems used for reducing Au^{3+} and Ag^{+} ions.

Nanoparticle formation was investigated by reacting $HAuCl_4$ with two series of compounds. The first series consists of benzoic acid derivatives (**1-5**) in which the substitutents on the aromatic rings are systematically varied and the second series (**6-10**) is based on phenolic derivatives. Stable nanoparticles were obtained on mixing $HAuCl_4$ with either gallic acid

(**1**) or protocatechuic acid (**2**). The formation of plasmon absorption is clearly visible in both the cases and absorption spectrum of gold nanoparticles obtained by using protocatechuic as the reductant is shown in Figure 2.17A. In contrast, no spectral change was observed upon mixing $HAuCl_4$ with either 4-hydroxybenzoic acid (**3**) or benzoic acid (**4**).

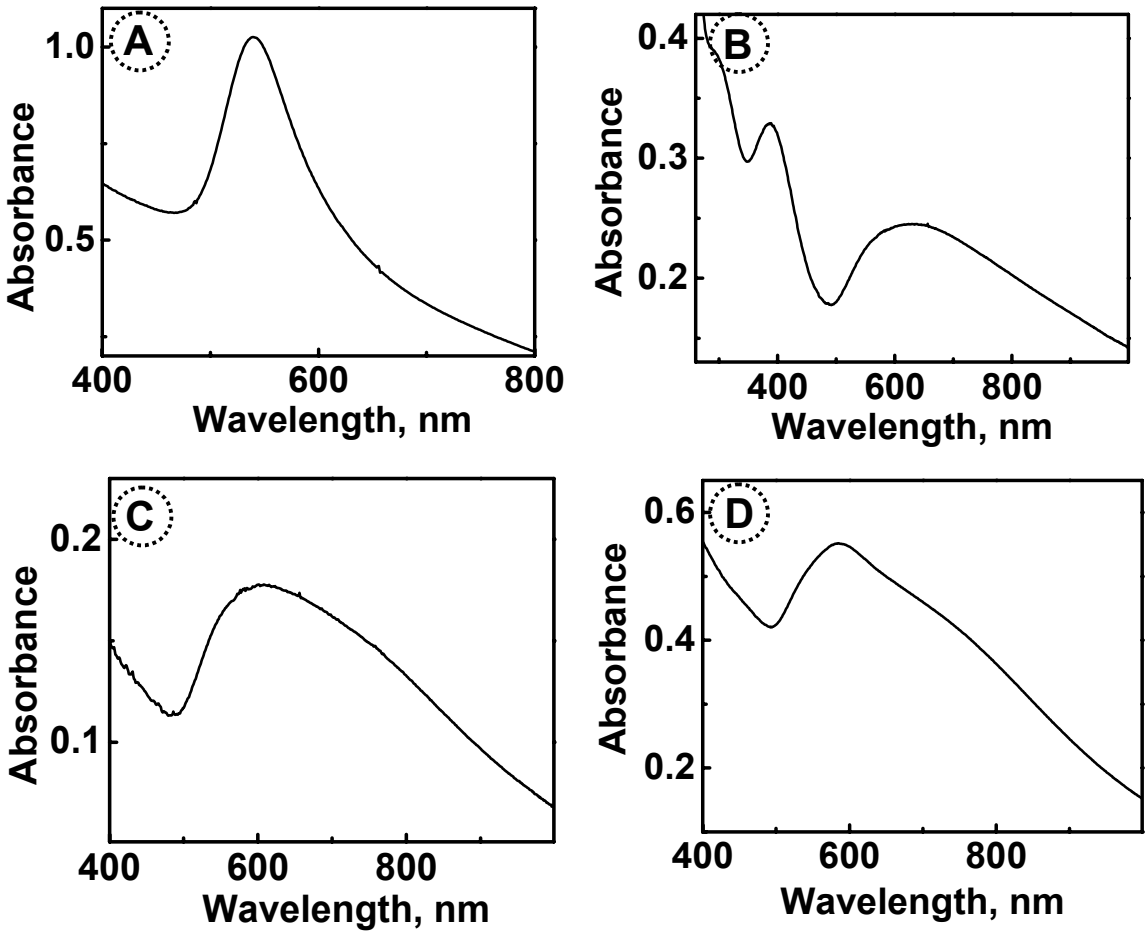

Figure 2.17. Absorption spectrum of nanoparticles prepared by mixing $HAuCl_4$ (0.2 mM) solution and various polyphenols(A) protocatechuic acid (180 μM) (B) catechol (180 μM) (C) pyrogallol (180 μM) and (D) hydroquinone (180 μM). The solutions B-D turned colorless after 5 min indicating the precipitation of nanoparticles.

These results clearly indicate that at least two hydroxyl groups are essential on benzoic acid for the formation of nanoparticles. Further the role of free hydroxyl groups was confirmed by protecting them as methoxy derivatives (**5**) and no spectral changes were observed.

The role of carboxylic acid group was confirmed by following the reaction between $HAuCl_4$ and a series of phenolic derivatives (**6**-**10**). The spectral changes corresponding to the formation of nanoparticles were observed on addition of $HAuCl_4$ to pyrogallol (**6**) or catechol (**7**). The color of the solution changed initially from green to red and further grayish blue, indicating the formation of large aggregates (Figures 2.17B,C). However, the color of solution faded due to precipitation, in both cases, and finally turned colorless. The major difference between compounds **6** and **7** (pyrogallol and catechol) in the second series and compounds **1** and **2** (gallic acid and protocatechuic acid) in the first series is that the former ones lack carboxylic functionality. These results clearly indicate that phenolic hydroxyl groups are involved in the reduction of Au/Ag cations and the carboxylic acid moiety in the stabilization of nanoparticles. Nanoparticle formation was further investigated by reacting $HAuCl_4$ with compounds **8**-**10** in the second series. The plasmon absorption indicating the formation of nanoparticles was not observed in the case of phenol (**10**) or resorcinol (**9**). In contrast, nanoparticle formation was observed

when the two hydroxyl groups are present in the *para* positions (for example hydroquinone, **8**) however they are unstable due to the absence of any stabilizer group. From these studies it is concluded that benzoic acid derivatives with at least two hydroxyl groups, either in the *ortho* or *para* positions can reduce Au^{3+}/Ag^{+} ions yielding stable nanoparticles. The hydroxy groups at the *ortho* or *para* postions undergo two-electron oxidation to the corresponding quinone and the nanoparticles thus formed are stabilized through the interaction of carboxylic acid group. A representative example illustrating the reduction process is shown in Scheme 2.1. A decrease in the pH of the medium from ~5.0 to ~3.0 was observed during the course of the reaction further supporting the release of the protons during the reduction process.

Further to prove this mechanism we have investigated the possibility of nanoparticle formation by mixing two molecules separately, having individual functions. Stable nanoparticles were obtained by reacting Au^{3+} ions with a mixture of pyrogallol (**6**) and *p*-hydroxybenzoic acid (in 3:1 molar equivalent) which was indicated by the appearance of sharp plasmon absorption (Figure 2.18).

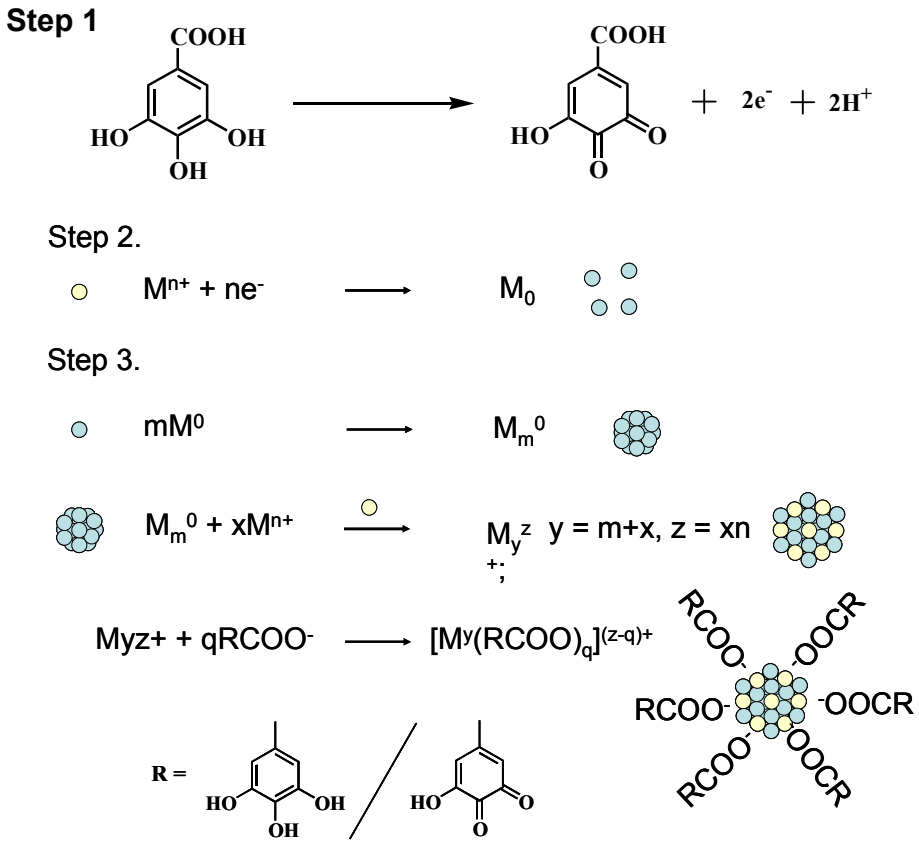

Scheme 2.1. Two-electron oxidation of gallic acid to the corresponding quinone form and the reduction of Au^{3+}/Ag^{+} ions resulting in the formation of nanoparticles.

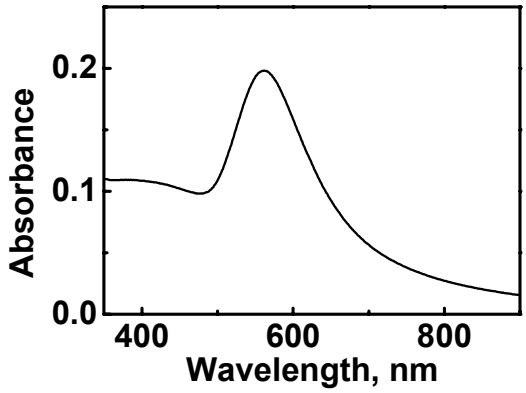

Figure 2.18. Absorption spectrum of gold nanoparticles prepared by adding a 1:3 mixture of 4-hydroxy benzoic acid (45 μM) and pyrogallol (135 μM) to $HAuCl_4$ solution (0.2 mM).

A similar mechanism for the reduction of Au^{3+} ions by L-DOPA has been reported by Willner and co-workers (scheme 2.2).[58,59] L-DOPA is well known to undergo decarboxylative oxidation to corresponding aminochrome or indole-5,6-quinone. This mechanism was supported by the fact that a decrease in pH of the medium was observed due to the release of protons during the course of reaction. Under acidic conditions both the aminochrome and indole quinones exists in the protonated form. In the present case the nanoparticles formed may be stabilized either through electrostatic interaction or through the coordination of nitrogen.

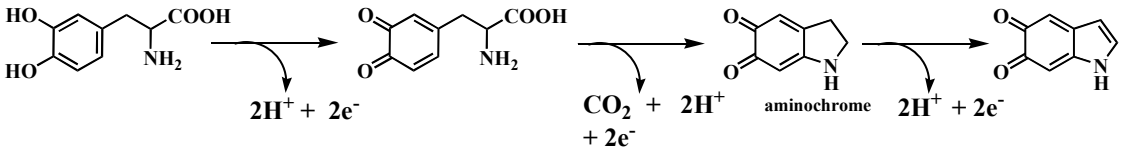

$$Au^{3+} + 3e^- \longrightarrow Au(0)$$

Scheme 2.2. Redox reactions illustrating the oxidation of L-DOPA and the reduction of Au^{3+} ions. (*adapted from reference 59*)

2.4.7. Characterization of Capping Agents on Au/Ag Nanoparticles

Attempts were made to characterize the chemical composition of the capping agents on the surface of nanoparticles by various spectroscopic methods. Absorption spectrum of gallic acid recorded before and after the addition of Au^{3+} ions is presented in Figure 2.19A. Gallic acid possesses two absorption bands in the UV region at 214 and 264 nm. Based on the deconvoluted absorption spectrum, it is clear that ~75 % of gallic acid

underwent oxidation during the course of nanoparticle formation. Similarly the FTIR spectrum of gallic acid and gold nanoparticles were recorded using ATR facility. In the FTIR spectrum (Figure 2.19B), C=O stretching frequency of gallic acid was observed at 1680 cm^{-1}.[54,62] After the reaction, a broad band was observed in the region of 1570-1730 cm^{-1} (with a maximum at 1630 cm^{-1} having a shoulder at 1690 cm^{-1}) attributed to the combined effect of the (i) interaction of carboxylate group on to the surface of nanoparticle and (ii) presence of *o*-quinone derivative arising from the oxidation of gallic acid. The binding of carboxylic moiety on to the nanoparticle surface was further indicated by the disappearance of the broad band in the region 2900-3100 cm^{-1}, which is the characteristic OH stretching vibration of carboxylic acid group.[63] In addition, the broad absorption band observed in the region 3100-3500 cm^{-1} is attributed to the presence of intermolecular hydrogen bonded network of phenolic groups on the surface of nanoparticle. The possibility for the formation of such a hydrogen bonded network between the gallic acid and its oxidized form, is much higher when these molecules are bound on to nanoparticle surface (due to high local concentration) compared to unbound ones in water. Further it is noticed that the peaks at 1540, 1446, 1333, 1256 cm^{-1} (corresponding to aromatic C=C and phenolic C-O vibrations) possess comparatively low intensity indicating that majority of the gallic acid are present in its oxidized form.

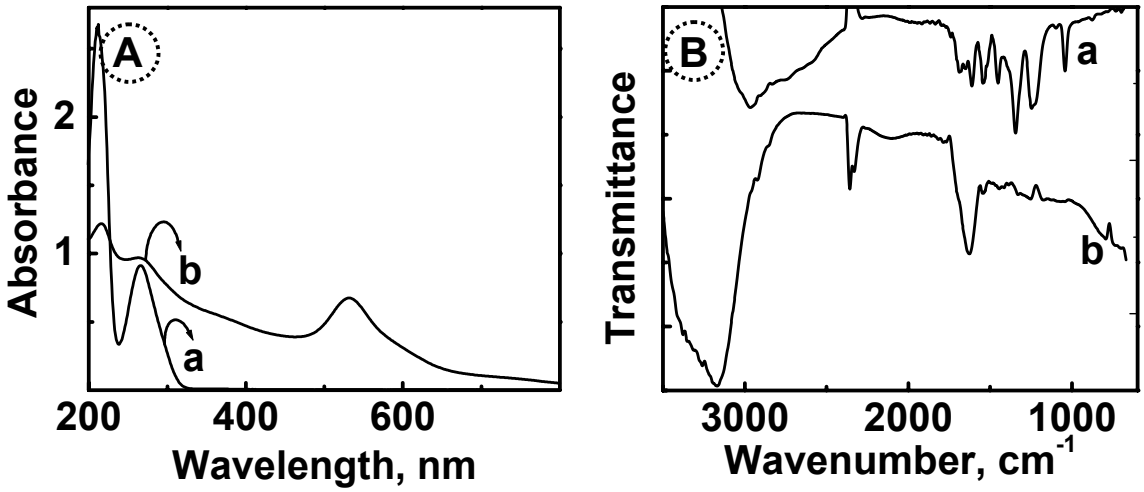

Figure 2.19. Absorption spectra of gallic acid (trace a) and gold nanoparticles (trace b). (B) FTIR spectra of gallic acid (trace a) and gold nanoparticles (trace b)

Attempts were made to characterize the capped nanoparticles using ^{1}H NMR studies, however the concentration of surface bound molecules is too low for any meaningful conclusions. Efforts to separate and purify the capped nanoparticles were also not successful due to their poor solubility in organic medium and metallization of centrifuged nanoparticles upon drying. It may be noted that the carboxylate stabilized nanoparticles (for example, citrate stabilized Au nanoparticle) usually have similar problems of isolation and characterization.[64] Based on the UV-Vis and IR studies, it is proposed that the Au/Ag nanoparticles are stabilized through electrostatic interaction of carboxylic group present in gallic acid and its oxidized form as represented in Figure 2.20.

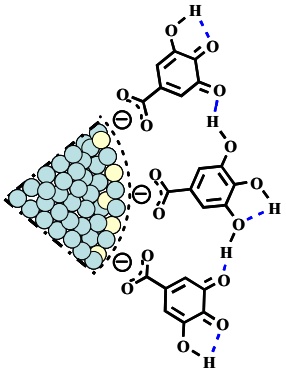

Figure 2.20. Representation of the electrostatic interaction of carboxylic groups on the nanoparticle surface and hydrogen bonding between the surface capped molecules.

2.5. Conclusion

A novel methodology for the synthesis of Au and Ag nanoparticles, in aqueous medium, was demonstrated by mixing the corresponding metal cations (Au^{3+} or Ag^{+}) and naturally occurring bifunctional molecules (gallic acid/DOPA) at room temperature. Detailed kinetic studies indicated that the formation of nanoparticles is autocatalytic in nature. Mechanistic aspects of the nanoparticle formation were elucidated by using a variety of model compounds and it is concluded that the hydroxyl group of gallic acid is involved in the reduction of Au^{3+}/Ag^{+} ions and the carboxylate group binds strongly on to the surface of nanoparticles. The observed stability of nanoparticles, for several months, is attributed to their high negative zeta potentials which prevent them from aggregation due to electrostatic repulsion. The characterization of nanoparticles using various techniques suggests that they are stabilized through the electrostatic interaction of

carboxylic acid groups on the nanoparticle surface and the hydrogen bonding between the surface capped molecules. These observations open a novel approach for the in situ synthesis of water soluble metal nanoparticles using a variety of biocompatible molecules which may have potential applications in biomedical field.

2.6. References

1. Kerker, M., *J. Colloid Interface Sci.* **1985,** *105*, 297-314.
2. Rao, C. N. R.; Kulkarni, G. U.; Thomas, P. J.; Edwards, P. P., *Chem. Soc. Rev.* **2000,** *29*, 27 - 35.
3. Link, S.; El-Sayed, M. A., *Int. Rev. Phys. Chem.* **2000,** *19*, 409-453.
4. Mishra, L. C., *Scientific Basis for Ayurvedic Therapies*. CRC Press: 2004; p 560.
5. Brown, C. L.; Bushell, G.; Whitehouse, M. W.; Agrawal, D. S.; Tupe, S. G.; Paknikar, K. M.; Tiekink, E. R. T., *Gold Bull.* **2007,** *40*, 245-250.
6. Daniel, M. C.; Astruc, D., *Chem. Rev.* **2004,** *104*, 293-346.
7. Barber, D. J.; Freestone, I. C., *Archaeometry* **1990,** *32*, 33-45.
8. Wagner, F. E.; Haslbeck, S.; Stievano, L.; Calogero, S.; Pankhurst, Q. A.; Martinek, K. P., *Nature* **2000,** *407*, 691-692.
9. Hunt, L. B., *Gold Bull.* **1976,** *4*, 134-139.
10. Faraday, M., *Philos. Trans.* **1857,** *147*, 145-181.
11. Evanoff Jr., D. D.; Chumanov, G., *ChemPhysChem* **2005,** *6*, 1221-1231.
12. Liz-Marzan, L. M., *Langmuir* **2006,** *22*, 32-41.
13. El-Sayed, I. H.; Huang, X.; El-Sayed, M. A., *Cancer Lett.* **2006,** *239*, 129-135.
14. Templeton, A. C.; Wuelfing, W. P.; Murray, R. W., *Acc. Chem. Res.* **2000,** *33*, 27-36.

15. Murphy, C. J.; Sau, T. K.; Gole, A. M.; Orendorff, C. J.; Gao, J.; Gou, L.; Hunyadi, S. E.; Li, T., *J. Phys. Chem. B* **2005,** *109*, 13857-13870.
16. Jain, P. K.; Huang, X.; El-Sayed, I. H.; El-Sayed, M. A., *Plasmonics* **2007,** *2*, 107-118.
17. Mie, G., *Ann. Phys.* **1908,** *25*, 377.
18. Eustis, S.; El-Sayed, M. A., *Chem. Soc. Rev.* **2006,** *35*, 209 - 217.
19. Kelly, K. L.; Coronado, E.; Zhao, L. L.; Schatz, G. C., *J. Phys. Chem. B* **2003,** *107*, 668-677.
20. Turkevich, J.; Stevenson, P. C.; Hillier, J., *Discuss. Faraday Soc.* **1951,** *11*, 55-75.
21. Henglein, A.; Giersig, M., *J. Phys. Chem. B* **1999,** *103*, 9533-9539.
22. Brust, M.; Walker, M.; Bethell, D.; Schiffrin, D. J.; Whyman, R., *J. Chem. Soc., Chem. Commun.* **1994**, 801 - 802.
23. Huang, Z.-Y.; Mills, G.; Hajek, B., *J. Phys. Chem.* **1993,** *97*, 11542-11550.
24. Wiley, B.; Sun, Y.; Xia, Y., *Langmuir* **2005,** *21*, 8077-8080.
25. Thomas, K. G.; Kamat, P. V., *Acc. Chem. Res.* **2003,** *36*, 888-898.
26. Kanaras, A. G.; Kamounah, F. S.; Schaumburg, K.; Kiely, C. J.; Brust, M., *Chem. Commun.* **2002**, 2294-2295.
27. Storhoff, J. J.; Elghanian, R.; Mucic, R. C.; Mirkin, C. A.; Letsinger, R. L., *J. Am. Chem. Soc.* **1998,** *120*, 1959-1964.
28. Lee, S.-J.; Han, M. S.; Mirkin, C. A., *Angew. Chem. Int. Ed.* **2007,** *46*, 4093-4096.
29. Lin, S.-Y.; Wu, S.-H.; Chen, C.-h., *Angew. Chem. Int. Ed.* **2006,** *45*, 4948-4951.
30. He, X.; Liu, H.; Li, Y.; Wang, S.; Li, Y.; Wang, N.; Xiao, J.; Xu, X.; Zhu, D., *Adv. Mater.* **2005,** *17*, 2811-2815.
31. Liu, J.; Lu, Y., *Chem. Mater.* **2004,** *16*, 3231-3238.
32. You, C.-C.; Chompoosor, A.; Rotello, V. M., *Nano Today* **2007,** *2*, 34-43.

33. You, C. C.; Verma, A.; Rotello, V. M., *Soft Matter* **2006,** *2*, 190-204.
34. Schultz, S.; Smith, D. R.; Mock, J. J.; Schultz, D. A., *Proc. Natl. Acd. Sci. U. S.A.* **2000,** *97*, 996–1001.
35. Ipe, B. I.; Mahima, S.; Thomas, K. G., *J. Am. Chem. Soc.* **2003,** *125*, 7174-7175.
36. Yoon, T. J.; Kim, J. S.; Kim, B. G.; Yu, K. N.; Cho, M. H.; Lee, J. K., *Angew. Chem. Int. Ed.* **2005,** *44*, 1068 –1071.
37. Michalet, X.; Pinaud, F. F.; Bentolila, L. A.; Tsay, J. M.; Doose, S.; Li, J. J.; Sundaresan, G.; Wu, A. M.; Gambhir, S. S.; Weiss, S., *Science* **2005,** *307*, 538-544.
38. Debouttière, P.-J.; Roux, S.; Vocanson, F.; Billotey, C.; Beuf, O.; Favre-Réguillon, A.; Lin, Y.; Pellet-Rostaing, S.; Lamartine, R.; Perriat, P.; Tillement, O., *Adv. Funct. Mater.* **2006,** *16*, 2330-2339.
39. Everts, M.; Saini, V.; Leddon, J. L.; Kok, R. J.; Stoff-Khalili, M.; Preuss, M. A.; Millican, C. L.; Perkins, G.; Brown, J. M.; Bagaria, H.; Nikles, D. E.; Johnson, D. T.; Zharov, V. P.; Curiel, D. T., *Nano Lett.* **2006,** *6*, 587-591.
40. O'Neal, D. P.; Hirsch, L. R.; Halas, N. J.; Payne, J. D.; West, J. L., *Cancer Lett.* **2004,** *209*, 171-176.
41. Willner, I.; Baron, R.; Willner, B., *Biosens. Bioelectron.* **2007,** *22*, 1841-1852.
42. Ghosh, S. K.; Pal, T., *Chem. Rev.* **2007,** *107*, 4797-4862.
43. Guo, S.; Wang, E., *Anal. Chim. Acta* **2007,** *598*, 181.
44. Stoeva, S. I.; Lee, J.-S., Thaxton, C. S. Mirkin, C. A., *Angew. Chem. Int. Ed.* **2006,** *45*, 3303-3306.
45. Raveendran, P.; Fu, J.; Wallen, S. L., *J. Am. Chem. Soc.* **2003,** *125*, 13940 -13941.
46. Sarma, T. B.; Chattopadhyay, A., *Langmuir* **2004,** *20*, 3520-3524.
47. Esumi, K.; Hosoya, T.; Suzuki, A.; Torigoe, K., *J. Colloid Interface Sci.* **2000,** *226*, 346-352.

48. Shankar, S. S.; Rai, A.; Ahmad, A.; Sastry, M., *Chem. Mater.* **2005,** *17*, 566-572.
49. Friedman, M.; Ju¨rgens, H. S., *J. Agric. Food Chem.* **2000,** *48*, 2101–2110.
50. Polewski, K.; Kniat, S.; Slawinska, D., *Curr. Top. Biophys.* **2002,** *26*, 217-227.
51. Fiuza, S. M.; Gomes, C.; Teixeira, L. J.; Cruz, M. T. G.; Cordeiro, M. N. D. S.; Milhazes, N.; Borgesa, F.; Marques, M. P. M., *Bioorg. Med. Chem.* **2004,** *12*, 3581–3589.
52. Polewski, K.; Kniat, S.; Slawinska, D., *Curr. Top. Biophys.* **2002,** *26*, 217-227.
53. Fink, D. W.; Stong, J. D., *Spectrochim. Acta.* **1982,** *38*, 1295-1298.
54. Ogata, T.; Nakano, Y., *Water Res.* **2005,** *39*, 4281–4286.
55. Kim, J.-S.; Morita, H.; Choi, G.-M.; Ohmid, T., *J. Electrochem. Soc.* **1999,** *146*, 4281-4289.
56. Mu, S., *Synth. Met.* **2003,** *139*, 287.
57. Pedrosa, R.; Soares-da-Silva, P., *Br J Pharmacol* **2002,** *137*, 1305.
58. Baron, R.; Zayats, M.; Willner, I., *Anal. Chem.* **2005,** *77*, 1566-1571.
59. Willner, I.; Baron, R.; Willner, B., *Adv. Mater.* **2006,** *18*, 1109-1120.
60. Wünsche, F.; Bund, A.; Plieth, W., *J Solid State Eletrochem.* **2004,** *8*, 209-213.
61. Sudeep, P. K.; Kamat, P. V., *Chem. Mater.* **2005,** *17*, 5404-5410.
62. Rouchon-Quillet, V.; Remazeilles, C.; Bernard, J.; Wattiaux, A.; Fournes, L., *Appl. Phys. A* **2004,** *79*, 389–392.
63. Giannakopoulos, E.; Christoforidis, K. C.; Tsipis, A.; Jerzykiewicz, M.; Deligiannakis, Y., *J. Phys. Chem. A* **2005,** *109*, 2223-2232.
64. Qi, Z. M.; Zhou, H. S.; Matsuda, N.; Honma, I.; Shimada, K.; Takatsu, A.; Kato, K., *J. Phys. Chem. B* **2004,** *108*, 7006-7011.

CHAPTER 3

Colorimetric Sensing of Metal Cations through Plasmon Coupling

3.1. Abstract

The metal binding properties of gallic acid reduced gold nanoparticles were investigated as a function of pH of the medium. At low pH values (< 4.2), precipitation of nanoparticles was observed on addition of various metal cations such as Ca^{2+}, Cu^{2+}, Cd^{2+}, Hg^{2+}, Mg^{2+}, Ni^{2+}, Zn^{2+}, Pb^{2+}. In the pH range of 4.5 to 5.2, additions of these metal cations, except Pb^{2+} cations, resulted in negligible changes to the plasmon absorption. Interestingly, addition of micromolar amounts of Pb^{2+} ions resulted in gradual red-shift in the absorption maximum. TEM, AFM, and FTIR studies indicate that the observed bathochromic shift in the plasmon absorption is due to interplasmon coupling arising from the supramolecular organization nanoparticles. The unique coordination behavior of Pb^{2+} ions (coordination number up to 12, flexible bond length and geometry) allows the formation of stable supramolecular complex resulting in the plasmon coupling and a visual color change. Due to the rigid coordination geometry, other metal cations interacts only with lesser number of ligands, leaving the nanoparticles isolated and

hence no spectral changes were observed under the experimental conditions. The ratiometric plots of the aggregated to the isolated forms indicate high sensitivity as well as selectivity of Au and Ag nanoparticles towards Pb^{2+} ions. One of the significant features of the present system is its ability to detect micromolar quantities (ppm level) of Pb^{2+} ions in the presence of other metal cations from water. Further, we have theoretically modeled the interaction between the newly synthesized nanoparticles and Pb^{2+} ions and various optimized geometries are evaluated. Based on the experimental and theoretical studies a tentative structure of the supramolecular complex leading to strong interparticle interaction has been provided.

3.2. Introduction

Controlled organization of metal nanoparticles, both in solution and surfaces, opens newer possibilities of designing nanoscale optoelectronic and sensor devices.[1-7] Among the various methodologies adopted, supramolecular approaches by exploiting weak noncovalent forces such as hydrogen bonding, coordination and electrostatic interactions are more attractive.[8-13] The ability of functionalized metal nanoparticles to undergo supramolecular organizations has been successfully employed for the colorimetric sensing of various analytes. These include the colorimetric detection of single DNA mismatches,[14-16] aminoacids,[17-19] metal cations[20-25] and monitoring kinase inhibitor activity.[26,27] The unique sensing abilities of

metal nanoparticle arise from the high optical cross-section of their surface plasmon, in the visible region, which is typically four to five orders of magnitude higher than that of conventional dyes[28-35] and plasmon coupling when they are brought in proximity.[17,30,36-40]

Theoretical methods have been developed recently for investigating electromagnetic interactions in arrays of spherical nanoparticles by varying their particle size, array spacing, array symmetry, and polarization direction.[17,38-40] The coupled plasmon absorption band of the noble metal nanoparticles undergo bathochromic shift, either on decreasing the distance between the interacting particles or on increasing the number of neighboring particles (Figure 3.1).[17,30,36-40] These aspects were experimentally verified by various groups and effectively utilized as “plasmon ruler” for measuring the distance in biological samples.[41-43]

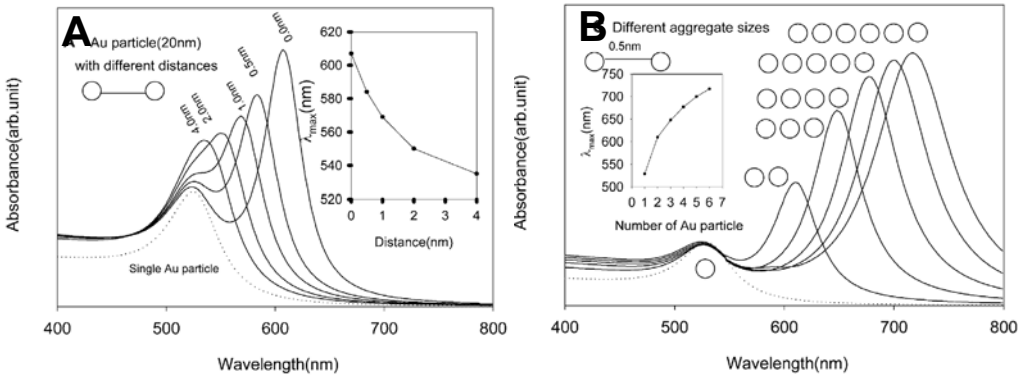

Figure 3.1. Electrodynamic modeling calculations for Au nanoparticles: (A) change of extinction spectra for 20 nm diameter particles with varying interparticle distances and (B) extinction spectra of ‘‘line aggregates’’ of varying number (d = 40 nm, s = 0.5 nm). (*adapted from reference 17*)

Due to the high extinction cross section of metal nanoparticles, the interplasmon coupling is usually accompanied by a visual color change (for example, red to blue for Au nanoparticles and yellow to red for Ag nanoparticles) which enables the potential use of metal nanoparticles in colorimetric sensing. The practical utility of interplasmon coupling, through a supramolecular approach, has been first demonstrated by Mirkin and coworkers. In this classic work, authors have used oligonucleotide functionalized gold nanoparticles for the one-pot colorimetric detection of single base-pair mismatches.[14,15]

The potential application of interplasmon coupling was further extended by many groups for the colorimetric sensing of various analytes such as metal cations,[20-25] nucleic acids[14-16] and amino acids.[17-19] In the presence of analytes, nanoparticles possess two distinct absorptions in its isolated and assembled state. The general strategy adopted for the colorimetric sensing is by monitoring either the formation or the dissociation of the supramolecular assembly in presence of analytes (Scheme 3.1). For example, the complexation of metal cations with the organic chelators bound to nanoparticles can effectively bring them very close to each other resulting in plasmon coupling. Spectral changes associated with such supramolecular organizations of functionalized noble metal nanoparticles have been utilized for the colorimetric detection of various metal cations such as Hg^{2+}, Pb^{2+},

Cd^{2+}, $Ca^{2+}$and Li^{+}.[20-25] For example, mercaptoundecanoic acid capped Au nanoparticles have been utilized as excellent colorimetric sensors for "Spectroscopically Silent Heavy" metal cations such as Pb^{2+}, Hg^{2+}, and Cd^{2+}.[24] Similarly, phenanthroline functionalized Au nanoparticles were used for the selective colorimetric detection for lithium ions.[23] A variation of this methodology for the selective colorimetric sensing of Pb^{2+} ions has been reported by utilizing Pb^{2+} ion specific DNAzyme which breaks the supramolecular network of DNA linked Au nanoparticles.[22,44,45]

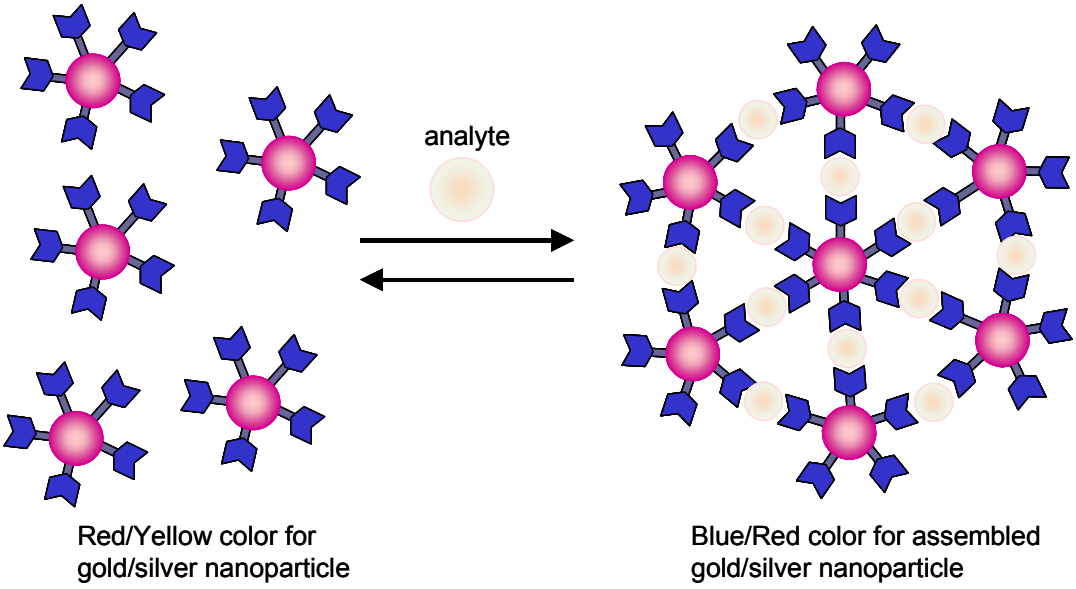

Scheme 3.1. Pictorial representation of the analyte induced formation or dissociation of supramolecular organization.

Both the hydroquinone and benzoquinone derivatives are well known to form supramolecular networks based on polymeric metal-organic coordination systems.[46,47] Polyphenolic compounds such as gallic acid,

catechol, pyrogallol forms complexes with heavy and transition metal cations.[46-53] For example, the organic matter present in the soil such as humic acid and fulvalic acid adsorb lead ions and other heavy metal cations.[53,54] This methodology has been widely used for the removal of toxic cations from water. It was also found that the incorporation of gallic acid to clay can increase its Pb^{2+} ion sorption ability.[55] Experimental and theoretical investigations on such metal complexes have revealed that the Pb^{2+} ions preferentially bind to the phenolic group as well as salicylic acid moiety.[55] It is reported in literature that the stability and solubility of phenolic metal complexes are highly dependant on the pH and ionic strength of the medium.[47,48,56]

In Chapter 2, we have reported the synthesis of Au and Ag nanoparticles in water by mixing the corresponding metal cations (Au^{3+} or Ag^{+}) with gallic acid/L-DOPA. The newly synthesized nanoparticles possess outer organic shell having both the bifunctional molecule (gallic acid/ L-DOPA) and its oxidized form. The ligand functionalized nanoparticles can be brought close to each other through complexation with metal cations. Formation of such supramolecular complexes results in strong plasmon coupling and in this chapter we investigate the metal binding properties of the newly synthesized metal nanoparticles (**Au-GA** and **Ag-GA**) by adopting this strategy.

3.3. Experimental Section

Lead(II) acetate, mercury(II) chloride, nickel(II) acetate, magnesium(II) sulphate, copper(II) sulphate, zinc(II) sulphate, calcium(II) chloride, cadmium(II) bromide, iron(III) chloride, EDTA, sodium hydroxide, and hydrochloric acid were obtained from sd fine chemicals (all analar grade) and used as received. Stock solutions of all the reagents were prepared in doubly distilled water. For adjusting the pH, use of buffer solutions was intentionally excluded to avoid complications arising from the interaction of nanoparticle surface and the buffering material. Hence in the present study, the pH of the medium was varied by either the addition of sodium hydroxide or hydrochloric acid. Metal binding studies were carried out by adding micromolar quantities of metal cations to Au/Ag nanoparticle solution (3 mL) kept at the desired pH and the corresponding absorption spectral changes were monitored. IR spectral changes in aqueous medium were carried out on an infrared spectrophotometer (IRPrestige-21, SHIMADZU) using ATR technique and the electronic spectra were recorded on a UV-Vis-NIR scanning spectrophotometer (Shimadzu Model UV-3101). Samples for TEM studies were prepared by drop casting Au/Ag nanoparticle solution on to a formvar coated Cu grid. The solvent was allowed to evaporate and the samples were imaged on a Hitachi H600 transmission electron microscope (operating at an acceleration voltage of 75 kV). AFM measurements were carried out by drop

casting the solution on a freshly cleaved mica surface. Samples were imaged, under ambient conditions, on a multimode scanning probe microscope (Nanoscope IV controller, Digital Instruments, Veeco) using the tapping mode technique. pH of the solution was measured using Elico LI 612 pH analyser. The zeta potentials of nanoparticles were measured using Malvern Zetasizer 3000HSA.

3.4. Results and Discussion

3.4.1. Metal Binding Studies with Au-GA Nanoparticles

The interaction of various metal cations with **Au-GA** nanoparticles were investigated by titrating micromolar quantities of metal cations (Pb^{2+}, Hg^{2+}, Ni^{2+}, Mg^{2+}, Cu^{2+}, Zn^{2+}, Ca^{2+}, Cd^{2+} and Fe^{3+}) and the corresponding absorption spectral changes were recorded. At a lower pH of 3.0, addition of micromolar quantities of various metal cations such as Pb^{2+} , Fe^{3+}, Cu^{2+} and Ca^{2+} ions to **Au-GA** nanoparticle solution resulted in their precipitation. Corresponding absorption spectral changes are presented in Figure 3.2. A decrease in the intensity of plasmon absorption at 530 nm, with increase in base line is indicative of precipitation and the solution finally turned colorless. The first ionization constant of gallic acid is 4.2;[57,58] the carboxylic acid group in the capping agents exists in its neutral form below this pH, which reduces the electrostatic interaction with the nanoparticle surface. Thus in solutions having pH < 4.2, surface coverage of capping ligands may be low. Either an

increase in ionic strength of the medium or the complexation of the surface bound molecules results in the formation of larger agglomerates of nanoparticles which eventually precipitate out of the solution.

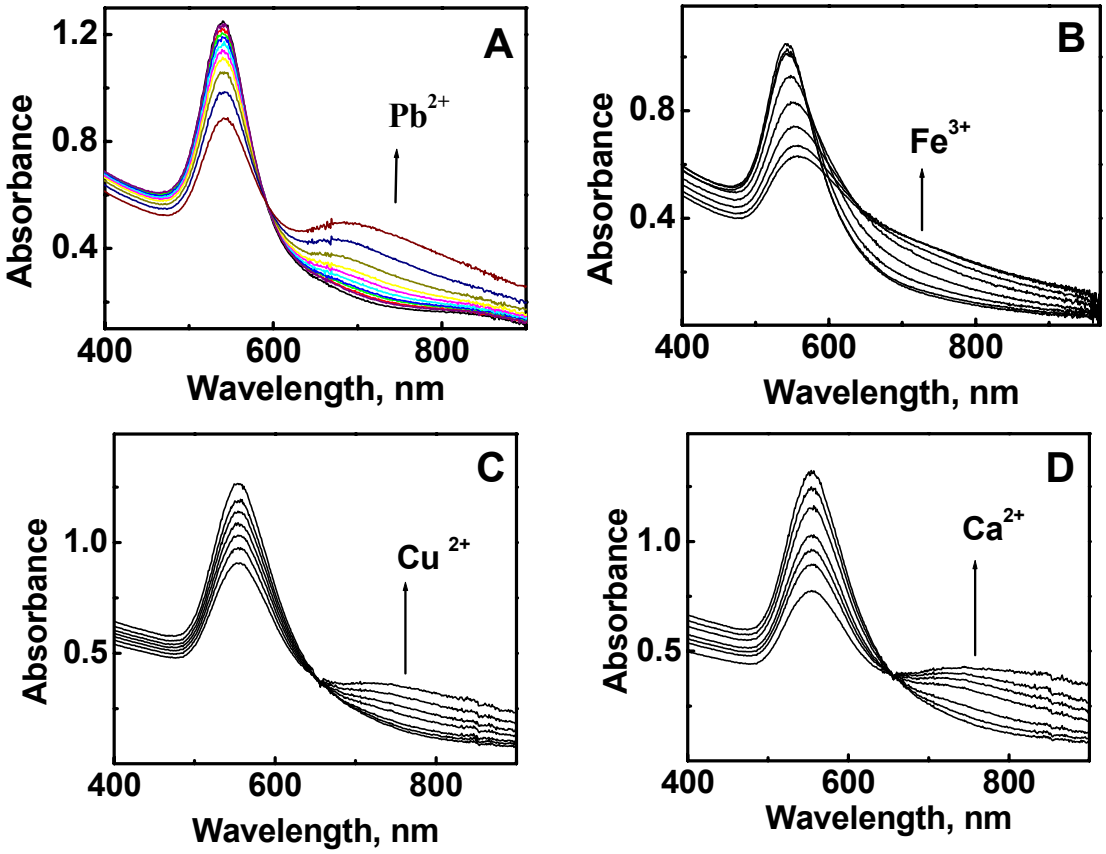

Figure 3.2. Absorption spectral changes of **Au-GA** nanoparticles in water (pH 3.0) on addition of (A) Pb^{2+} (B) Fe^{3+} (C) Cu^{2+} (D) Ca^{2+}; $[M^{n+}]$ = 0-100 μM.

Interestingly, when the pH of the **Au-GA** nanoparticle solution was raised above 4.2 (for e.g., pH 4.5) addition of Hg^{2+}, Cd^{2+}, Fe^{3+}, Cu^{2+}, Ni^{2+}, Zn^{2+}, Ca^{2+} and Mg^{2+} ions showed negligible spectral changes (Figure 3.3). At this pH, carboxylic moiety of the capping agent exists in its ionized form which enhances the electrostatic interaction with the nanoparticle surface. Under

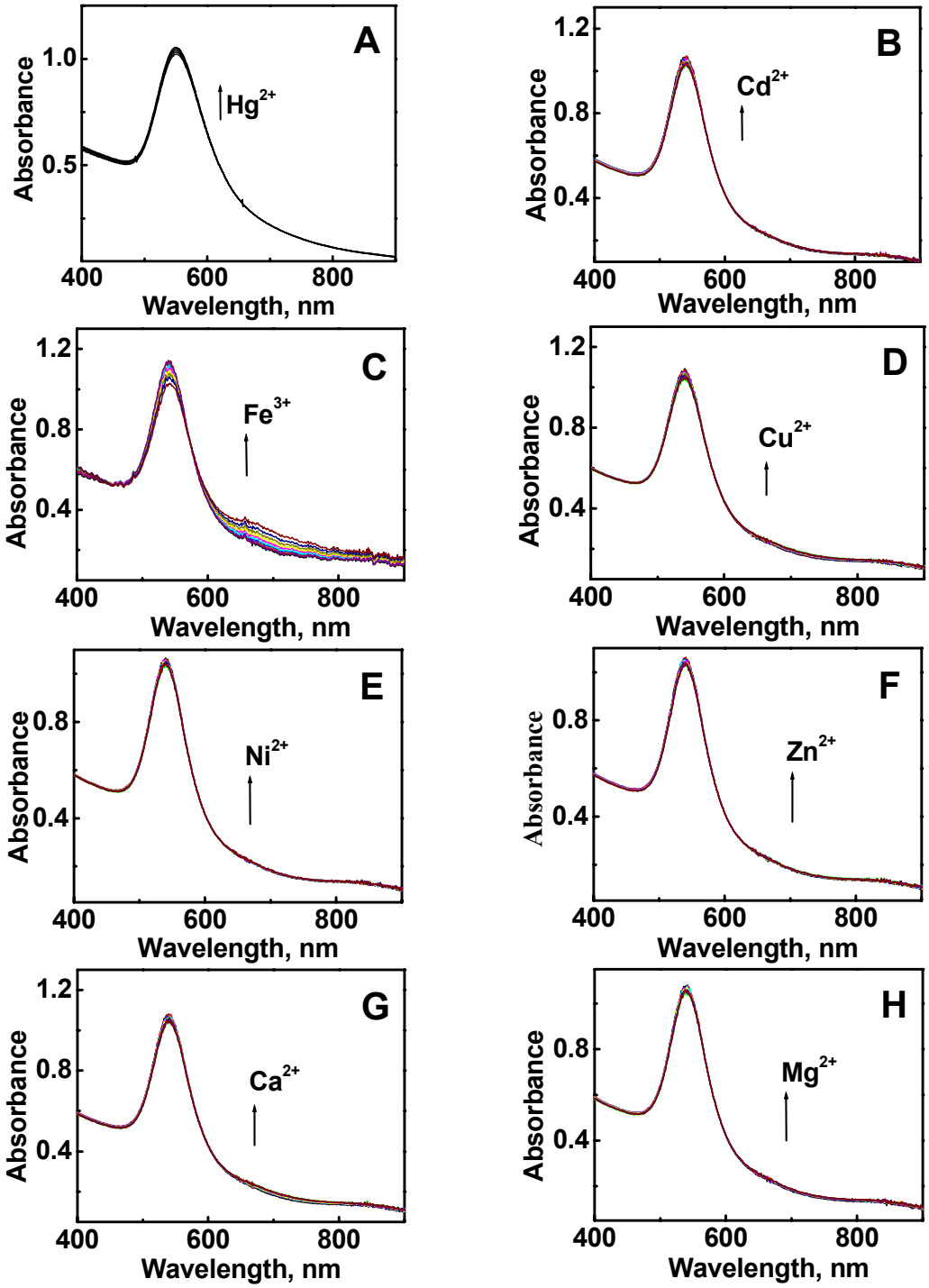

Figure 3.3. Absorption spectral changes of **Au-GA** in presence of varying concentrations of metal cations in water (A) Hg^{2+} (B) Cd^{2+} (C) Fe^{3+} (D) Cu^{2+} (E) Ni^{2+} (F) Zn^{2+} (G) Ca^{2+} (F) Mg^{2+}; $[M^{n+}]$ = 0-100 μM.

this condition, **Au-GA** nanoparticles are stable in water and remain isolated. In contrast, addition of micromolar amounts of Pb^{2+} ions resulted in a gradual bathochromic shift in the plasmon absorption band and the spectral changes are presented in Figure 3.4. Furthermore, the solution underwent a visual color change from red to blue in presence of Pb^{2+} ions (Figure 3.4B) indicating potential use of this system for naked eye detection. The bathochromic shift in plasmon absorption band and the accompanied visual color change is attributed to the assembling of **Au-GA** nanoparticles in presence of Pb^{2+} ions, which was further confirmed through various microscopic investigations (AFM/TEM).

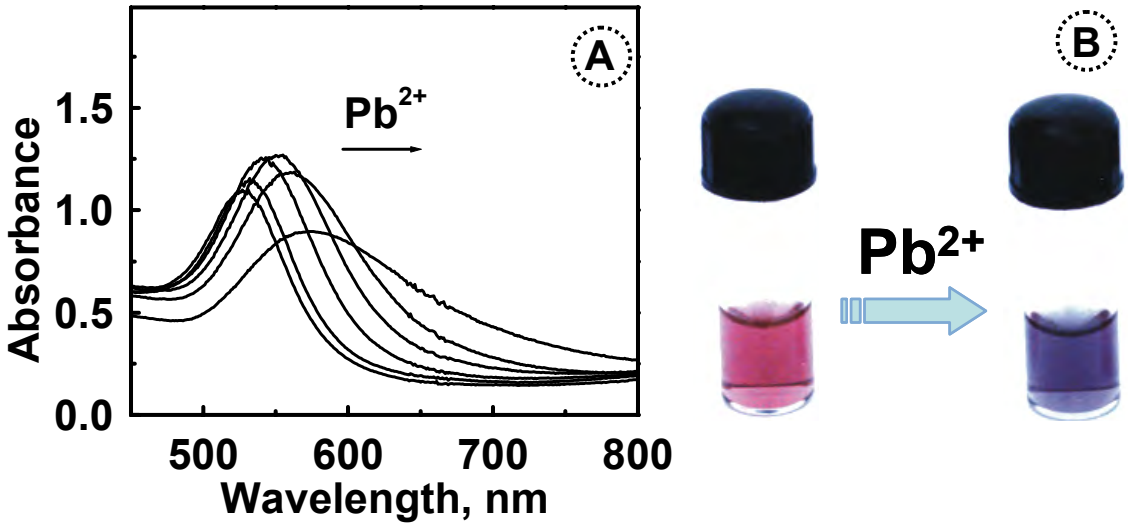

Figure 3.4. (A) Absorption spectral changes of Au nanoparticles in water on addition of Pb^{2+} ions; [Pb^{2+}] = 0-150 μM and (B) color photograph of nanoparticle solution in the absence and presence of Pb^{2+} ions (150 μM).

AFM and TEM investigations: Detailed AFM and TEM studies were carried out to investigate the metal ion induced assembling of **Au-GA** nanoparticles. At very low concentrations of Pb^{2+} ions (~8 μM), a small bathochromic shift in the plasmon absorption was observed (Figure 3.4). The **Au-GA** nanoparticles containing Pb^{2+} ions (~8 μM) were imaged by drop casting the solution on to a freshly cleaved mica surface. The corresponding tapping mode AFM images showed the presence of isolated **Au-GA** nanoparticles along with smaller aggregates of the size range 200-300 nm (Figure 3.5A). The plasmon absorption of **Au-GA** nanoparticles underwent a bathochromic shift on further increase in the concentration of Pb^{2+} ions (Figure 3.4) and the corresponding AFM images showed the presence of larger aggregates (Figure 3.5B-E). Interestingly the size of the nanoparticle aggregates reaches the order of micrometer at higher concentrations of Pb^{2+} ions (~150 μM). Under these conditions the plasmon absorption band of **Au-GA** nanoparticle assembly underwent a large red shift (> 30 nm) and broadening resulting in a visual color change from wine red to blue (Figure 3.4B).

TEM images of the **Au-GA** nanoparticles were recorded both in the presence and absence of Pb^{2+} ions, under identical conditions. Nanoparticles remain isolated and randomly distributed in the absence of Pb^{2+} ions (Figure 3.6A). In contrast, large aggregates of **Au-GA** nanoparticles were observed

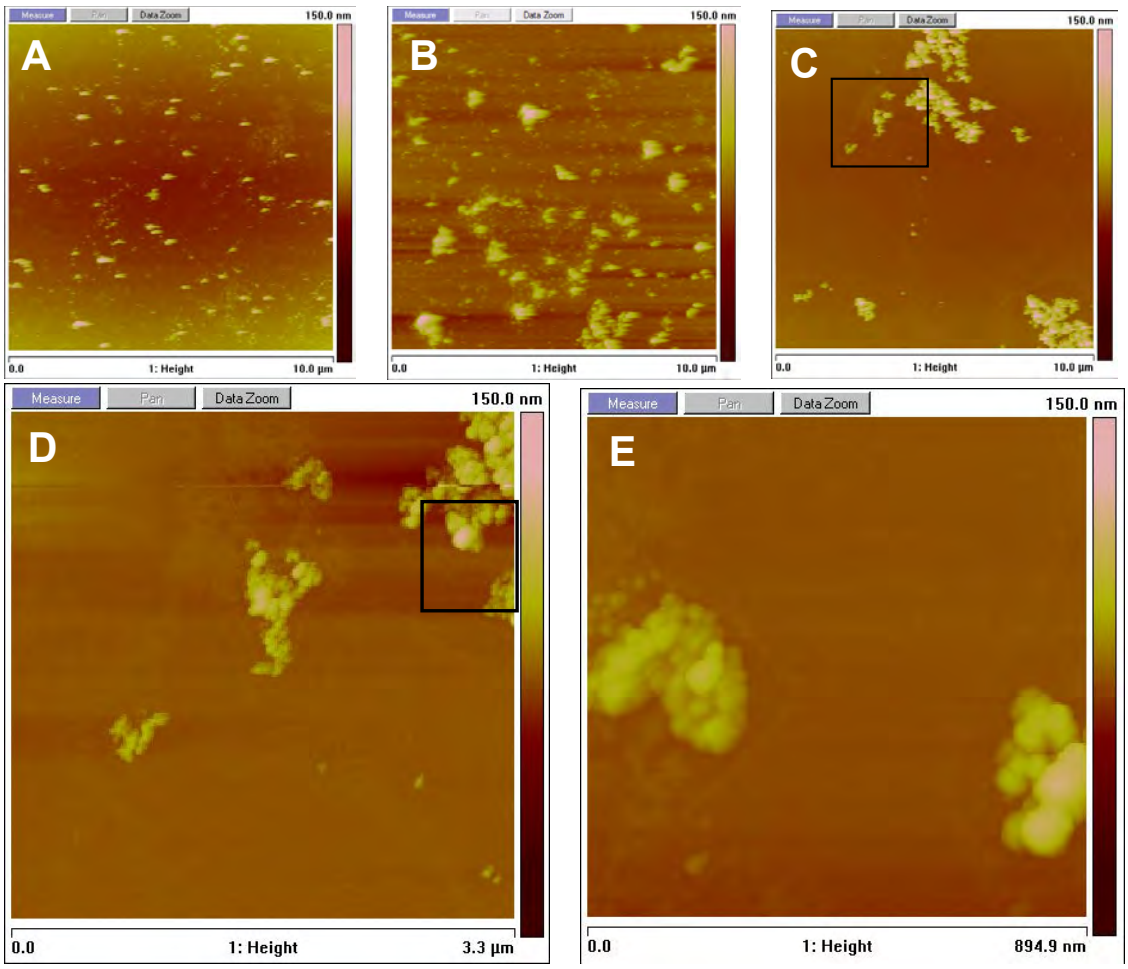

Figure 3.5. Tapping mode AFM images of **Au-GA** nanoparticles in presence of varying concentration of Pb^{2+} ions; [Pb^{2+}] = (A) 8, (B) 16 and (C) 150 µM. Real time zoomed images of the area with in the black square of C and D respectively are shown as (D) and (E). Samples for AFM studies were prepared by drop casting the corresponding solutions on to freshly cleaved mica surface.

at specific locations on the TEM grid in presence of Pb^{2+} ions (Figure 3.6B). Both the AFM and TEM studies clearly indicate that Pb^{2+} ions induces aggregation of nanoparticles which results in a bathochromic shift in the plasmon absorption and a visual color change from red to blue.

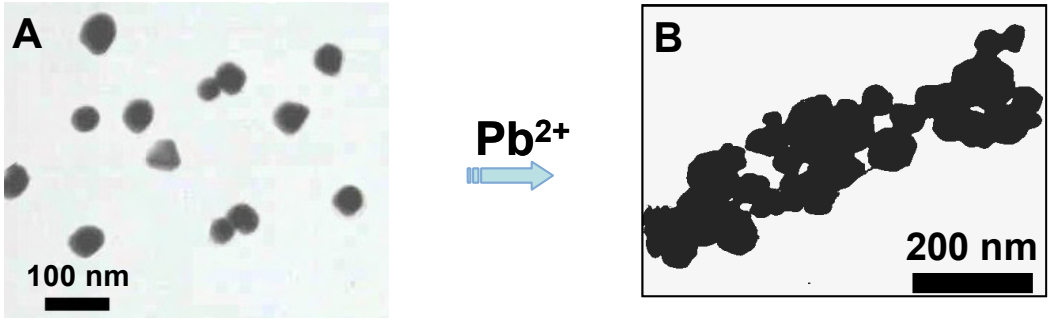

Figure 3.6. TEM images of **Au-GA** nanoparticles in the (A) absence and (B) presence of Pb^{2+} ions (100 μM). Samples for TEM were prepared by drop casting the corresponding solutions on to a formvar coated copper grid.

Supramolecular assembly arises through the interaction of a Pb^{2+} ion with the surface bound ligands present on two or more nanoparticles. Since the nanoparticles are isotropic in nature these interactions can lead to the formation of three dimensional aggregates. The close proximity of the nanoparticles induces coupling of their plasmon oscillation (interplasmon coupling) resulting in a bathochromic shift in the absorption band. The role of surface bound ligands on the aggregate formation was further confirmed by checking the reversibility of the metal binding events by adding a stronger chelating agent and through FTIR investigations.

Reversibility of the aggregation: To check the reversibility of aggregation, micromolar amounts of a stronger chelating agent, namely EDTA, was added to **Au-GA** nanoparticle (OD at 527 nm = 1.1) solution containing Pb^{2+} ions (80 μM). The corresponding absorption spectral changes are shown in

Figure 3.7. The plasmon absorption band of **Au-GA** nanoparticles at 528 nm (curve 'a' in Figure 3.7) underwent a bathochromic shift of ~ 30 nm in presence of 80 μM of Pb^{2+} ions (curve 'b') due to aggregate formation. The nanoparticle aggregates are found to be stable under this experimental condition and a reversal of the plasmon absorption to the initial value (~528 nm) was observed upon addition of 95 μM of EDTA (curve 'c'). Being a stronger chelating agent, EDTA extracts the Pb^{2+} ions from the supramolecularly organized nanoparticle aggregates, leaving the nanoparticles isolated and restoring the plasmon absorption of isolated nanoparticles. A complete reversal of the plasmon absorption band on addition of EDTA confirms the existence of the complex between the Pb^{2+} ions with the surface bound ligands of Au nanoparticles.

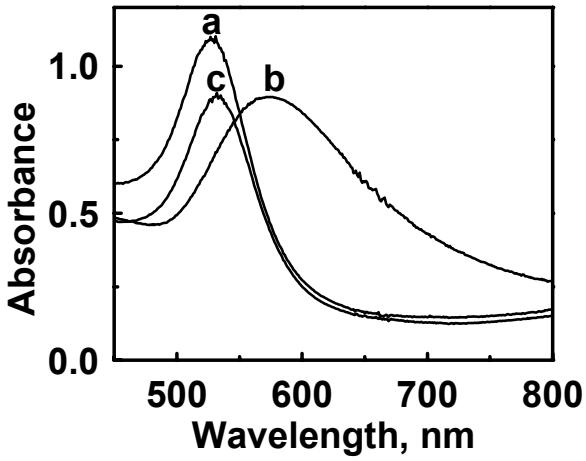

Figure 3.7. Absorption spectral changes of Au nanoparticles in water at pH 4.5 (trace 'a'), on addition of 80 μM Pb^{2+} (trace 'b') and after the addition of 95 μM EDTA (trace 'c').

FTIR studies: Further to confirm the interaction of metal cations with surface bound ligands, FTIR studies were performed using ATR facility. A comparison of FTIR spectra of **Au-GA** nanoparticles in the absence and presence of Pb^{2+} ions is presented in Figure 3.8. The broad IR band observed in the region 3100-3400 cm^{-1}, in the case of isolated nanoparticles, is attributed to the strong intermolecular hydrogen bonding between the hydroxyl groups on the surface of nanoparticles.[59,60] Interestingly, this broad band turned sharp on addition of Pb^{2+} ions indicating the disruption of hydrogen-bonded network between the hydroxyl groups due to the complexation with Pb^{2+} ions. From these results, it can be attributed that the Pb^{2+} ions predominantly interact through the phenolic group on the surface bound ligands. The C=O stretching frequency at 1600-1640 cm^{-1} underwent a

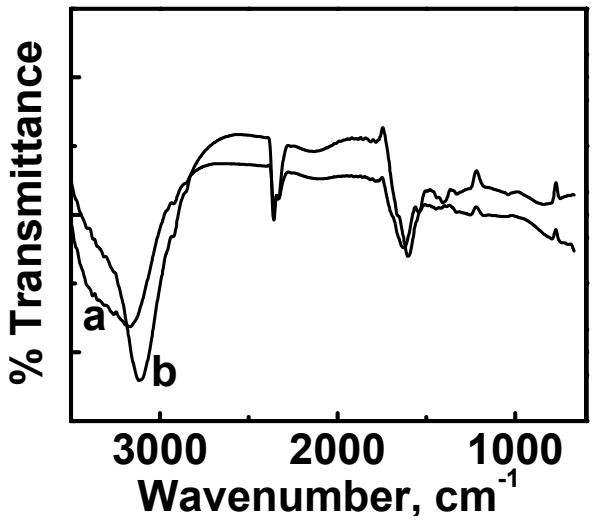

Figure 3.8. FTIR spectra **of Au-GA** nanoparticles before (trace 'a') and after the addition of 75 μM Pb^{2+} (trace 'b') (FTIR spectrum were recorded using ATR facility).

small hypsochromic shift upon complexation with Pb^{2+} ions, may be due to the changes in the electronic distribution of the carbonyl group. These results clearly indicate that complexation of Pb^{2+} ions with the surface bound ligands results in the supramolecular organization **Au-GA** nanoparticles in solution which induces the interplasmon coupling.

Sensitivity and selectivity: Lead ranks second in the list of toxic substances and often encountered by many due to its wide distribution in environment.[61-64] The toxicity of lead in humans mainly originate from its destructive mimicking action by occupying the calcium binding sites on numerous calcium dependant proteins in cells (for example, calmodulin and enzyme protein kinase C), thus impairing physiological functions.[62,63] Lead is also a potent central neurotoxin and gets accumulated in bones and kidneys resulting in their damage.[64] The usual techniques adopted for the detection of lead ions involve spectrophotometric methods using chromoionophores and ICP analysis.[65-75] Even though several chromoionophores are available for the detection of lead ions, most of them are soluble in organic solvents which limit their day to day applications (for example, detection of lead ions in drinking water). Ideally, procedures for selective 'naked-eye' detection of an analyte from aqueous medium which do not require any specialized instrumentation are desirable.[15,18,21,22,24,45,71-77] Among various optical reporting methodologies enlisted in the literature for the detection of lead ions,

sensing based on the plasmon absorption of Au and Ag nanoparticles is rather promising.[21,22,24,45,76] The high extinction coefficient of metal nanoparticles enables the naked-eye detection of the analyte even in ppm level. The present system enables the selective detection of Pb^{2+} ions from aqueous medium at moderate pH values; for example, Pb^{2+} ions induce a bathochromic shift at pH 4.5 due to plasmon coupling where as other metal cations has negligible effects (*vide supra).* A color photograph of the nanoparticle solution in presence of different metal cations (150 μM) is presented in Figure 3.9 and the color changes from red to blue in presence of Pb^{2+} ions. Thus experimental procedure reported here can be utilized for the selective naked eye detection of Pb^{2+} ions from aqueous medium.

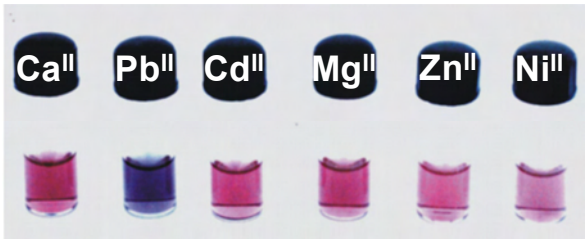

Figure 3.9. Color photographs of the Au nanoparticle solution in presence of different metal ions ([M^{2+}] = 150 μM).

The plasmon absorption of metal nanoparticle is highly dependant on the dielectric environment and hence it is essential to have a calibration graph for any practical applications. The sensitivity and selectivity of nanoparticles towards various metal cations at pH 4.5 were quantified by plotting the ratio of

the absorbance of aggregated form at 575 nm to that of the monomer form at 530 nm (A_{575}/A_{530}) as a function of the metal ion concentration. The ratiometric plots are presented in Figure 3.10A and the ratio increases with concentration for Pb^{2+} ions whereas it remains constant for other metal cations. These results clearly indicate that the Pb^{2+} ions can selectively bind with the ligands on the surface of metal nanoparticles leading to plasmon coupling. More interestingly, the plot of the bathochromic shift in the plasmon absorption maximum ($\Delta\lambda$) of Au nanoparticles against the concentration of Pb^{2+} ions showed a linear relationship (Figure 3.10B) indicating the versatility of this methodology for the quantitative determination of toxic metal cations from aqueous medium.

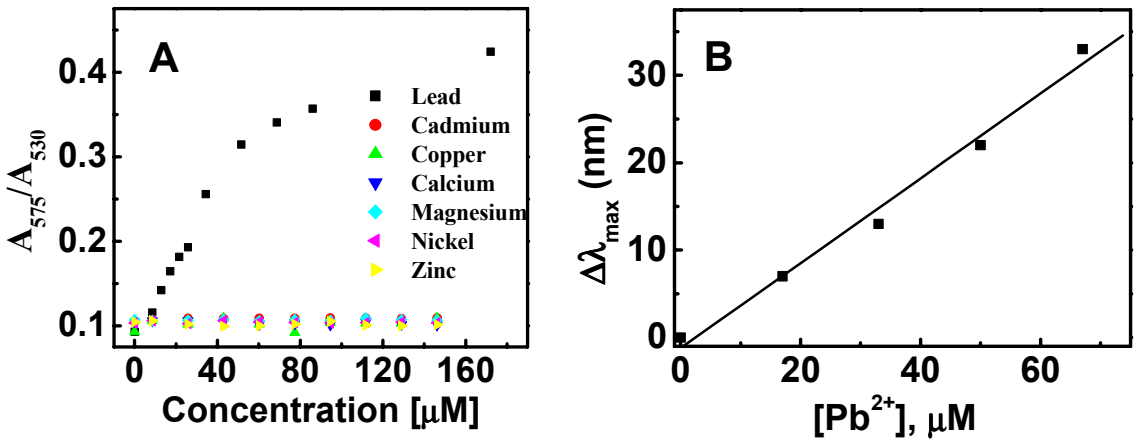

Figure 3.10. Plot illustrating (A) the changes in ratio of the absorbances of the aggregated to the isolated form of **Au-GA** nanoparticles (A_{575}/A_{530}) on addition of various metal cations and (B) shift in the plasmon absorption band ($\Delta\lambda$) as a function of Pb^{2+} ion concentration for nanoparticles.

Tuning the selectivity: Gallic acid and related molecules exist in various ionized forms depending on the pH of the medium. The complexation ability of Pb^{2+} cations is dependent on the nature of the surface bound molecule and the selectivity of metal ion sensing was further investigated by varying the pH of the medium. At very low pH values (< 4.2), the addition of micromolar amounts of various metal cations (i.e., Pb^{2+}, Fe^{3+}, and Cu^{2+}) resulted in the precipitation of **Au-GA** nanoparticles whereas in the pH ranges of 4.5-5.2, **Au-GA** nanoparticle system can selectively detect Pb^{2+} ions. These aspects were discussed in earlier section *(vide supra)*. At pH 5.5, both Pb^{2+} and Fe^{3+} ions induce a bathochromic shift in the plasmon absorption band (Figure 3.11A), whereas the spectral features remain unaffected for other metal cations. Apart from Pb^{2+} and Fe^{3+} ions, Cu^{2+} also induces a bathochromic shift in the plasmon absorption band when the pH of the solution is raised to

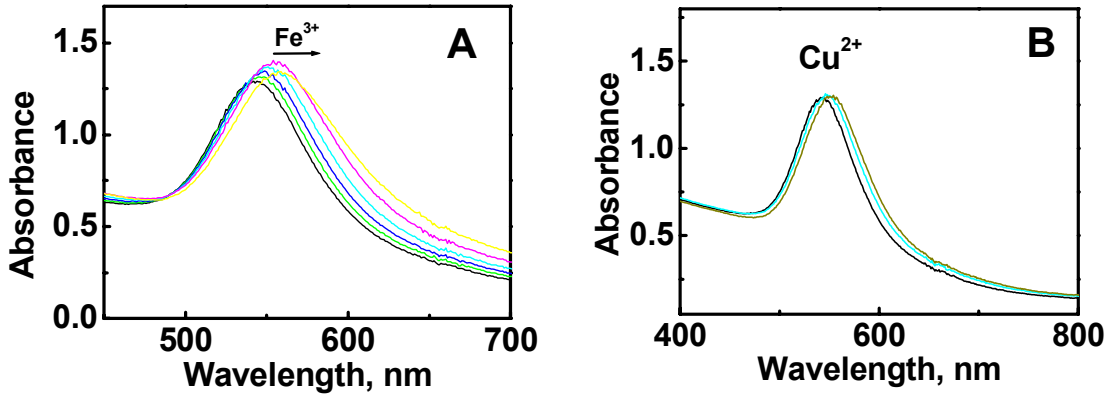

Figure 3.11. Absorption spectral changes of **Au-GA** nanoparticles in water in presence of varying concentrations of (A) Fe^{3+} ions at pH 5.5 (B) Cu^{2+} ions at pH 6.0 ($[M^{n+}]$ = 0-100 μM).

6.0 (Figure 3.11B). Thus it is clear that the metal cation induced interparticle interactions in the newly synthesized **Au-GA** nanoparticles are strongly influenced by the pH of the medium.

Role of zeta potential: To have a better understanding on the pH dependant selectivity, zeta potentials (ζ) of **Au-GA** nanoparticles were measured as a function of the pH of the medium. The results presented in Table 3.1 clearly indicate that the nanoparticles possess a negative surface charge which varies as a function of the pH of the medium. It is well established that the colloids having ζ value higher than +30 mV or lower than -30 mV are generally stable due to the strong electrostatic repulsion between the particles which prevent them from aggregation.[21,78] At a pH value of ~3.0, nanoparticles possess a low ζ value of -24 mV. The carboxylic acid group exists in its neutral form at this pH resulting in weak surface interaction. The ease of bringing nanoparticles having low zeta potential (ζ = -24 mV), close to each other, may result in the formation of larger aggregates which eventually precipitate out of the solution. At pH 4.5, the nanoparticles are fairly stable due to the high ζ value of -45 mV and the effective surface coverage of nanoparticles by the capping agents (*vide supra*). Thus at pH 4.5, two nanoparticles can be brought in proximity only through the effective chelation

Table 3.1. Zeta potential of nanoparticles at different pH and their metal ion sensing ability.

pH	Zeta Potential ζ (mV)	Selectivity of metal cation
3.0	-24	Precipitation
4.5	-45	Pb^{2+}
5.5	-42	Pb^{2+}, Fe^{3+}
6.0	-40	Pb^{2+}, Fe^{3+}, Cu^{2+}

of surface bound ligands with metal cations overcoming the electrostatic repulsion imposed by the nanoparticles. The overall stability of a supramolecular complex formed between ligands and metal cations depends on the steric and stereo requirements of the ligands around the metal cations, the co-ordination number of the metal cations and various other factors such as columbic and hydrogen bonding interactions.[8,46] It may be noted that the Pb^{2+} ions possess unique co-ordination properties compared to other metal cations. For example, Pb^{2+} ions display variable co-ordination number up to 12 with flexible bond length (up to 3 Å) and co-ordination geometry.[79-84] Due to this unique co-ordination ability, Pb^{2+} ions interact more effectively with a large number of ligands resulting in the formation of a stronger supramolecular complex. Also, similar to inner transition elements, sandwich complexes having higher co-ordination number are very common in the case of Pb^{2+} cations.[80,81] In a recent study, Parajuli et al. have found that the

selectivity of catechol modified lignin towards different metal cations varies in the order: $Pb^{2+} > Fe^{3+} > Al^{3+} > Ni^{2+} \sim Zn^{2+} \sim Cd^{2+} \sim Co^{2+}$.[85] The higher stability constant observed for Pb^{2+} ion is attributed to the presence of a large number of phenolic moieties in the modified lignin. By adopting this methodology, authors could isolate even the trace quantities of Pb^{2+} ions in presence of large excess of other metal cations such as Zn^{2+}. In the present case, ligands on Au nanoparticles possess large number of free phenolic groups (Figure 2.20, Chapter 2) which form multivalent co-ordination with Pb^{2+} cations, resulting in the formation of stable supramolecular aggregates. In contrast, other metal cations may interact with lesser number of ligands due to their rigid co-ordination geometry and the electrostatic repulsion between the nanoparticles may be dominant in these systems leaving the nanoparticles isolated. The observed interparticle interactions in presence of other metal cations (Fe^{3+} and Cu^{2+}) at higher pH is attributed to the gradual decrease in ζ value and increase in the nucleophilicity of hydroxyl groups. These results clearly indicate that small variations in the binding ability of different metal cations can be effectively utilized for their selective colorimetric detection through the fine control of the nanoparticle's zeta potentials.

Model calculations: The results presented in earlier section indicate that the chelation of Pb^{2+} ions with the surface bound ligands of **Au-GA** nanoparticles results in the supramolecular organization. Such interactions bring the

nanoparticles in the close proximity resulting in plasmon coupling. To have better understanding on the complex formation, model calculations have been carried out with density functional theory (DFT) method. The chosen method contains the MPWB1K functional[86,87] which is recently proposed as a good functional for the study of the interactive behavior of molecules. For C, O, and H atoms, standard split valence 6-31G(d,p) basis set and for Au and Pb the Los Alamos effective-core potential (ECP) Lanl2DZ basis set are used.[88,89] Further, to improve the accuracy of the metal-centered basis sets, additional 'f' polarization functions for Au[90] and additional 'd' polarization functions for Pb[91] are included in the LanL2DZ basis set. For all the calculations, Gaussian 03 suite of programs have been used.[92]

During the formation of nanoparticles, adsorption of any unreduced or partially reduced metal cations (Au/Ag) imparts residual positive charge on nanoclusters. The electrostatic interaction with the negatively charged carboxylate moiety makes the nanoparticle highly stable and water soluble. One of the simplest models of the above mentioned system can be obtained through the interaction of the positively charged three atom triangular model of gold cluster with the anion of the oxidized form of gallic acid ('Complex 1' in Figure 3.12). This interaction possesses a negative entropy and the free energy released in the reaction is found to be extremely high (131.58 kcal/mol), suggesting that the process is highly exergonic.

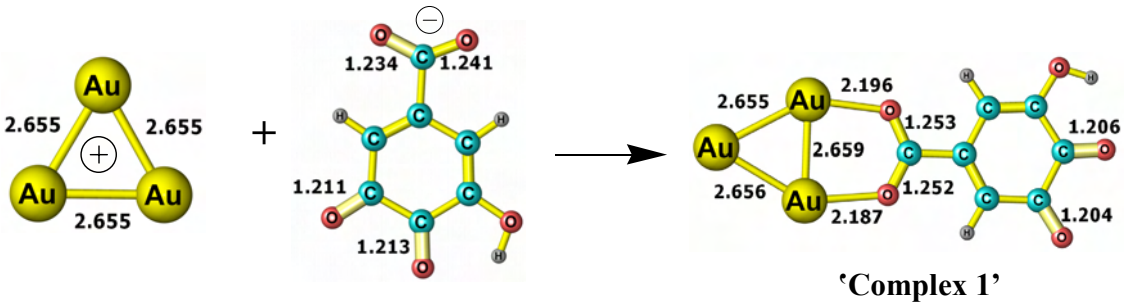

Figure 3.12. Electrostatic interaction between a positively charged model gold cluster with the oxidized form of gallic acid (the accompanying free energy change is found to be -131.58 kcal/mol).

Based on this thermodynamically favored interaction, we can assume that several such ligands may be bound electrostatically on to the surface of a large Au nanoparticle. Thus for every adsorbed molecule on the surface of Au nanoparticle, three oxygen atoms possessing lone pairs of electrons are available for further complexation with incoming metal ions. In order to model such a process, we have investigated the basic interaction of two units of 'Complex 1' with the Pb^{2+} cation. During this process, ionization of the O-H bond of Complex 1 may occur and the charge is balanced by the counter anion of Pb^{2+} namely acetate anion. The optimized geometry of the complex possesses a distorted square pyramidal structure having Pb^{2+} ions at the apical position ('Complex 2' in Figure 3.13A). The above mentioned geometric features of lead center are very often observed when it is connected to four oxygen atoms.[82] The side view (with respect to the gold rings) of 'Complex 2' is presented as Figure 3.13B. It is interesting to note

that the two Au_3 units are separated only by 1.1 nm indicating that both the ligands belong to the same nanoparticle and such a complexation will not lead to any interparticle interaction.

Based on X-ray structures, it is reported that lead possesses a variety of coordination geometries and coordination number as high as 12.[79-84] The coordination sphere around lead is highly flexible to the steric and electronic demands persisting in the system.[79-84] Therefore, further coordination possibilities exist for the lead center and it is reasonable to assume that two

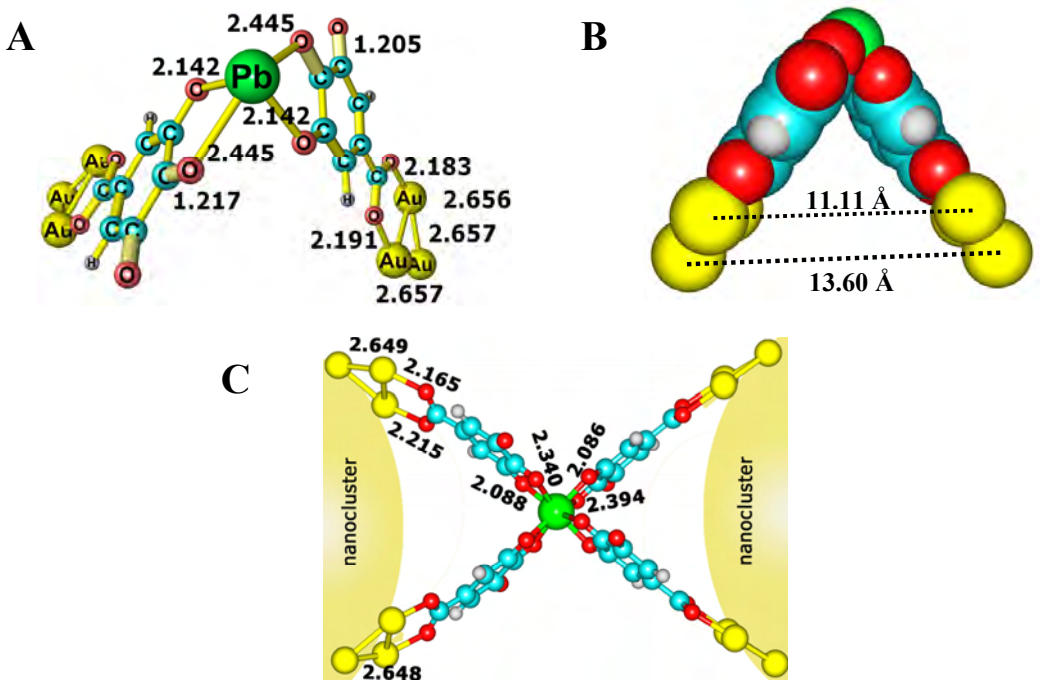

Figure 3.13. (A) Optimized structure of a distorted square pyramidal structure of Pb^{2+} complex ('Complex 2') (B) Side view of 'Complex 2' with respect to the Au_3 units (C) Optimized structure ('Complex 3') showing the interparticle interaction through coordination to Pb^{2+} ion (representative bond lengths are also shown in Angstrom unit).

or more ligands bound on the neighboring Au nanoparticle can interact with 'Complex 2'. One of the possibilities for such complexation is depicted as 'Complex 3' in Figure 3.13C (for optimization, the Au…Au distance within a nanocluster is kept as 13.60 Å to maintain the rigidity; see Figure 3.13B). Due to geometric reasons arising from the large size of the nanoparticle (~ 50 nm) compared to the tiny size of the ligand (~ 0.5 nm), further coordination of the ligands from third nanoparticle to the octahedrally coordinated lead in 'Complex 3' can be ruled out. These results indicate that within the supramolecular aggregate, a particular lead ion is bridged between only two Au nanoparticles. Based on the experimental and theoretical studies presented in the above sections, a tentative representation of the supramolecular complex is presented in Scheme 3.2.

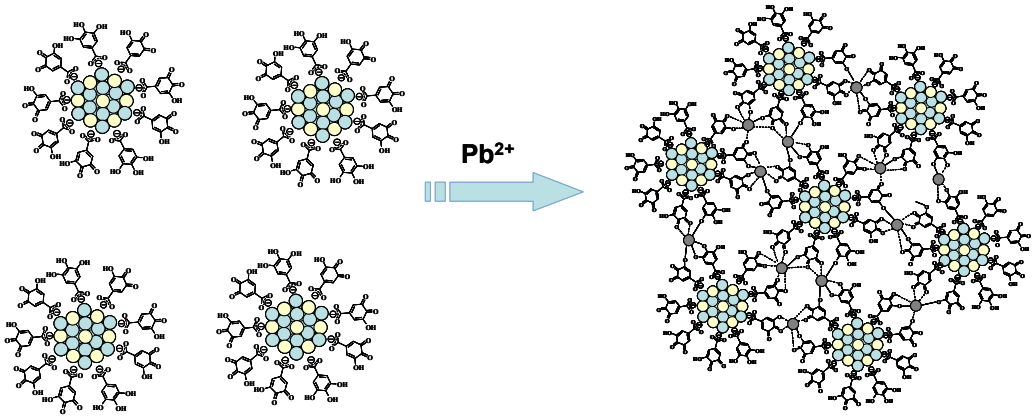

Scheme 3.2. Pictorial representation of formation of metal-ligand complex leading to the aggregation of nanoparticles (the size of the nanoparticle is highly minimized compared to the size of the ligand to magnify the interparticle interaction around the Pb^{2+} centers).

Competitive binding studies: To prove the versatility of present methodology for practical applications, competitive binding studies were performed in the presence of other interfering metal cations namely, Fe^{3+}, Cd^{2+}, Cu^{2+}, Hg^{2+}, Ni^{2+}, Zn^{2+}, Mg^{2+} and Ca^{2+}. Three separate solutions were prepared by mixing the above mentioned metal ions wherein the concentrations of the individual metal cations were varied as 14, 400 and 1500 μM and mixed with **Au-GA** nanoparticles. In first two cases, no spectral changes were observed in the presence of these interfering metal cations. The addition of Pb^{2+} ions to above mentioned solution resulted in a bathochromic shift, however, the detection limit depends on the concentration of interfering metal cations present. For example, the detection limit of Pb^{2+} ions was found to be in the range of 30-300 μM, when the concentration of interfering metal cations in the mixture was fixed as 14 μM. Further increase in the concentration of interfering metal ions to 400 μM resulted in a decrease in sensitivity of Pb^{2+} ions to 75-400 μM. Ratiometric plots showing the sensitivity of nanoparticles towards Pb^{2+} ions in presence of different concentrations of interfering metal cations is presented in Figure 3.14. The observed decrease in the detection limit may be due to (i) an increase in the ionic strength of the medium or (ii) the complexation of interfering metal cations with capping agents on isolated nanoparticles. It may be noted that at pH 4.5, other metal cations are not capable of forming supramolecular

organization through multivalent coordination. At higher concentrations of interfering metal cations (1500 μM), precipitation of nanoparticles was observed.

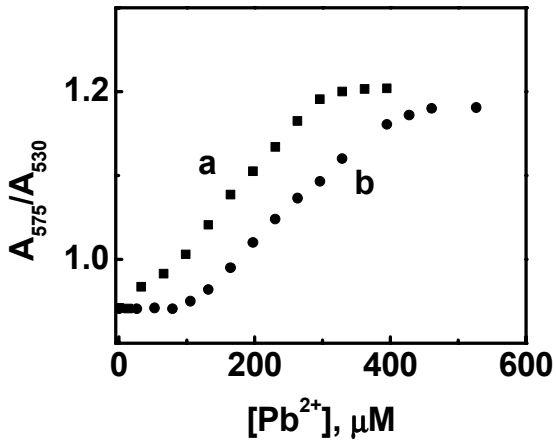

Figure 3.14. Ratiometric plot showing the sensitivity of nanoparticles towards Pb^{2+} ions wherein the concentrations of the individual metal cations (Fe^{3+}, Cd^{2+}, Cu^{2+}, Hg^{2+}, Ni^{2+}, Zn^{2+}, Mg^{2+} and Ca^{2+}) were varied as (a) $[M^{n+}]$ = 14 μM and (b) $[M^{n+}]$ = 400 μM.

***In situ* synthesis:** Further to demonstrate the versatility of the present method, synthesis of nanoparticles were carried out in solutions containing Pb^{2+} ions (*In situ* synthesis). Gallic acid and hydrogentetrachloroaurate were added sequentially to an aqueous medium containing different concentration (0-100 μM) of Pb^{2+} ions. The absorption spectrum obtained in each case is presented in Figure 3.15 and the absorption maximum underwent a bathochromic shift with increase in the concentration of Pb^{2+} ions. These studies indicate that the colorimetric method presented here allows the

detection of lead ions from aqueous medium in the presence of other interfering metal cations just by mixing gallic acid and Au(III) ions without the aid of any specialized equipment.

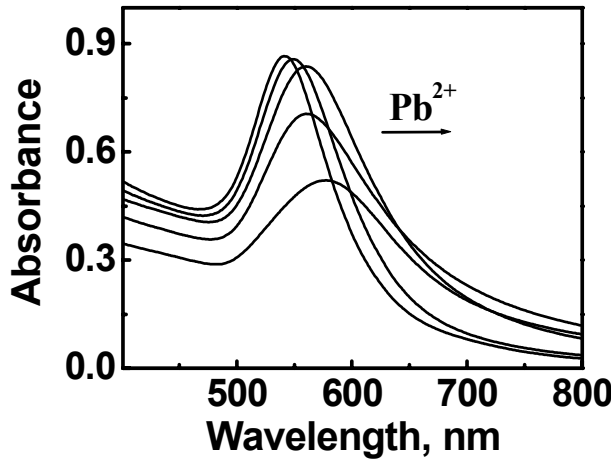

Figure 3.15. Absorption spectral changes indicating the formation of gold nanoparticles on addition of gallic acid (0.18 mM) and $HAuCl_4$ (0.2 mM) to solutions containing Pb^{2+} ions (0-100 μM).

3.5. Metal Binding Studies with Ag-GA Nanoparticles

Silver nanoparticles exhibits intense plasmon excitation when compared to the other two metals (Au and Cu) and are ideal for the colorimetric detection of aqueous metal cations. To invoke this aspect, the interactions of different metal ions with gallic acid stabilized silver nanoparticles (**Ag-GA**) were investigated. The pH of the silver nanoparticles were adjusted to 4.5-5.0 and metal binding studies were performed by adding micromolar amounts of different metal cations and the absorption spectral changes were monitored after each addition. Similar to the gold

nanoparticles, it has been observed that addition of most of the metal cations has a negligible effect on the plasmon absorption of nanoparticles (Figure 3.16). Interestingly, addition of micromolar amounts of Pb^{2+} ions resulted in a

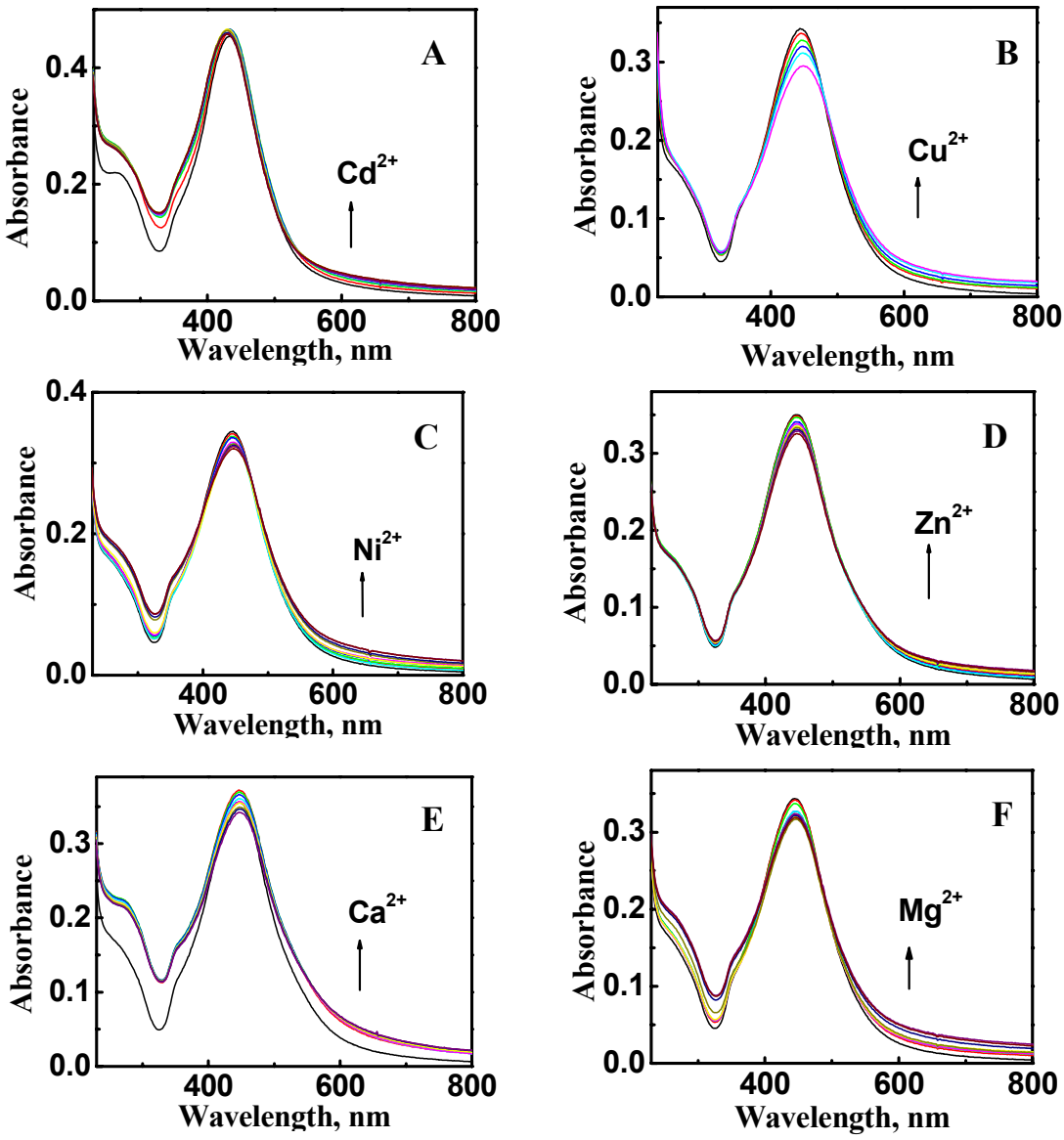

Figure 3.16. Absorption spectral changes of **Ag-GA** in presence of varying concentrations of metal cations in water (A) Cd^{2+}, (B) Cu^{2+}, (C) Ni^{2+}, (D) Zn^{2+}, (E) Ca^{2+} and (F) Mg^{2+}; $[M^{n+}]$ = 0-100 μM.

gradual bathochromic shift in the plasmon absorption and the color of the solution turned from yellow to red (Figure 3.17). The bathochromic shift to the plasmon absorption is attributed to the metal ion induced supramolecular organization of nanoparticles and confirmed through microscopic investigations.

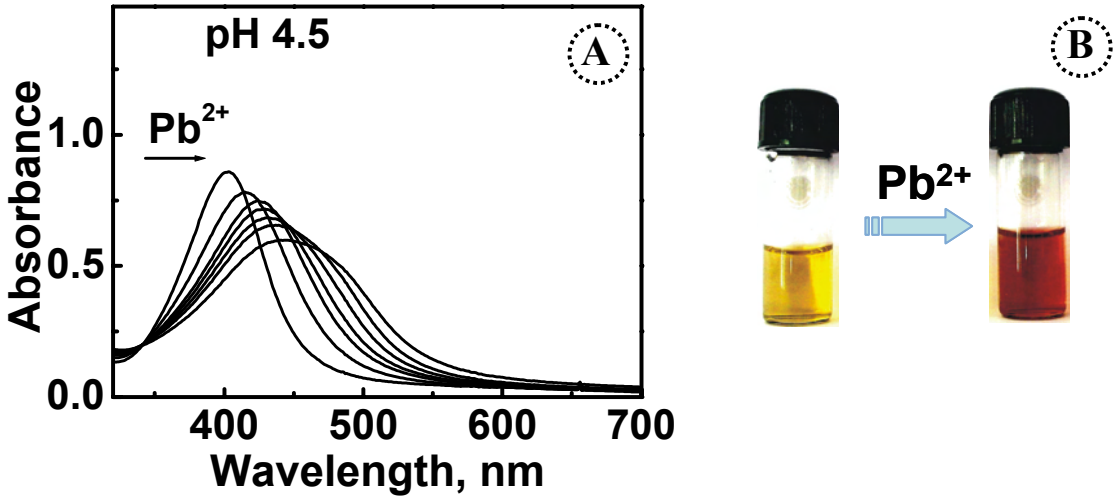

Figure 3.17. (A) Absorption spectral changes of **Ag-GA** nanoparticles in water on addition of varying concentrations of Pb^{2+} ions; [Pb^{2+}]=0-150 μM and (B) the color photograph of nanoparticle solution in the absence and presence of Pb^{2+} ions (150 μM).

The TEM and AFM images of the nanoparticles, before and after the addition of 100 μM Pb^{2+} ions, are presented in Figure 3.18. Nanoparticles remained isolated and randomly distributed in the absence of Pb^{2+} ions, whereas large aggregates of nanoparticles were observed on addition of Pb^{2+} ions (100 μM). These studies suggest that the observed bathochromic shift in

the plasmon maximum results from the metal ion induced supramolecular organization of nanoparticles. Similar to the **Au-GA** system, the complexation of Pb^{2+} ions with the surface capping ligands of nanoparticles brings the nanoparticles close to each other resulting in plasmon coupling.

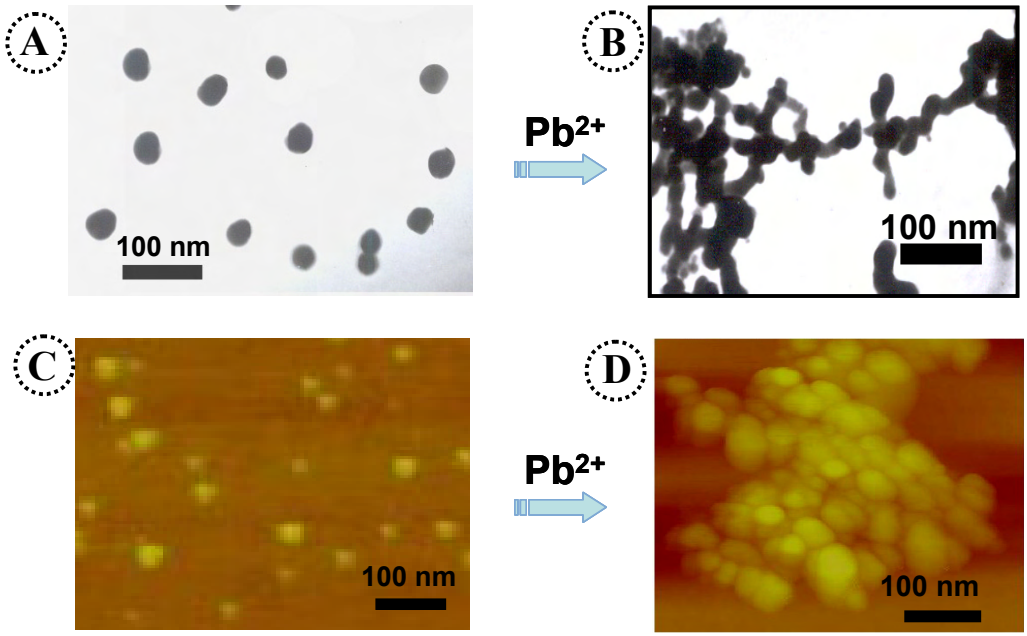

Figure 3.18. TEM (A,B) and AFM (C,D) images of **Ag-GA** nanoparticles in the absence (A, C) and presence (B,D) of Pb^{2+} ions (100 μM). Samples for TEM were prepared by drop casting the solution on to a formvar coated copper grid and AFM studies by drop casting on to freshly cleaved mica surface.

Reversibility of the aggregation process was further confirmed by adding a much stronger chelating agent namely, EDTA (Figure 3.19). The absorption spectrum of **Ag-GA** nanoparticles is characterized by strong plasmon absorption at 405 nm (trace 'a'). On addition of Pb^{2+} ions (80 μM), the plasmon absorption underwent a bathochromic shift of 25 nm (trace 'b')

due to the supramolecular organization of nanoparticles. A complete reversal of plasmon absorption was observed (trace 'c') on addition of EDTA (95 μM) indicating the reversibility of binding process.

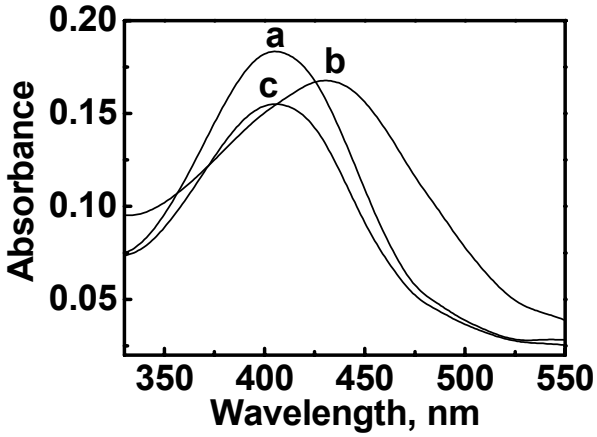

Figure 3.19. Absorption spectral changes of **Ag-GA** nanoparticles in water at pH 4.5 in the absence (trace 'a') and presence of 80 μM of Pb^{2+} (trace 'b'). Trace 'c' illustrates the spectral change on addition of EDTA (95 μM) to this solution.

Visual color changes of **Ag-GA** nanoparticles on addition of various metal cations (150 μM) are illustrated in Figure 3.20A and it is clear that the color changes (yellow to red) are only observed in the presence of Pb^{2+} ions. For any practical application, it is essential to quantify the metal cation sensing ability. A plot of ratio of the absorbance of aggregated nanoparticle (456 nm) to that of the isolated form (429 nm), as a function of Pb^{2+} ion concentration is presented in Figure 3.20B. The ratiometric plot indicates

that the **Ag-GA** nanoparticle system is sensitive only towards Pb^{2+} ions under the experimental conditions and sensitivity ranges from 5-100 μM.

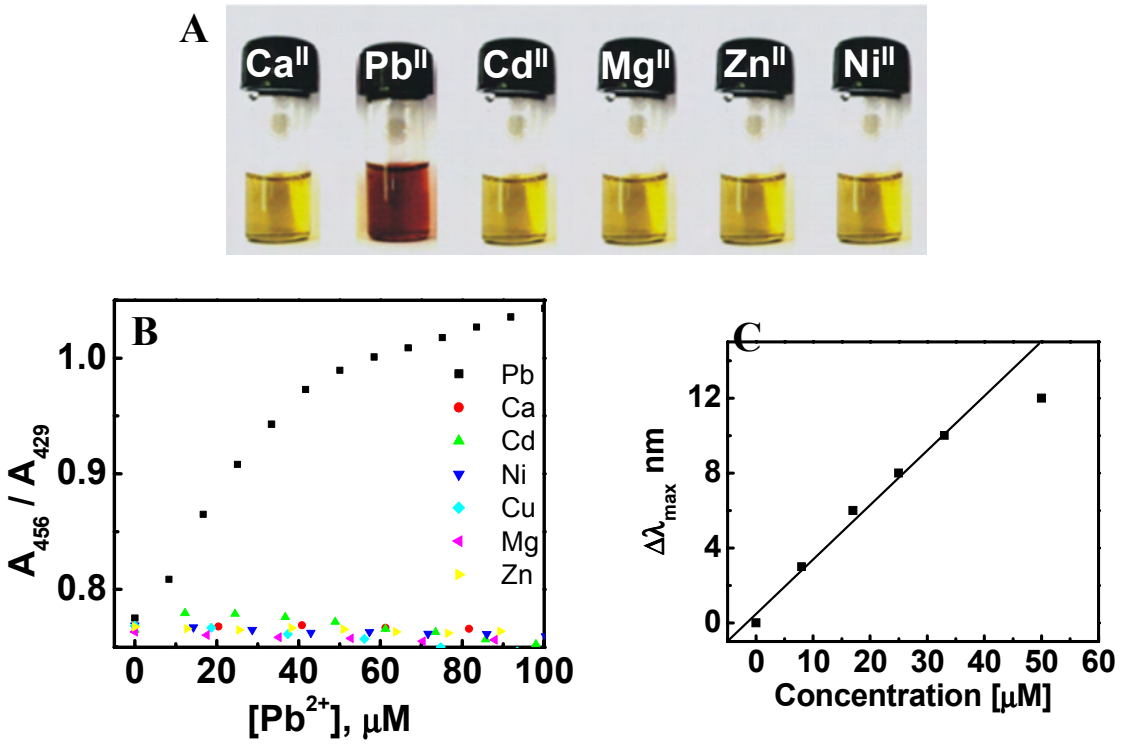

Figure 3.20. (A) Color photograph of the **Ag-GA** nanoparticle solutions in presence of various metal cations ([M^{2+}] = 150 μM); (B) plot illustrating the changes in ratio of the absorbances, of the aggregated to the isolated form of nanoparticles (A_{575}/A_{530}), on addition of various metal cations and (C) the shift in the plasmon absorption band ($\Delta\lambda$) as a function of Pb^{2+} ion concentration.

Further the plot of the shift in the plasmon absorption maximum ($\Delta\lambda$) of Au nanoparticles as a function of Pb^{2+} ion concentration showed a linear relationship (Figure 3.20C) indicating the versatility of this methodology for their quantitative determination from aqueous medium.

3.6. Conclusion

The newly synthesized nanoparticles (**Au-GA** and **Ag-GA**) possess a unique ability to detect micromolar quantities of Pb^{2+} ions in the presence of other interfering metal cations (Fe^{3+}, Cd^{2+}, Cu^{2+}, Hg^{2+}, Ni^{2+}, Zn^{2+}, Mg^{2+} and Ca^{2+}) resulting in a visual color change from pink to blue for Au nanoparticle and yellow to red for Ag nanoparticles. The linear shift in the plasmon absorption maximum against the concentration of Pb^{2+} ions indicates the versatility of the current methodology for their quantitative determination. The high selectivity and sensitivity of Pb^{2+} ions to the plasmon oscillation of **Au-GA** and **Ag-GA** nanoparticles is attributed to the unique coordination behavior of Pb^{2+} ions which overcomes the interparticle electrostatic repulsion. The extremely elegant colorimetric method presented here allows the detection of lead ions from aqueous media in the presence of other interfering metal cations, without the aid of any specialized instruments.

3.7. References

1. Jain, P. K.; Huang, X.; El-Sayed, I. H.; El-Sayed, M. A., *Plasmonics* **2007,** *2*, 107-118.
2. Guo, S.; Wang, E., *Anal. Chim. Acta* **2007,** *598*, 181-192.
3. Hegmann, T.; Qi, H.; Marx, V., *J. Inorg. Organomet. Polym. Mat.* **2007,** *17*, 483-508.
4. You, C. C.; Verma, A.; Rotello, V. M., *Soft Matter* **2006,** *2*, 190-204.

5. Burda, C.; Chen, X.; Narayanan, R.; El-Sayed, M. A., *Chem. Rev.* **2005,** *105*, 1025-1102.
6. Mirkin, C. A., *Small* **2005,** *1*, 14-16.
7. Mirkin, C. A.; Thaxton, C. S.; Rosi, N. L., *Expert Rev. Mol. Diagn.* **2004,** *4*, 749-751.
8. Lehn, J.-M., *Science* **2002,** *295*, 2400-2403.
9. Lehn, J.-M., *Proc. Natl. Acad. Sci. U.S.A.* **2002,** *99*, 4763-4768.
10. Oshovsky, G. V.; Reinhoudt, D. N.; Verboom, W., *Angew. Chem. Int. Ed.* **2007,** *46*, 2366-2393.
11. Schenning, A. P. H. J.; Meijer, E. W., *Chem. Commun.* **2005**, 3245-3258.
12. Mulder, A.; Huskens, J.; Reinhoudt, D. N., *Org. Biomol. Chem.* **2004,** *2*, 3409-3424.
13. Fialkowski, M.; Bishop, K. J. M.; Klajn, R.; Smoukov, S. K.; Campbell, C. J.; Grzybowski, B. A., *J. Phys. Chem. B* **2006,** *110*, 2482-2496.
14. Elghanian, R.; Storhoff, J. J.; Mucic, R. C.; Letsinger, R. L.; Mirkin, C. A., *Science* **1997,** *277*, 1078-1080.
15. Storhoff, J. J.; Elghanian, R.; Mucic, R. C.; Mirkin, C. A.; Letsinger, R. L., *J. Am. Chem. Soc.* **1998,** *120*, 1959-1964.
16. Hurst, S. J.; Han, M. S.; Lytton-Jean, A. K. R.; Mirkin, C. A., *Anal. Chem.* **2007,** *79*, 7201-7205.
17. Zhong, Z. Y.; Patskovskyy, S.; Bouvrette, P.; Luong, J. H. T.; Gedanken, A., *J. Phys. Chem. B* **2004,** *108*, 4046-4052.
18. Sudeep, P. K.; Joseph, S. T. S.; Thomas, K. G., *J. Am. Chem. Soc.* **2005,** *127*, 6516-6517.
19. Baron, R.; Zayats, M.; Willner, I., *Anal. Chem.* **2005,** *77*, 1566-1571.
20. Lee, J.-S.; Han, M. S.; Mirkin, C. A., *Angew. Chem. Int. Ed.* **2007,** *46*, 4093-4096.

21. Lin, S.-Y.; Wu, S.-H.; Chen, C.-h., *Angew. Chem. Int. Ed.* **2006,** *45*, 4948-4951.
22. Liu, J.; Lu, Y., *J. Am. Chem. Soc.* **2003,** *125*, 6642-6643.
23. Obare, S. O.; Hollowell, R. E.; Murphy, C. J., *Langmuir* **2002,** *18*, 10407-10410.
24. Kim, Y.; Johnson, R. C.; Hupp, J. T., *Nano Lett.* **2001,** *1*, 165-167.
25. Li, J.; Lu, Y., *J. Am. Chem. Soc.* **2000,** *122*, 10466-10467.
26. Xu, X.; Han, M. S.; Mirkin, C. A., *Angew. Chem. Int. Ed.* **2007,** *46*, 3468-3470.
27. Wang, Z.; Levy, R.; Fernig, D. G.; Brust, M., *J. Am. Chem. Soc.* **2006,** *128*, 2214-2215.
28. Link, S.; El-Sayed, M. A., *Int. Rev. Phys. Chem.* **2000,** *19*, 409-453.
29. Zhao, L. L.; Kelly, K. L.; Schatz, G. C., *J. Phys. Chem. B* **2003,** *107*, 7343-7350.
30. Liz-Marzan, L. M., *Langmuir* **2006,** *22*, 32-41.
31. Jain, P. K.; Lee, K. S.; El-Sayed, I. H.; El-Sayed, M. A., *J. Phys. Chem. B* **2006,** *110*, 7238-7248.
32. Evanoff Jr., D. D.; Chumanov, G., *ChemPhysChem* **2005,** *6*, 1221-1231.
33. Kelly, K. L.; Coronado, E.; Zhao, L. L.; Schatz, G. C., *J. Phys. Chem. B* **2003,** *107*, 668-677.
34. Sun, Y.; Xia, Y., *Analyst* **2003,** *128*, 686-691.
35. El-Sayed, M. A., *Acc. Chem. Res.* **2001,** *34*, 257-264.
36. Ghosh, S. K.; Pal, T., *Chem. Rev.* **2007,** *107*, 4797-4862.
37. Jain, P. K.; Eustis, S.; El-Sayed, M. A., *J. Phys. Chem. B* **2006,** *110*, 18243-18253.
38. Hutter, E.; Fendler, J. H., *Adv. Mater.* **2004,** *16*, 1685-1706.
39. Rechberger, W.; Hohenau, A.; Leitner, A.; Krenn, J. R.; Lamprecht, B.; Aussenegg, F. R., *Opt. Commun.* **2003,** *220*, 137-141.

40. Su, K.-H.; Wei, Q.-H.; Zhang, X.; Mock, J. J.; Smith, D. R.; Schultz, S., *Nano lett.* **2003,** *3*, 1087-1090.
41. Jain, P. K.; Huang, W.; El-Sayed, M. A., *Nano Lett.* **2007,** *7*, 2080-2088.
42. Sonnichsen, C.; Reinhard, B. M.; Liphardt, J.; Alivisatos, A. P., *Nat. Biotechnol.* **2005,** *23*, 741-745.
43. Reinhard, B. M.; Siu, M.; Agarwal, H.; Alivisatos, A. P.; Liphardt, J., *Nano Lett.* **2005,** *5*, 2246-2252.
44. Liu, J.; Lu, Y., *Chem. Mater.* **2004,** *16*, 3231-3238.
45. Liu, J.; Lu, Y., *J. Am. Chem. Soc.* **2004,** *126*, 12298-12305.
46. Oh, M.; Carpenter, G. B.; Sweigart, D. A., *Acc. Chem. Res.* **2004,** *37*, 1-11.
47. McDonald, M.; Mila, I.; Scalbert, A., *J. Agric. Food Chem.* **1996,** *44*, 599-606.
48. Charkoudian, L. K.; Franz, K. J., *Inorg. Chem.* **2006,** *45*, 3657-3664.
49. Sever, M. J.; Wilker, J. J., *Dalton Trans.* **2004**, 1061-1072.
50. Limson, J.; Nyokong, T., *Anal. Chim. Acta* **1997,** *344*, 87-95.
51. Dhungana, S.; Heggemann, S.; Heinisch, L.; Mollmann, U.; Boukhalfa, H.; Crumbliss, A. L., *Inorg. Chem.* **2001,** *40*, 7079-7086.
52. Hynes, M. J.; O Coinceanainn, M., *J. Inorg. Biochem.* **2001,** *85*, 131-142.
53. Kraemer, S.; Xu, J.; Raymond, K.; Sposito, G., *Environ. Sci. Technol.* **2002,** *36*, 1287-1291.
54. Strawn, D. G.; Sparks, D. L., *Soil Sci. Soc. Am. J.* **2000,** *64*, 144-156.
55. Giannakopoulos, E.; Christoforidis, K. C.; Tsipis, A.; Jerzykiewicz, M.; Deligiannakis, Y., *J. Phys. Chem. A* **2005,** *109*, 2223-2232.
56. Zhang, Z. Z.; Bailey, G. W. In *Proceedings of the Seventh International Symposium*, Fish Physiology, Toxicology, and Water Quality, Tallinn, Estonia, 2003; pp 297-324.
57. Fink, D. W.; Stong, J. D., *Spectrochim. Acta.* **1982,** *38*, 1295-1298.

58. Beltran, J. L.; Sanli, N.; Fonrodona, G.; Barron, D.; Ozkan, G.; Barbosa, J., *Anal. Chim. Acta* **2003,** *484*, 253-264.
59. Hizal, J.; Apak, R., *J. Colloid Interface Sci.* **2006,** *295*, 1-13.
60. Majcher, E. H.; Chorover, J.; Bollag, J.-M.; Huang, P. M., *Soil Sci. Soc. Am. J.* **2000,** *64*, 157-163.
61. Hernberg, S., *Am. J. Ind. Med.* **2000,** *38*, 244-254.
62. Lewis, J. A.; Cohen, S. M., *Inorg. Chem.* **2004,** *43*, 6534-6536.
63. Bridgewater, B. M.; Parkin, G., *J. Am. Chem. Soc.* **2000,** *122*, 7140-7141.
64. Schroeder, H.; Tipton, I. H., *Arch. Environ. Health* **1986,** *17*, 965-978.
65. Callan, J. F.; de Silva, A. P.; Magri, D. C., *Tetrahedron* **2005,** *61*, 8551-8588.
66. de Silva, A. P.; Gunaratne, H. Q. N.; Gunnlaugsson, T.; Huxley, A. J. M.; McCoy, C. P.; Rademacher, J. T.; Rice, T. E., *Chem. Rev.* **1997,** *97*, 1515-1566.
67. Kwon, J. Y.; Jang, Y. J.; Lee, Y. J.; Kim, K. M.; Seo, M. S.; Nam, W.; Yoon, J., *J. Am. Chem. Soc.* **2005,** *127*, 10107-10111.
68. Fitch, A., *Crit. Rev. Anal. Chem.* **1998,** *28*, 267-345.
69. Wu, D.-Y.; Xie, L.-X.; Zhang, C.-L.; Duan, C.-Y.; Zhao, Y.-G.; Guo, Z.-J., *Dalton Trans.* **2006**, 3528-3533.
70. Kadarkaraisamy, M.; Sykes, A. G., *Inorg. Chem.* **2006,** *45*, 779-786.
71. Basheer, M. C.; Alex, S.; George Thomas, K.; Suresh, C. H.; Das, S., *Tetrahedron* **2006,** *62*, 605-610.
72. Xue, H.; Tang, X. J.; Wu, L. Z.; Zhang, L. P.; Tung, C. H., *J. Org. Chem.* **2005,** *70*, 9727-9734.
73. Schmittel, M.; Lin, H.-W., *Angew. Chem. Int. Ed.* **2007,** *46*, 893-896.
74. Folmer-Andersen, J. F.; Lynch, V. M.; Anslyn, E. V., *Chem. Eur. J.* **2005,** *11*, 5319-5326.
75. Prodi, L., *New. J. Chem.* **2005,** *29*, 20-31.
76. Lu, Y.; Liu, J., *Acc. Chem. Res.* **2007,** *40*, 315-323.

77. Rex, M.; Hernandez, F. E.; Campiglia, A. D., *Anal. Chem.* **2006,** *78*, 445-451.
78. Muller, R. H.; Jacobs, C.; Kayser, O., *Adv. Drug Delivery Rev.* **2001,** *47*, 3-19.
79. Esteban-Gomez, D.; Platas-Iglesias, C.; Enriquez-Perez, T.; Avecilla, F.; deBlas, A.; Rodriguez-Blas, T., *Inorg. Chem.* **2006,** *45*, 5407-5416.
80. Kotch, F. W.; Fettinger, J. C.; Davis, J. T., *Org. Lett.* **2000,** *2*, 3277-3280.
81. Rogers, R. D.; Bond, A. H., *Inorg. Chim. Acta* **1992,** *192*, 163-171.
82. Parr, J., *Polyhedron* **1997,** *16*, 551-566.
83. Manceau, A.; Boisset, M. C.; Sarret, G.; Hazemann, J. L.; Mench, M.; Cambier, P.; Prost, R., *Environ. Sci. Technol.* **1996,** *30*, 1540-1552.
84. Soudi, A. A.; Marandi, F.; Ramazani, A.; Ahmadi, E.; Morsali, A., *C. R. Chimie* **2005,** *8*, 157-168.
85. Parajuli, D.; Inoue, K.; Ohto, K.; Oshima, T.; Murota, A.; Funaoka, M.; Makino, K., *React. Funct. Polym.* **2005,** *62*, 129-139.
86. Zhao, Y.; Schultz, N. E.; Truhlar, D. G., *J. Chem. Theory Comput.* **2006,** *2*, 364-382.
87. Wodrich, M. D.; Corminboeuf, C.; Schleyer, P. v. R., *Org. Lett.* **2006,** *8*, 3631-3634.
88. Hay, P. J.; Wadt, W. R., *J. Chem. Phys.* **1985,** *82*, 270-283.
89. Hay, P. J.; Wadt, W. R., *J. Chem. Phys.* **1985,** *82*, 299-310.
90. Ehlers, A. W.; Bohme, M.; Dapprich, S.; Gobbi, A.; Hollwarth, A.; Jonas, V.; Kohler, K. F.; Stegmann, R.; Veldkamp, A.; Frenking, G., *Chem. Phys. Lett.* **1993,** *208*, 111-114.
91. Hollwarth, A.; Bohme, M.; Dapprich, S.; Ehlers, A. W.; Gobbi, A.; Jonas, V.; Kohler, K. F.; Stegmann, R.; Veldkamp, A.; Frenking, G., *Chem. Phys. Lett.* **1993,** *208*, 237-240.
92. Frisch, M. J.; Trucks, G. W.; Schlegel, H. B.; Scuseria, G. E.; Robb, M. A.; Cheeseman, J. R.; Montgomery, J. J. A.; Vreven, T.; Kudin, K. N.; Burant, J. C.; Millam, J. M.; Iyengar, S. S.; Tomasi, J.; Barone, V.; Mennucci, B.; Cossi,

M.; Scalmani, G.; Rega, N.; Petersson, G. A.; Nakatsuji, H.; Hada, M.; Ehara, M.; Toyota, K.; Fukuda, R.; Hasegawa, J.; Ishida, M.; Nakajima, T.; Honda, Y.; Kitao, O.; Nakai, H.; Klene, M.; Li, X.; Knox, J. E.; Hratchian, H. P.; Cross, J. B.; Adamo, C.; Jaramillo, J.; Gomperts, R.; Stratmann, R. E.; Yazyev, O.; Austin, A. J.; Cammi, R.; Pomelli, C.; Ochterski, J. W.; Ayala, P. Y.; Morokuma, K.; Voth, G. A.; Salvador, P.; Dannenberg, J. J.; Zakrzewski, V. G.; Dapprich, S.; Daniels, A. D.; Strain, M. C.; Farkas, O.; Malick, D. K.; Rabuck, A. D.; Raghavachari, K.; Foresman, J. B.; Ortiz, J. V.; Cui, Q.; Baboul, A. G.; Clifford, S.; Cioslowski, J.; Stefanov, B. B.; Liu, G.; Liashenko, A.; Piskorz, P.; Komaromi, I.; Martin, R. L.; Fox, D. J.; Keith, T.; Al-Laham, M. A.; Peng, C. Y.; Nanayakkara, A.; Challacombe, M.; Gill, P. M. W.; Johnson, B.; Chen, W.; Wong, M. W.; Gonzalez, C.; Pople, J. A. *Gaussian 03*, Version 6.1; Gaussian, Inc.: Pittsburgh PA, 2003.

CHAPTER 4

Supramolecular Organization of Phenyleneethynylenes on Surfaces

4.1. Abstract

Self-organization of a series of phenyleneethynylenes compounds (**1-4**) on HOPG surface were investigated using scanning tunneling microscopy. Phenyleneethynylene molecule (**1**), which does not possess any functional groups, self-organizes into wire like structures on surfaces. High resolution STM imaging revealed that molecules are arranged in a skewed 1D fashion. Analysis of various domains indicated the formation of three types of molecular packing. The initial steps of molecular assembly involve the interdigitation of alkoxy chains and the alkyl CH-acteylinic π interactions leading to the organization of molecules as a strip. It can be seen that with respect to the hexyloxy groups, the alkyl chain of the adjacent molecules interact with the acetylenic moiety, either from the '*ortho'* or '*meta'* position, leading to the formation of two types of strips, which further interlocks to various molecular assemblies. The spacing between the molecular wires was successfully modulated by increasing the length of the alkyl chains (**2**). Phenyleneethynylene molecule having hydroxyl groups at the terminal

positions (**3)** form linear assemblies through strong intermolecular hydrogen bonding between the hydroxyl groups. The 1D organization of dumbbell shaped fullerene having phenyleneethynylene spacer (**4**) is attributed to the higher surface potential near the step-edge.

4.2. Introduction

Organic electronics, a fast developing field of research having potential technological applications, aims at the use of organic molecules as active components in electronic devices.[1-4] Recent developments in the organization of photo- or electroactive molecules on two-dimensional surfaces, with atomic level precision, provides excellent possibilities for designing nanoscale optoelectronic devices.[2,5-10] Among the various molecular systems, π-conjugated organic molecules have been extensively utilized in various opto-electronic devices.[3,11-13] These include, light emitting devices such as organic light emitting diodes (OLEDs), thin film transistors (OTFTs), photovoltaic cells such as organic photovoltaic systems (OPVs) and dye sensitized solar cells (DSSC).[1] Fabrications of above mentioned optoelectronic devices involve the organization of molecules on surfaces and their efficiency is often controlled by the way in which molecules are arranged. Among the various methodologies adopted, self-organization of molecules has been emerged as an efficient bottom up strategy for the creation well defined molecular architectures on both surfaces and interfaces. Various noncovalent

interactions between the molecules and with surfaces play a decisive role in their organization.[14-17] An in-depth understanding of these interactions is essential for device fabrication. Scanning Tunneling Microscopy (STM) has been emerged as an excellent tool for probing these aspects with atomic scale resolution.[18-25]

Scanning tunneling microscopy:

Scanning Tunneling Microscope often referred as STM was invented by Binnig and Rohrer[26] of IBM Zurich laboratory in 1982 for which they were awarded the Nobel Prize in physics for the year 1986. The instrument was initially developed with an objective of imaging structural and electronic properties of surfaces.[26,27] Before its invention, information on the sub-micrometer scale length was accessible only using indirect techniques such as electron or X-ray diffraction or with electron microscopes that required vacuum environment and conductive materials. Over the years, STM has been emerged as a powerful tool for studying and manipulating materials with atomic scale precision. Compared to other imaging techniques STM has the advantage that it can image surfaces under a variety of conditions: at ambient conditions and high vacuum conditions by varying the temperature and also in air or liquid. In addition to these, STM can perform as a two terminal device for the direct determination of conductivity of even single molecules and nanoparticles.

Principle: The basic principle of STM is the measurement of the tunneling current at various points on the sample and an atomically sharp metallic tip is used to probe the sample surface. The technique is based on the well known quantum mechanical phenomenon called electron tunneling effect; when two conductors of varying Fermi energies are separated by a gap (or insulating layer), electrons flow (tunnel) from one conductor to other, crossing the potential barrier imposed by the gap.[28] The resulting current is known as tunneling current, which decays exponentially with the distance between the two conductors (gap width). The tunneling effect can be further induced and controlled by the application of a small bias voltage (V) between the sample and the tip. Depending upon the polarity of the applied potential, tunneling of electrons occurs by the transfer of electrons either from occupied states of the sample into the unoccupied states of the tip or from the tip to the sample. Figure 4.1 illustrates a typical tunnel junction formed between an atomically sharp metallic tip and a conductive surface.

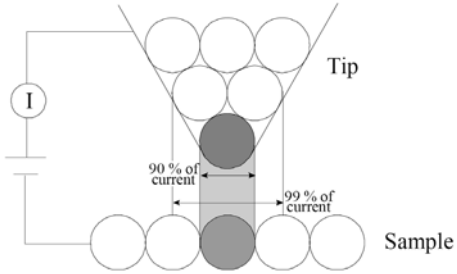

Figure 4.1. Schematic representation of the tunnel junction formed between the tip and sample surface (contribution of tip atoms to the tunneling current is shown). (*adapted from reference 28*)

For a given bias voltage V, the tunneling current (I) passing through a junction can be expressed as

$$I \approx Ve^{-cd}$$

where, c = constant; d = tip sample separation distance

Due to the exponential relationship, a variation of the gap by one Ångström causes the tunneling current to change by an order of magnitude resulting in a high vertical resolution of < 1 Å. Furthermore, for an atomically sharp tip, the apex atom contributes to more than 90% of the tunneling current providing a lateral resolution of ~1 Å (Figure 4.1).

In a topographic mode of STM operation, the tip scans over the surface in a raster mode (point by point, line by line) and tunneling current at various points are measured. When the tip scans the sample surface, it encounters sample features at different heights and depths, resulting in an exponential change in the tunneling current. A feed back loop is used to maintain a constant tunneling current during the scanning by vertically moving the scanner at each (x,y) data point until the desired set point is reached. Hence the a plot of the vertical position of the scanner as a function of (x,y) data points represent the contours of the sample surface (constant current mode, Figure 4.2A). In an alternative mode, STM image is constructed by recording the tunneling current as the tip rapidly scans over the surface at a constant distance often called constant height mode (Figure 4.2B).

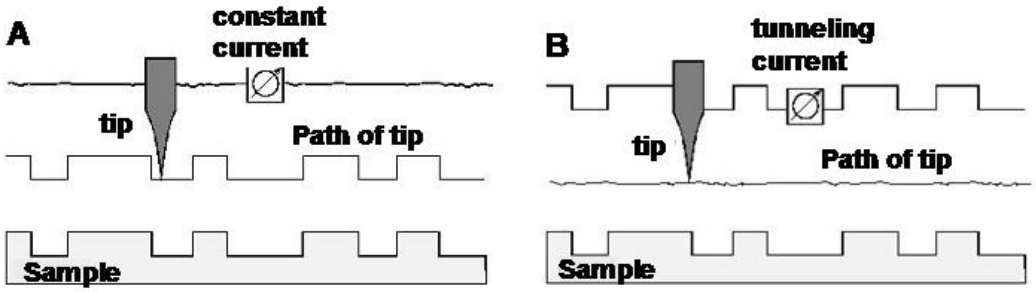

Figure 4.2. Different STM imaging techniques: (A) constant current and (B) constant height modes. (*adapted from reference 28*)

Self-organization of molecules: It is possible to control the organization of molecules on surfaces by varying the functional groups present. A review on the recent developments is presented in section 3 of Chapter 1. Among the various molecular building blocks, π-conjugated molecular systems such as oligo(phenyleneethynylene)s (OPE) have been proposed as elements in optoelectronic devices due to their fascinating structural and optical properties.[11,29-38] They possess rigid structure which does not involve any possibility of isomerization and the cylindrical symmetry of acetylene unit maintains the π-electron conjugation at any degree of rotation. Due to the unique structural and optical properties phenyleneethynylenes are suggested as elements in optoelectronic devices.[11,29-38]

Recent photophysical and electrochemical investigations of these compounds from our group[30,31] and others[33-38] have revealed that OPE based systems possess excellent luminescent properties in solution and may find potential applications in electroluminescent devices and as organic

light emitting diodes (OLEDs).[31, 39] However interchromophoric interactions of such molecules in solids can alter their optoelectronic properties and hence the way in which OPEs organize on surfaces is very crucial for device applications. Herein we describe scanning tunneling microscopic investigations of the self-organization of a few phenyleneethynylenes and a dumbbell shaped fullerene dimer, having phenyleneethynylene as linker (Chart 4.1), on highly oriented pyrolitic graphite (HOPG) surface and the various intermolecular interactions leading to their assembly are discussed.

All the compounds listed in Chart 4.1, possess three phenyl units interconnected with two acetylinic triple bonds. Alkyl substitution was introduced to impart solubility and studied the effect of varying the alkyl chain length. Influence of hydrogen bonding on self-organization was further investigated by using a phenyleneethynylene which possess hydroxyl groups at the terminal positions.

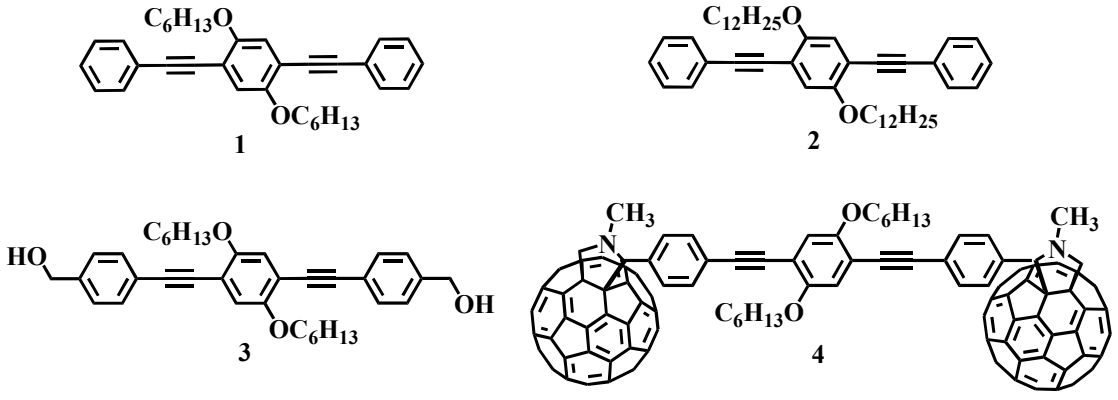

Chart 4.1. Molecular systems used for self-organization

4.3. Experimental Section

In the present study, STM investigations were performed on Multimode Scanning Probe Microscope (Nanoscope IV controller, Digital Instruments, Veeco). Special care was taken during various stages of sample preparation to avoid any type of impurities, since we are mapping the electron density.

***Preparation of the substrate**:* The quality (particularly the neatness) of the substrate is very crucial in STM studies and impurities on surfaces can disturb molecular organization. Atomically flat substrates with precisely controlled chemical functionalities, preferably freshly prepared just before the deposition are highly desirable for obtaining reproducible results. For the present investigations, we have used one of the commercially available flat supports, namely highly oriented pyrolitic graphite (HOPG) purchased from SPI supplies. A 5 x 5 x 2 mm piece of HOPG was fixed on to a steel metal disc using silver paste. Just before the sample preparation, the top layers of HOPG were cleaved with an adhesive tape to obtain a clean surface and the electrical connectivity of the sample surface through metallic disc was checked using a mulitimeter.

***Preparation of the tip**:* The quality and sharpness of the tip (probe) is crucial in obtaining highly resolved STM images. Ideally, a tip with one atom at the apex provides atomic resolution. In the present investigations,

Pt/Ir (80:20) wire was used for preparing the tip. Platinum is well known for its chemical inertness and the small percentage of the Ir increases the stiffness of the material, there by reducing the free vibration of the tip, providing images with high signal to noise ratio. Two approaches usually adopted for the sharpening of the tip are (i) mechanical cutting and (ii) electrochemical etching. Among these the later one is well known to produce reproducible tips capable of atomic resolution hence we have adopted this methodology. A schematic representation of the electrochemical set up used is presented in Figure 4.3.

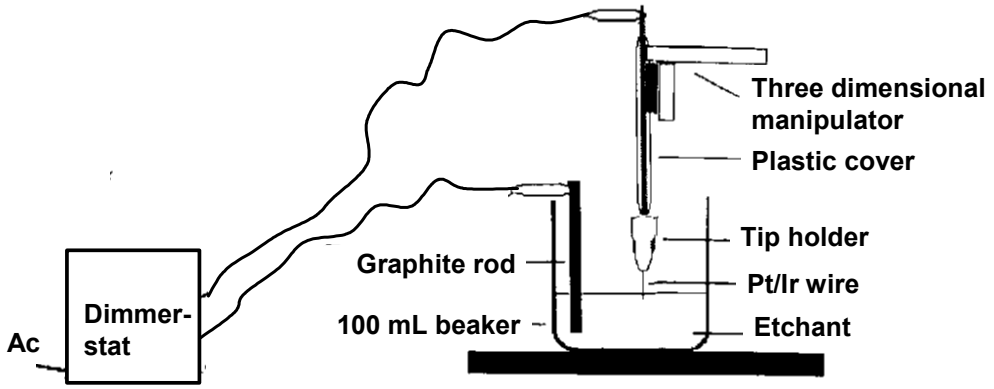

Figure 4.3. Schematic representation of the electrochemical set up used for the preparation of STM tips.

In a typical procedure, electrochemical etching of 0.25 mm diameter Pt/Ir wire were carried out using 1N aqueous KOH containing 5 % acetone as electrolyte and copper rod as the counter electrode. The presence of acetone in the electrolyte solution reduces the surface tension and controls the rate of formation of hydrogen gas and etching of tip. The electrolysis

was performed by vertically immersing about 1 mm of Pt/Ir wire in the electrolyte solution at a constant voltage of 20-30 V (ac; 50 Hz) between the electrodes. A dimmerstat was used to regulate the voltage to the desired value (~20 V). When a potential is applied between the wire and counter electrode, the tip undergo oxidation and slow etching. At a certain point, the lower part drops off and a sharp tip is formed at the breaking point. Any contaminant adhered near to the tip was removed using an ultra sharp forceps. The tip is then thoroughly washed with doubly distilled water, followed by acetone and air dried.

***Preparation of the sample**:* All the samples for STM investigations were prepared by drop casting the solution on HOPG surface. Typically, 0.1 mM of the respective compounds were prepared in either 1,2-dichlorobenzene or 1,2,4-trichlorobenzene and ~ 75 μL of the solution was drop casted on to the top layer of the freshly cleaved HOPG substrate and allowed to dry under ambient conditions. Before the analysis, samples were checked for electrical connectivity using a multimeter.

Synthesis: The synthesis of all the molecules **1-4** were carried out using a reported procedure[31,40] as shown in Scheme 4.1 and characterized using various analytical and spectroscopic techniques.

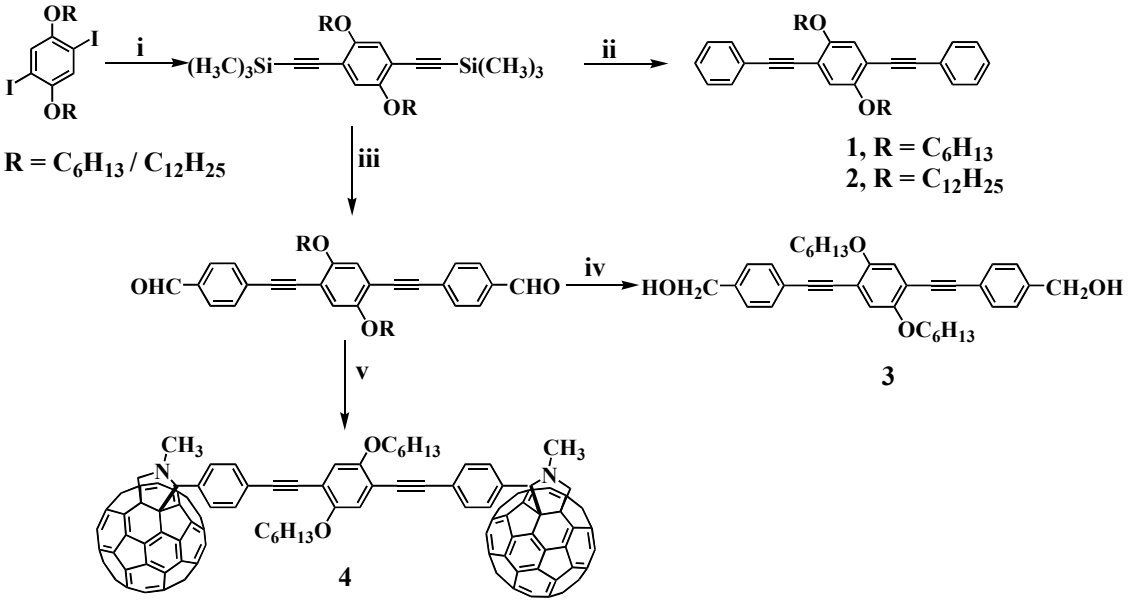

Scheme 4.1. Synthetic route adopted for the preparation of **1-4**: (i) (trimethylsilyl)acetylene, $Pd(PPh_3)_2Cl_2$, CuI, $(i\text{-}pr)_2NH$, 80 ^{0}C, 1h (ii) CH_3OH, K_2CO_3, THF, C_6H_5I, $Pd(PPh_3)_4$, CuI, PPh_3 (iii) CH_3OH, K_2CO_3, THF, BrC_6H_4CHO, $Pd(PPh_3)_4$, CuI, PPh_3 (iv) (v) C_{60}, sarcosine, tolune, reflux.

4.4. Results and Discussions

To have a fundamental understanding on the ability of our experimental set up to produce atomically resolved data, we have recorded the STM images of atomically flat HOPG substrate at different scan sizes and are presented in Figure 4.4. At higher scan size of 13 x 13 nm^2 (Figure 4.4A) a number of dots like features arranged in a periodic fashion was observed. On further decreasing the scan size to 1.9 x 1.9 nm^2 (Figure 4.4B) and 1 x 1 nm^2 (Figure 4.4C), a threefold symmetry arrangement of bight spots was clearly visible in the images. The distance

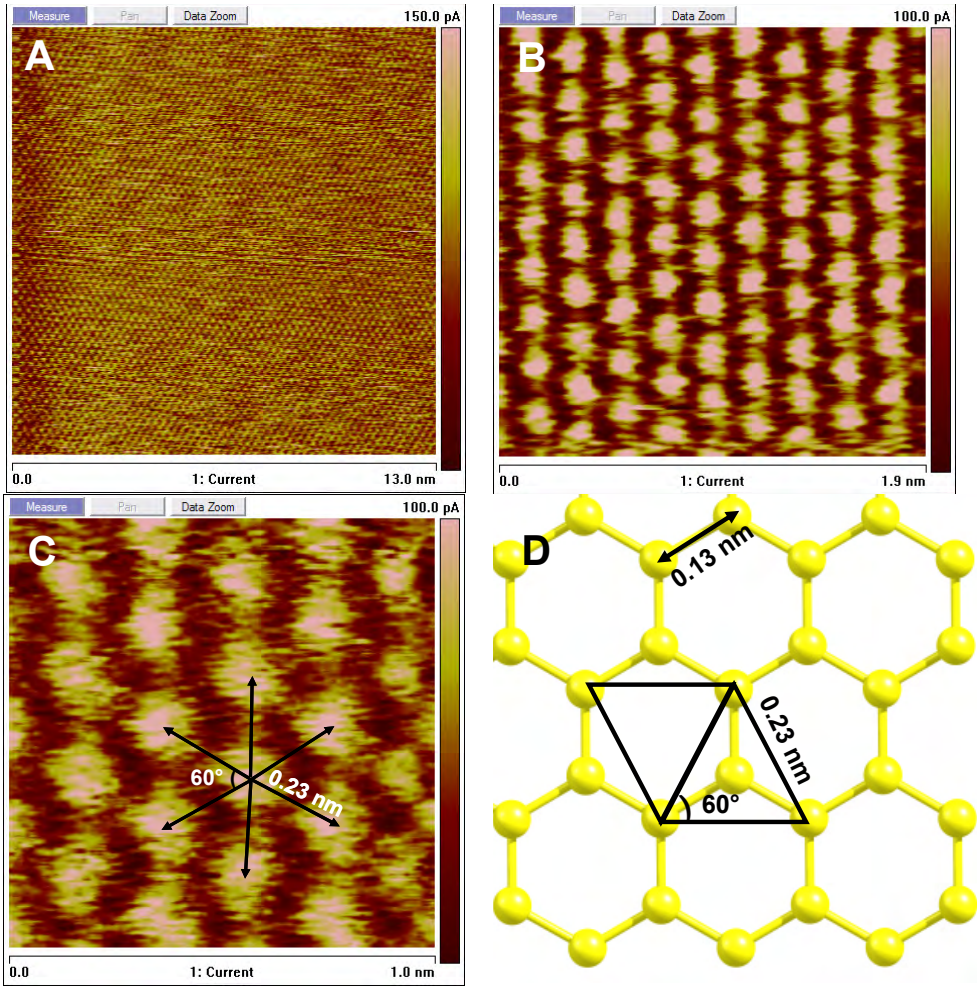

Figure 4.4. STM current images of HOPG substrate recorded at different scan sizes: (A) scan size 13 x 13 nm^2; V_{bias} = 466 mV; I_t = 0.5 nA, (B) scan size 1.9 x 1.9 nm^2; V_{bias} = 466 mV; I_t = 0.5 nA, (C) scan size 1 x 1 nm^2; V_{bias} = 466 mV; I_t = 0.5 nA and (D) schematic representation of the graphite model structure constructed by extending benzene units. Interatomic distances and angular measurements are also presented.

between adjacent spots is measured to be ~0.23 nm in all directions having an angle of 60^0 between two adjacent vectors. These bright spots are essentially the graphitic carbon atoms.

Figure 4.2D represents the carbon atoms of a graphite layer constructed by extending benzene units and show hexagonal honeycomb arrangement. The distance between the two neighboring atoms is estimated to be 0.13 nm and the angle between three adjacent atoms is found to be 120^0. Several attempts have been made by various groups[41-44] to understand the STM images of HOPG surface and brief summary is provided below. It has been concluded that due to the electronic structures that affects from the atomic plane below the surface, only every other atom (half of the atoms) of the honey comb lattice will be visible in STM data.[44] The surface of graphite possesses two types of atoms, namely α and β. In the case of a single layer of graphite sheet, the $2P_z$ states of both α and β sites have the same energy. In contrary, for crystalline graphite, the $2P_z$ states centered at the α sites of one layer overlap with that of the neighboring layer which lowers their bonding energy. This result in $2P_z$ states centered at the β sites as the highest occupied and lowest unoccupied surface states. In such cases the tunneling currents at α sites will be considerably lower than that at β sites[43] and hence only β can be visible in the STM images. In a more recent study, Hembacher et al. proved this aspect by successfully combining low force (pN) AFM with STM.[42] They could observe a number of bright spots arranged in a threefold symmetry with the lattice parameter 0.245 nm and the atomic

spacing of the HOPG surface has been reported to be 0.142 nm. Figure 4.5 shows the overlay of a benzene unit over the STM image which indicate the position of α (pink) and β atoms (green).

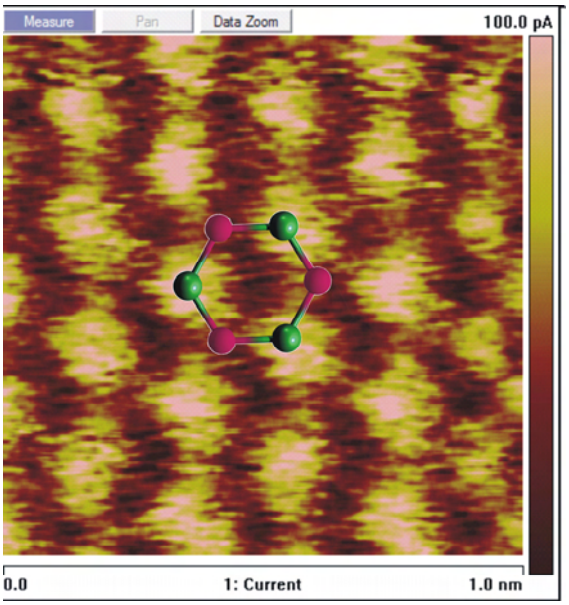

Figure 4.5. Overlay of a single benzene unit over the STM image of the graphite indicating the position of α (pink) and β atoms (green)

4.4.1. Self-organization of Phenyleneethynylenes

The samples for STM investigation were prepared by drop casting ~75 μL of a 0.1 mM solution of respective compounds (Chart 4.1) on to a freshly cleaved HOPG substrate. The samples were allowed to dry under ambient conditions and imaged on multimode scanning probe microscope in the constant height mode. As the samples were prepared through drop casting, uniform coverage is not expected over the entire HOPG substrate. The specific areas of molecular packing were located by carefully changing

the 'X' and 'Y' positions of the sample and well organized domains were observed at various locations on HOPG surface. Usually the areas of molecular packing appear as patches over the atomically flat substrate and a representative example showing the self-organization of **1** is presented in Figure 4.6.

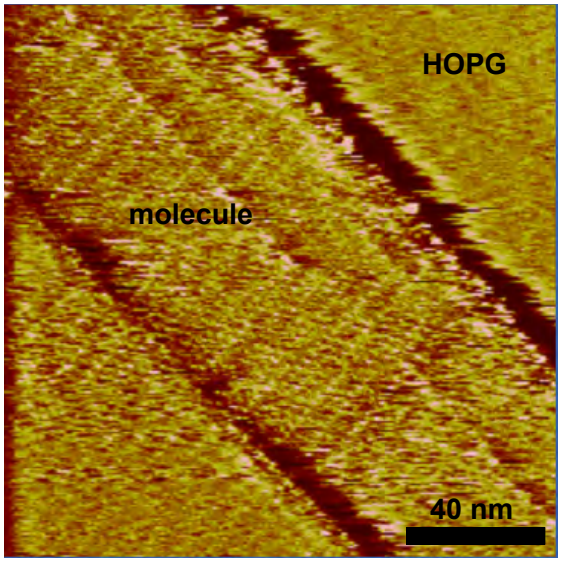

Figure 4.6. STM current image of showing the patches of self-organized regions of **1** on HOPG surface; scan size 150 x 150 nm^2; V_{bias} = -396 mV; I_t = 100 pA.

Model phenyleneethynylenes (1): To have a better understanding on molecular packing of **1** on HOPG surface, STM images were recorded at different scan sizes and are presented in Figure 4.7. When imaged at larger scan size of 45 x 45 nm^2 (Figure 4.7A) parallel arrangements of wire like structures running over several hundreds of nanometers were observed. In order to probe the organization of molecules leading to wires,

high resolution STM images were further recorded at lower scan sizes (18 x 18 nm^2) and interestingly an end to end arrangement of molecules was observed (Figure 4.7B). Usually a molecule having functional groups at both ends organizes in an end to end fashion leading to the formation of wire like structures. However, in the present case, the molecule **1** does not possess any functional groups and a wire like arrangements is not expected.

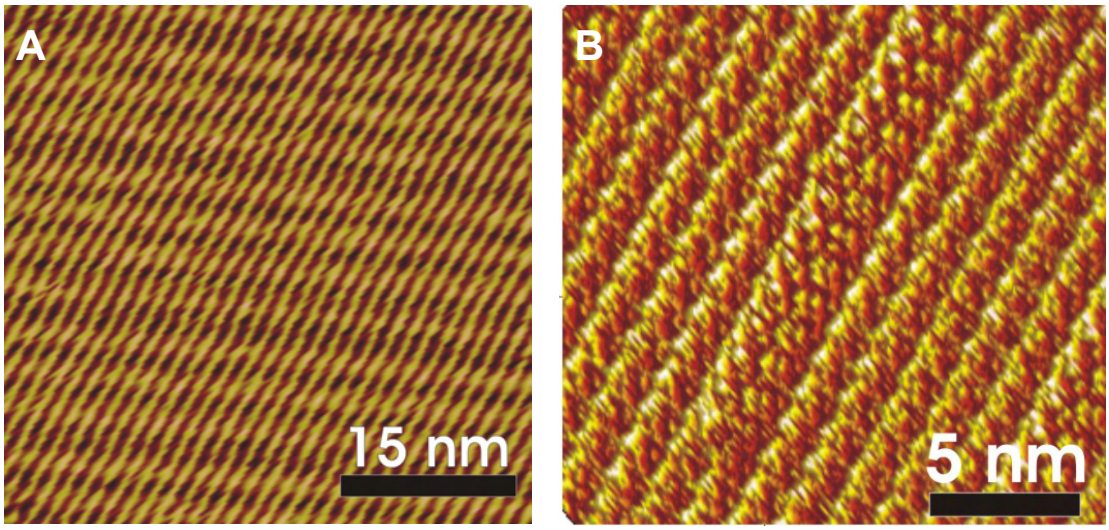

Figure 4.7. STM current images of **1** on HOPG: (A) scan size 45 x 45 nm^2; V_{bias} = 700 mV; I_t = 700 pA and (B) the real time zoomed image over a scan area of 18 x 18 nm^2; V_{bias} = -969 mV; I_t = 118 pA.

To have a better insight on the molecular interaction, high resolution images were recorded by decreasing the scan size to 6 x 6 nm^2 (Figure 4.8). Well defined bright rod like structures arranged as skewed 1D rows, each of them having an average length of 1.8±0.1 nm, were observed

throughout. In the present case the phenyleneethynylene molecules possess higher electron density along its longitudinal axis compared to the alkoxy side chains. The probability of electron tunneling is much higher along longitudinal axis consisting of π rich aromatic unit compared to the alkyl regions. Thus the well defined bright rod like structures obtained in the STM image is identified as the phenyleneethynylene core unit. This was further supported by the fact that the average length of each bright region is in good agreement with the molecular length of phenyleneethylene core (1.844 nm) calculated from the X-ray crystal structure of **1** reported by West and co workers.[37] In contrast, the alkyl regions appeared as dark due to the large energy difference between the electronic states of the aliphatic chain and the Fermi level of the substrate.[19-25] In order to have a better understanding on the self-organization of **1,** we have manually reconstructed the image by positioning the molecules on the top of bright rod like features. Further the intermolecular interactions leading to the organization of molecules along two axes were considered: interactions leading to the parallel arrangement of molecules along 'a' axis and skewed 1D organization along 'b' axis. The organization of the molecule was further characterized by measuring the unit cell parameters 'a', 'b' and 'γ' and the average distance between identical points along 'a' axis is measured as 1.3 nm and that along 'b' axis

as 1.2 nm. The angle between these two vectors is calculated as $\gamma = 98^0$. The inner distance between bright regions is 1.19±0.1 nm suggesting that there is enough room for alkyl chains to interdigitate. The hexyloxy group has a length of 9.496 Å in the extended conformation. The analysis of the manually reconstructed image indicates that with in each of the wire like structures (along 'b' axis), the molecules are arranged such a way that the phenyl unit of one molecule is in close proximity to the acetylinic triple bond of the neighboring molecule.

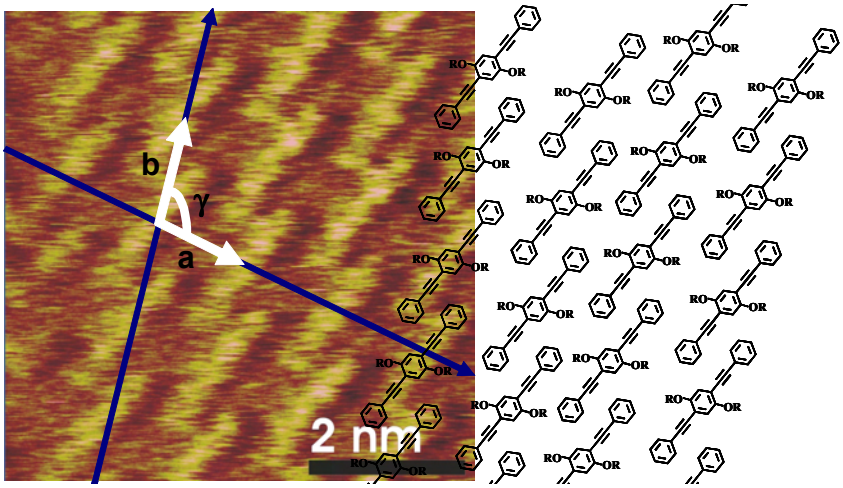

Figure 4.8. High resolution STM current image showing the skewed 1D organization of **1**; scan size 6 x 6 nm^2; V_{bias} = -1072 mV; I_t = 400 pA. A tentative model of the molecular organization constructed by manually positioning the molecules above the bright features is shown on the right side of the image.

To have a better understanding on the various intermolecular interactions leading to the formation of organized structure, the crystal packing[37] of the molecule were analyzed. The 3D crystal structure shows a

herrine-bone fashion arrangement of molecules (Figure 4.9) and the organization is stabilized by very weak non-conventional hydrogen bonding interactions. A careful slicing analysis of the crystal structure revealed that the 3D organization is mainly stabilized through the (i) acetylenic π-alkyl CH, (ii) acetylenic π-aromatic CH, (iii) alkoxy oxygen-aromatic CH interactions. These interactions can be clearly viewed in Figure 4.10. The sliced image presented in Figure 4.10A shows that the molecules in a plane are stabilized through the interdigitation of alkyl chains and the hydrogen bonding interaction between the alkyl CH (of the terminal CH_3 group) and the acetylenic π-electron cloud of the neighbouring molecule. Similarly, the orthogonal arrangement of the molecule is stabilized through the hydrogen bonding interaction of the aromatic CH with alkoxy oxygen and the π-electron cloud of the acetylenic bond (Figure 4.10B).

From the X-ray crystal structure[37] it is clear that a constant distance of 1.36 nm is maintained between the molecules in a plane through the interdigitation of the hexyloxy chain and the hydrogen bonding between the terminal alkyl CH and acetylenic π-bond. Interestingly, this value has close resemblance with the intermolecular distances observed along the 'a' axis of the STM images (1.3±0.1 nm), indicating that the interdigitation of hexyloxy chains and CH**...**π interactions assist the organization of molecules as strips along 'a' axis.

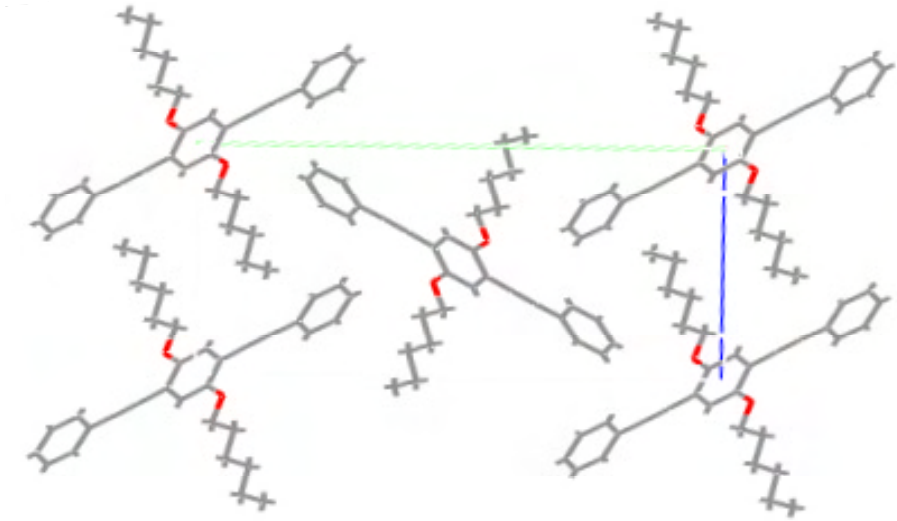

Figure 4.9. Crystal structure of molecule **1** (reported by west and coworkers; adapted from reference 37)

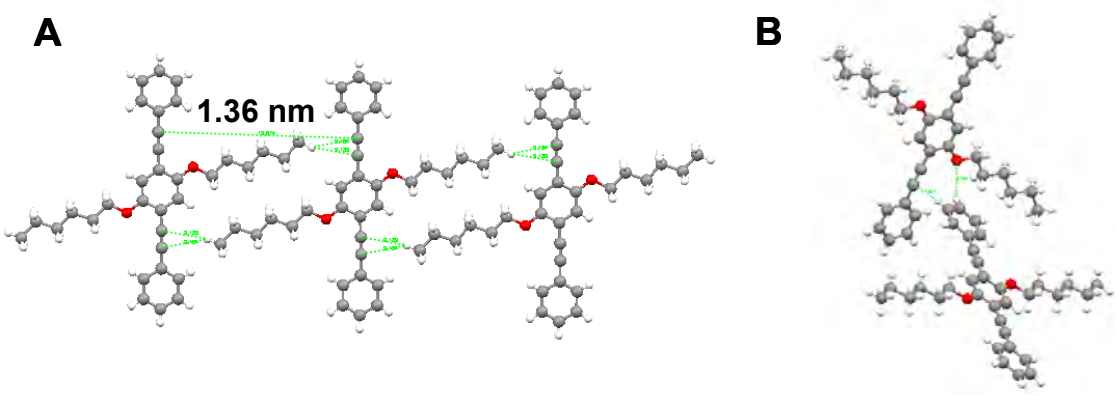

Figure 4.10. Sliced crystal structures showing the interdigitation of alkyl chains and weak noncovalent interactions.

Thus, the initial steps of molecular assembly involve the interdigitation of hexyloxy chains and the hydrogen bonding interaction between the alkyl CH-acteylinic π interactions leading to the organization of molecules as strips along the 'a' axis. Interlocking of two such strips leads to the formation of self-assembled structures which results in the

organization of molecules along 'b' axis in skewed 1D fashion. The interaction of molecules along 'b' axis may be further stabilized through the hydrogen bonding between the aromatic CH and acetylenic π bond.

Further we have analyzed the organization of molecules on a larger area. Interestingly, domains with three types of molecular organizations (type I, II and III) having close resemblance were observed (Figures 4.11). Each domain extends over an area of ~150-200 nm^2. It is interesting to note that these molecular packing have several similarities: (i) possess a parallel strip like arrangement along the 'a' axis ('*a-strip'*) and (ii) a skewed 1D arrangement along the 'b' axis ('*b-strip'*). In all the case, the average distance between identical points on adjacent molecules along '*a-strip'* is 1.3±0.1 nm (averaged over 10 images) suggesting that the strip is formed through the interdigitation of hexyloxy chains (*vide supra*). The major difference between these arrangements is the extent to which the phenyleneethynylene molecules on adjacent '*a-strips'* overlap: decreases in the order of type I > type II > type III (see the encircled portions). In the case of type I arrangement, the end phenyl group of one molecule is interlocked up to the acetylenic region of the neighbouring molecules where as the end phenyl groups are in the close proximity for the type II packing. An entirely different organization, in a staircase fashion, was observed in the case of type III image. A close analysis of these images

further showed that the angle of orientation of phenyleneethynylene core (bright features) with respect to the 'a' axis is the same (70°) for Figures 4.11A,D and different for 4.11B (83°). This raises another interesting question how various types of organizations are formed from the same molecule. These aspects were further analyzed using computational methods.

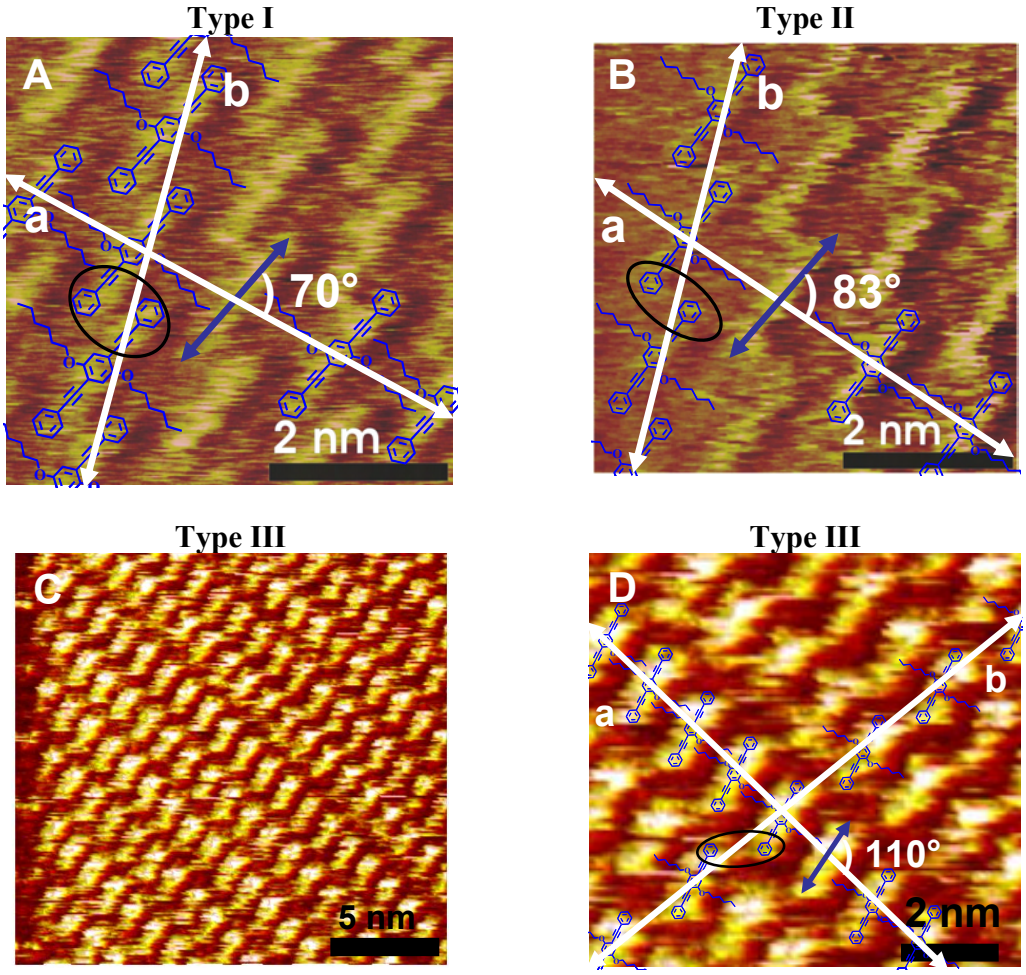

Figure 4.11. STM images of **1** at various domains illustrating different types of molecular packing (A, B) scan size 5 x 5 nm^2; (C) scan size 20 x 20 nm^2; V_{bias} = -1274 mV; I_t = 638 pA (D) Zoomed image of C, scan size 8.5 x 8.5 nm^2.

From the results presented above, it is clear that interdigitation of hexyloxy chains plays a major role in the self-organization of **1**: various possible modes of hexyloxy chain interdigitation were analyzed for explaining the three types of molecular assemblies observed in STM studies (Figure 4.11). It can be seen that with respect to the hexyloxy groups, the adjacent molecules can interact with the acetylenic moiety (through alkyl CH interaction), either from the '*ortho'* or '*meta'* position, leading to type I or type II interaction, respectively ('x' and 'x'' in Scheme 4.2). The extension of such structures can lead to the formation of 1D organization ('y' and 'y'' in Scheme 4.2) similar to that observed as '*a-strips'* in the STM images. It has been further noticed that the phenyleneethynylene core unit makes an acute angle with the 'a' axis which has close resemblance with the '*a-strips*' of type I and type III organization (Figures 4.11A, D). In contrast, the molecules are arranged in more or less right angle to the 'a' axis in 'y'' of Scheme 4.2 and show close resemblance with the '*a-strip*' of type II packing (Figure 4.11B).

Various possibilities of interlocking of '*a-strips*' were analyzed to explain the formation of 2D assemblies (Schemes 4.2 and 4.3). However, the extent to which the strips interlock differs in type I and type II assemblies due to the steric restrictions imposed by the hexyloxy group. The '*ortho*' arrangement of type I interactions result in the close packing of

hexyloxy groups, leaving enough space for interlocking of adjacent '*a-strips'*. In contrast, due to the '*meta*' arrangement, hexyloxy chains are more separated to each other in the case of type II interaction.

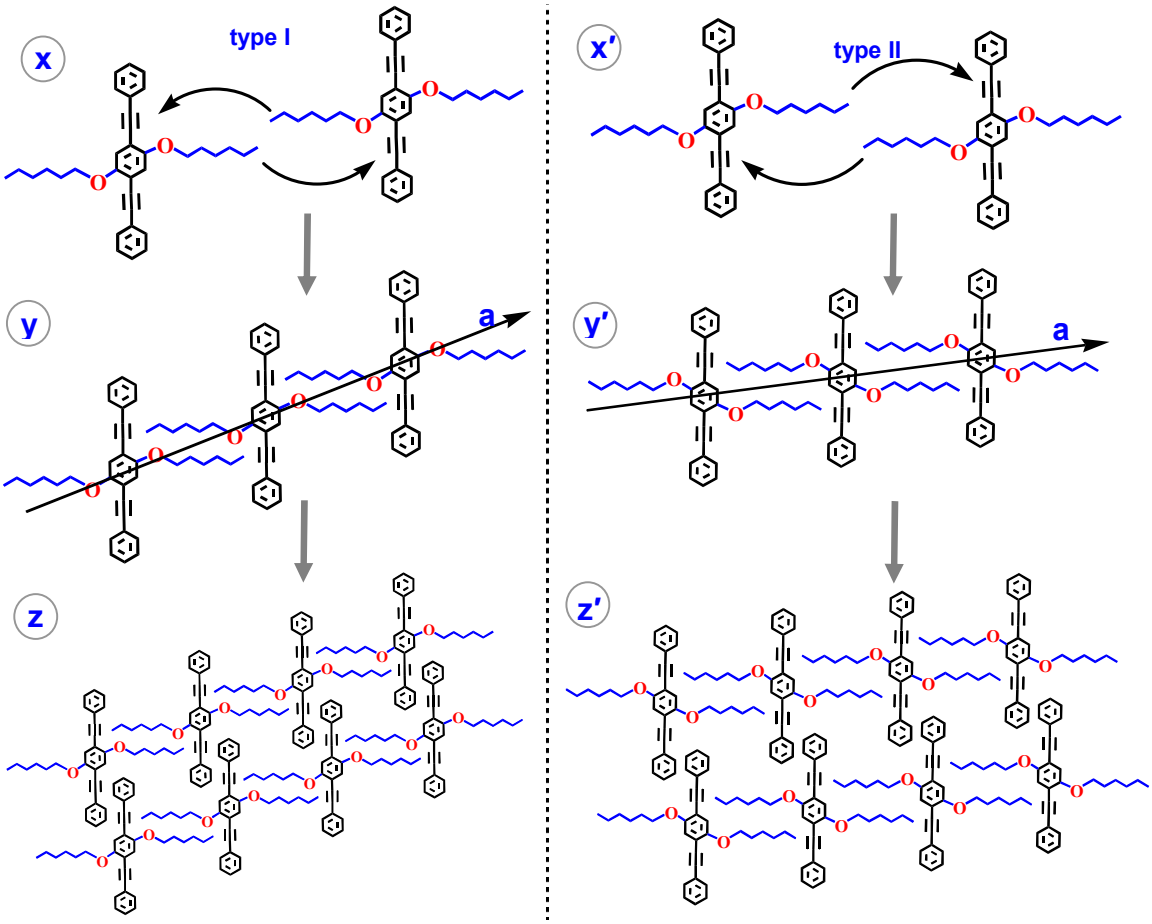

Scheme 4.2. Two possible modes of (x) *ortho* and (x') *meta* interdigitation of hexyloxy chains leading to the formation of two types of '*a-strips*' (y and y') and their interlocking into extended 2D assemblies (z and z').

The major difference between the type I/II and type III images are the way in which the adjacent '*a-strips*' are interlocked. In type III images (Figure 4.11D) strong acetylenic π-aromatic CH interactions allows the

interlocking of adjacent '*a-strips*' in a tilted fashion as shown in 'b' of Scheme 4.3. Such an interaction is only possible if the interlocking strips are out of plane to each other (a_1 and a_2 in Scheme 4.3 are rotated by 180° along the molecular axis) leading to a close packed structure. Extension of

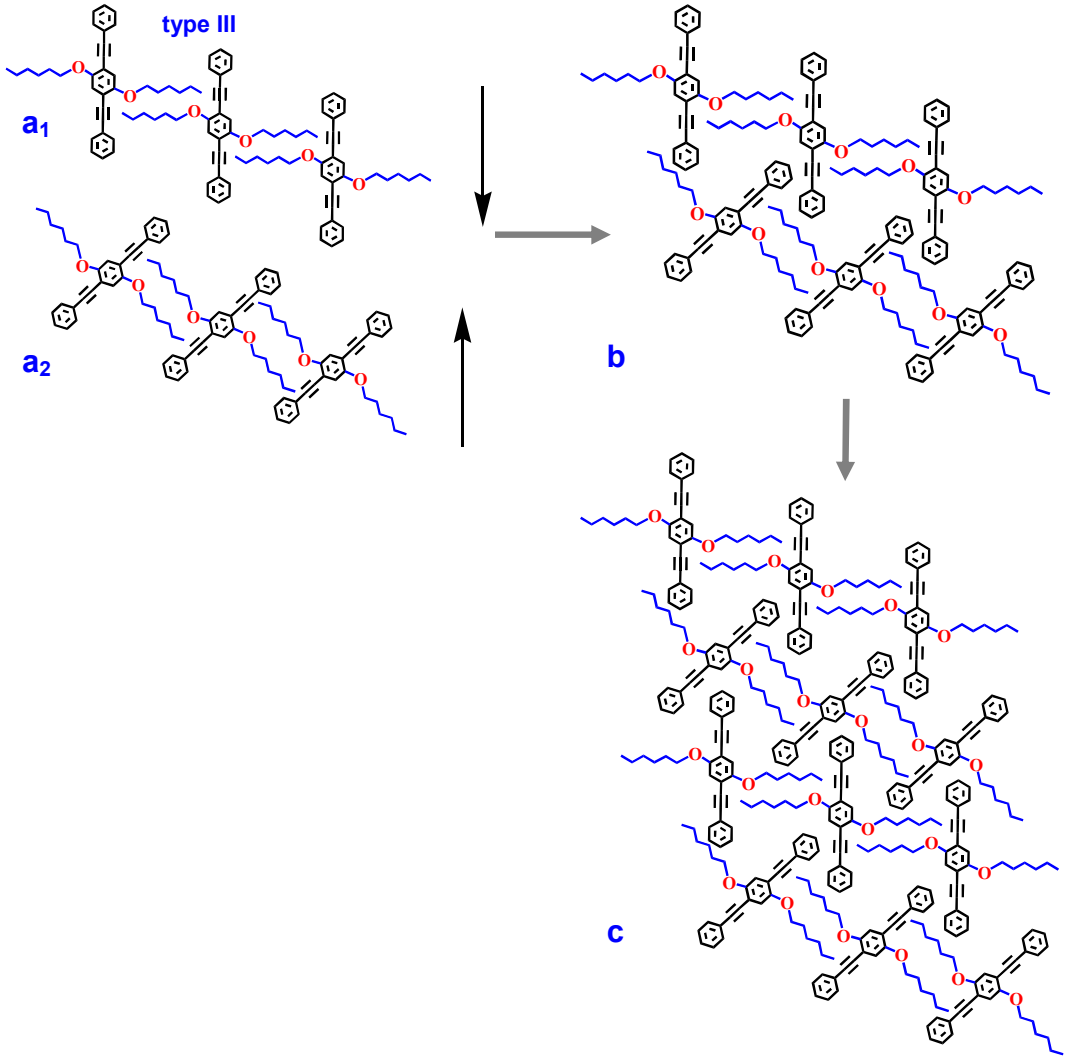

Scheme 4.3. Interlocking of two similar '*a-strips*' in a tilted fashion, with two different faces, leading to the formation of type III structures.

this organization lead to the type of molecular packing presented in Figure 4.11D. It is interesting to note that in type III organization, alternate layers of molecules are arranged parallel fashion.

Further, the mechanism of formation of self-organized structures was analyzed through molecular modeling experiments (Figure 4.12 and 4.13). The formation of '*a-strips*' is modeled by optimizing the geometry of a pack of three molecules each which were formed by interdigitating the alkyl chains at the AM1 level. For mimicking the molecular packing on surface, constraints were applied during the geometry optimization, to keep the carbon atoms of along the molecular axis of two adjacent molecules in the same plane by fixing appropriate dihedral angles. However, this restriction will allow the free rotation of the phenyl rings and the movement of the hexyloxy chains. The optimized geometries presented in Figures 4.12 clearly indicate that the two modes of interdigitation of hexyloxy chains resulted in two types of '*a-strips*'. The '*ortho*' interdigitation showed close packing of the hexyloxy chains with CH**...**π interactions and relatively strong alkyl CH**...**O interactions (Figure 4.12A). This packing is characterized by the orientation of molecules at an angle 65° with respect to the strip axis and closely resembles with the experimentally observed values of type I and type III images. On the other hand, '*a-strip*' formed through *meta* interdigitation possesses only alkyl

CH•••π interactions on the acetylenic π bond (Figure 4.12B). The analysis of the structure showed that the phenyleneethynylene units are oriented at an angle 84º with respect to the strip axis and this value is in close resemblance with the orientation of bright spots presented in Figure 4.11B (type II packing).

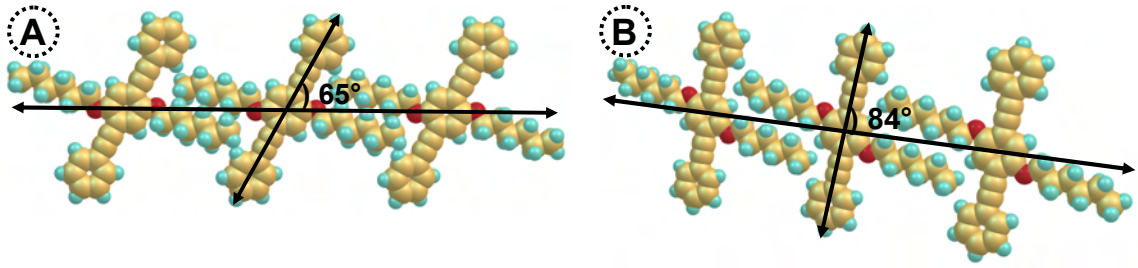

Figure 4.12. AM1 level optimized structures of two types of '*a-strips*': (A) *ortho* and (B) *meta* interactions of hexyloxy groups. (*optimized using Gaussian 03*[†])

Further the geometry optimization of molecular assemblies was performed with a pack of six molecules at the AM1 level and the corresponding energy minimized structure is presented in Figure 4.13. Theoretical calculations clearly indicate that the way in which the hexyloxy chains interdigitate play a decisive role on the extent of interlocking of two '*a-strips*'. For example, in the optimized structure of type I assembly (Figure 4.13A), the terminal phenyl groups in an '*a-strip*' is inserted up to the acetylenic regions of adjacent '*a-strip*'. Thus the extent of overlap of phenyleneethynylenes in adjacent '*a-strips*' is maximum in type I arrangement and the interlocking is very effective. This molecular packing

is in close resemblance with the STM image presented in Figure 4.11A. From the molecular calculations, it can also be seen that the 2D-organization is further stabilized through CH**...**π interactions between the aromatic CH and acetylenic π bond. In contrast, type II assembly has a lesser extent of interlocking of '*a-strips*' and the optimized 2D assembly is stabilized by aromatic CH**...**aromatic π interactions. The optimized molecular packing (Figure 4.13B) resembles well with the STM image shown in Figure 4.11B. This was further supported by the fact that the

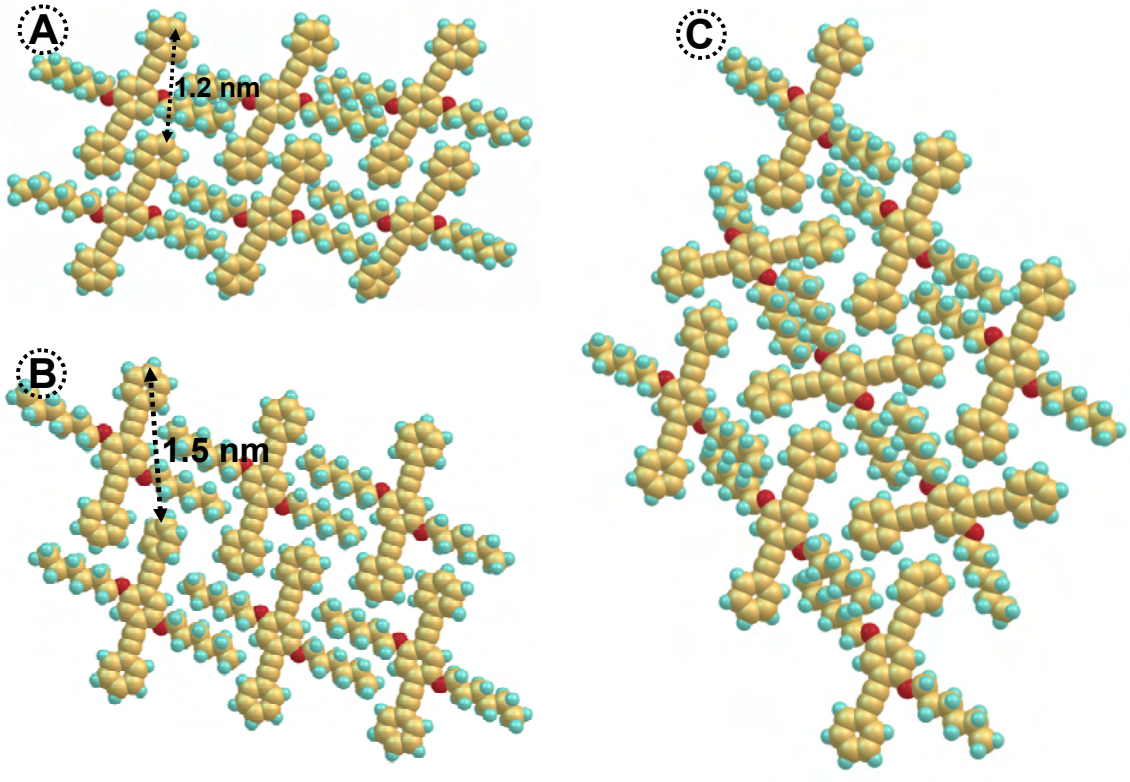

Figure 4.13. AM1 level optimized structures of 2D molecular packing formed through interlocking of '*a-strips*': (A) type I, (B) type II and (C) type III organizations. (*optimized using Gaussian 03*[†])

orientation of molecules along 'a' axis and the measured distances between the identical points along the '*b-strip*' in the STM images (70° and 1.2 nm in Figure 4.11A; 83° and 1.5 nm in Figure 4.11B) are in good agreement with the values presented in Figures 4.13A,B through molecular modeling experiments.

Further the molecular organization of type III assembly is investigated by the geometry optimization of a pack of 9 molecules at the AM1 level and presented in Figure 4.13C. Analysis of the energy minimized structure revealed that the organization is stabilized through aromatic CH-aromatic π hydrogen bonding interactions.

Effect of alkoxy chain length: Further the effect of alkoxy chains on the self-organization was investigated by synthesizing a phenyleneethynylene molecule bearing $OC_{12}H_{25}$ on the 2,5 positions of the central phenyl ring (**2**). The STM current images of **2** over a larger scan size of 75 x 75 nm^2 (Figure 4.14A) indicate that the molecule self-assemble in a parallel wire like arrangement. However, the spacing between the wires is found be much higher than that observed for **1**. The organization of molecules was further investigated by reducing the scan size. STM current image recorded at scan sizes 10 x 10 nm^2 shows bright rod like features arranged in an end to end fashion (Figure 4.14B). The length of each bright rod like feature is measured to be 1.8±0.1 nm which is assigned as

phenyleneethynylene units. The molecular packing is characterized by measuring the 2D unit cell parameters as a = 2.2 nm; b = 1.3 nm; γ = 72º. The distance between identical points along 'a' axis is

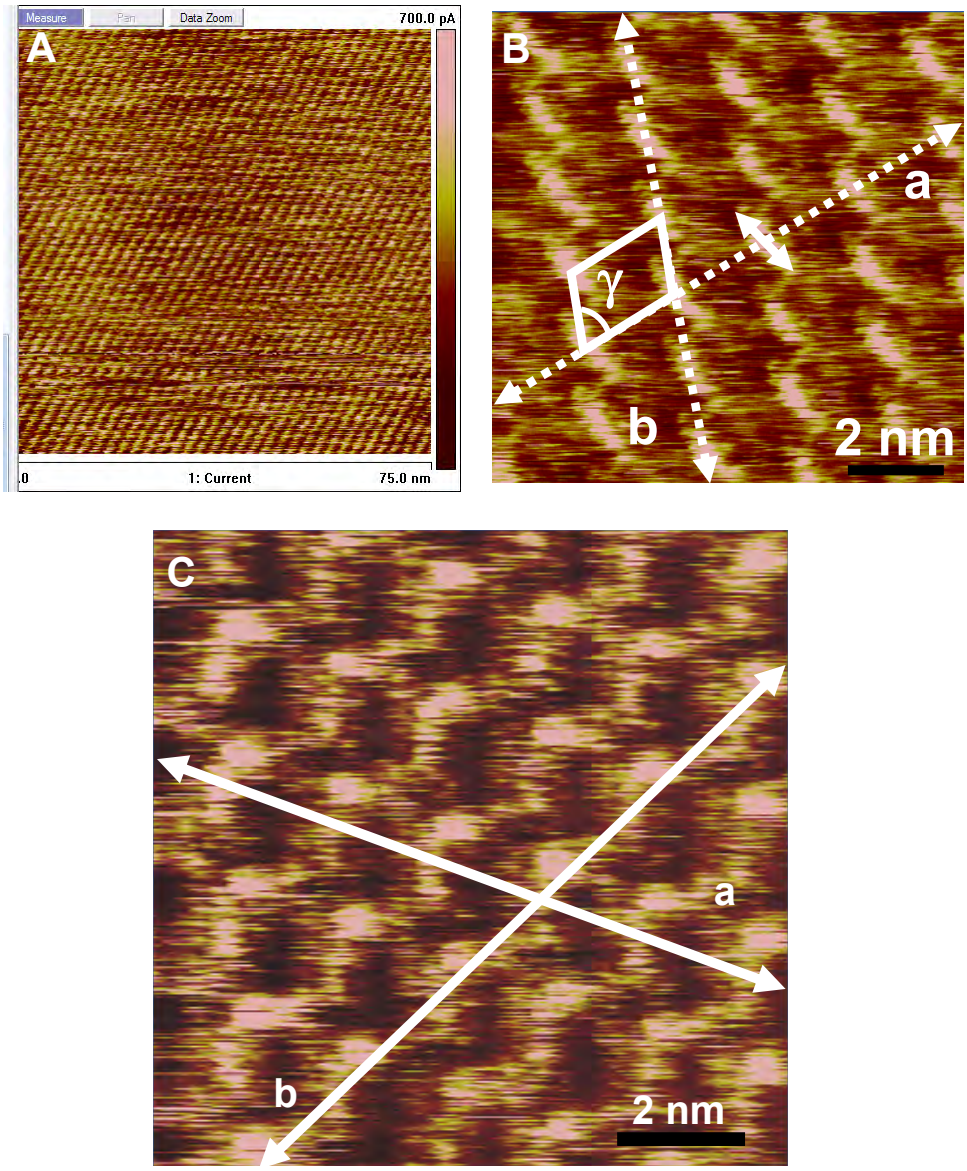

Figure 4.14. STM current images of self-organized structures of **2**; Scan sizes (A) 75 x 75 nm^2 V_{bias} = -1040 mV; I_t = 0.9 nA, (B) 20 x 20 nm^2 V_{bias} = 1010 mV; I_t = 500 pA and (C) 10 x 10 nm^2 V_{bias} = -615 mV; I_t = 534 pA.

found to be 2.2 nm indicating that there is enough room to accommodate $OC_{12}H_{25}$ chains in its extended conformation. A comparison of this data with that observed for molecule **1** suggests that the spacing between the molecular wires can be controlled by the appropriate choice of the alkoxy group.

Careful STM imaging revealed that molecule **2** also forms domains having different types of molecular packing. For example, a staircase type of organization of molecules was observed at various locations (Figure 4.14 C). In all the cases, the distance between identical points along 'a' axis remains constant as 2.2 nm indicating that interdigitation of alkoxy chains drives the organization of molecules as '*a-strips*'. As in the previous case, the mechanism of self-organization of **2** can be explained based on various interactions. These include (i) interdigitation of alkoxy chains leading to the formation of molecular strips along 'a' axis and (ii) interlocking of '*a-strips*' leading to the formation of extended 2D organization, stabilized through weak aromatic CH-acetylenic as well as aromatic π interactions. Various modes of interlocking of '*a-strips*' lead to the formation of different types of molecular packing and the detailed mechanism is presented in Scheme 4.4. The STM images presented in Figures 4.14A and 4.14B has the molecular arrangements as shown in Scheme 4.4C and 4.4D, respectively.

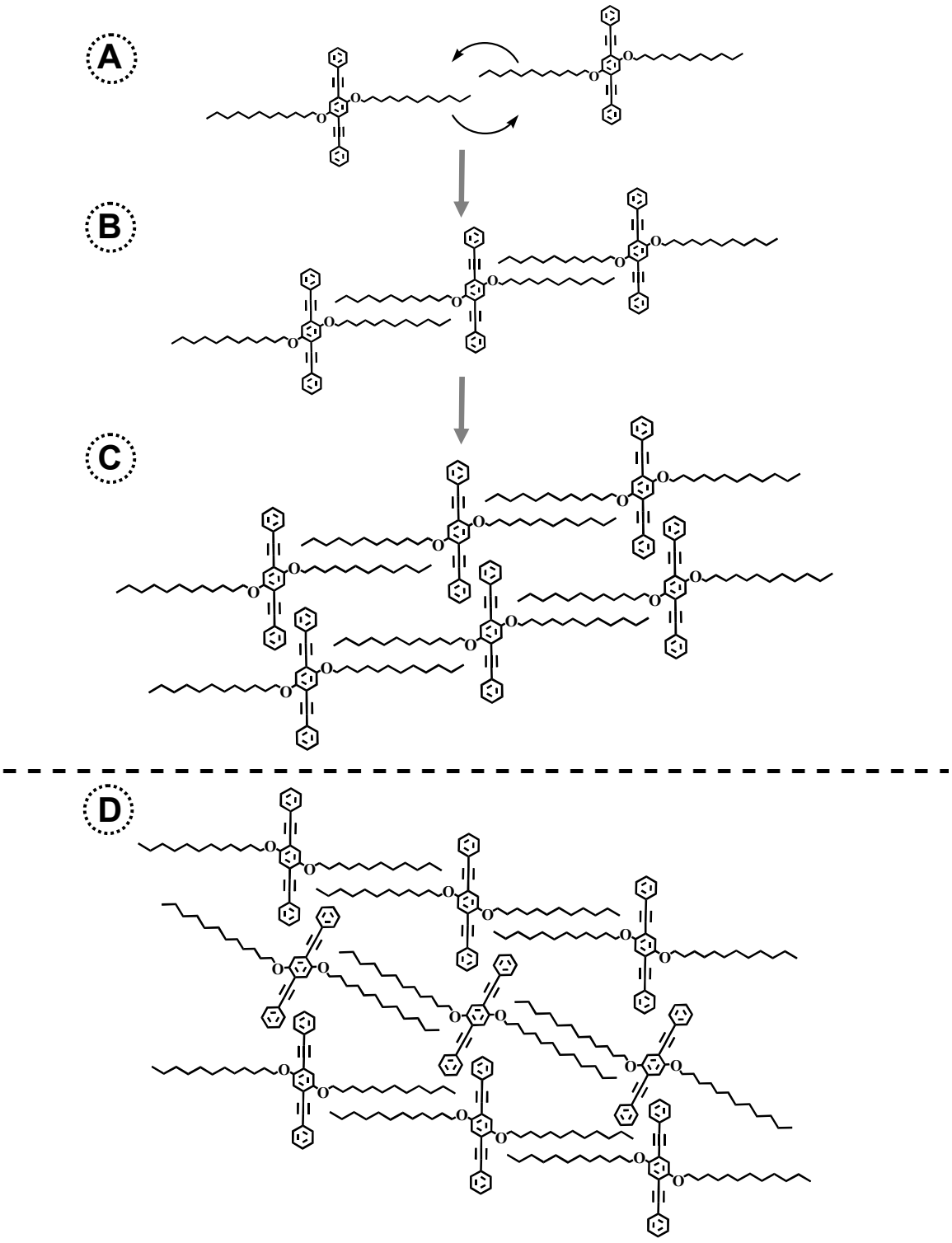

Scheme 4.4. Interdigitation of alkoxy chains leading to the formation of '*a-strips*' and their interlocking into extended 2D assemblies.

Chiral molecular arrangements on surface: Interestingly, analysis of STM images of various domains indicated the presence of mirror image type arrangements. A representative example from two domains is presented in Figure 4.15. Phenyleneethynylene core can be visible as bright rods having a length of ~1.8 nm, and the unit cell parameters of packing are the same in both cases. It can be seen that the phenyleneethynylenes are oriented at an angle of ~70º with respect to the 'a' axis and the way in which these molecules orient on surface clearly support mirror image arrangement.

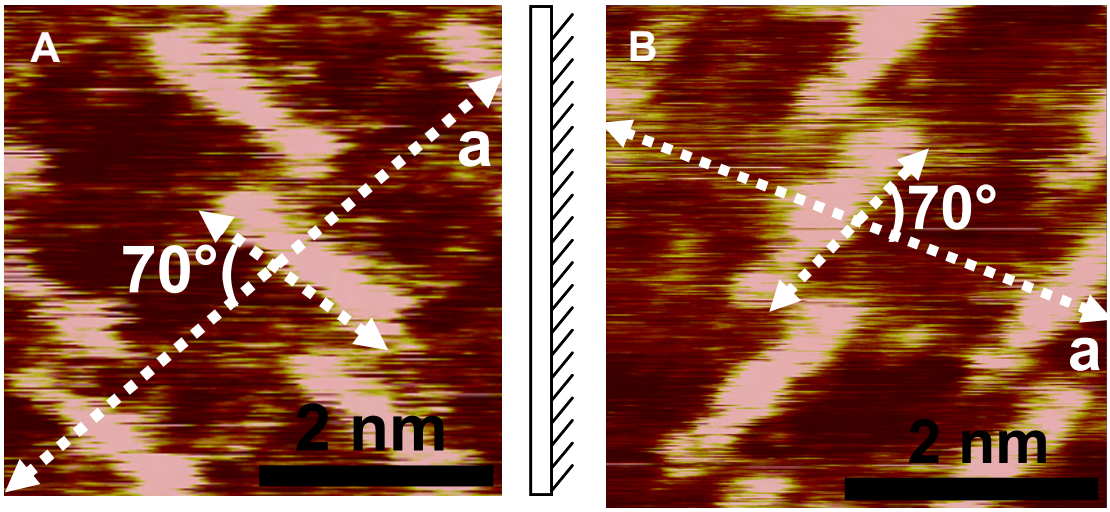

Figure 4.15. STM current images of **2** illustrating enantiomeric assembly: (A) scan size 5 x 5 nm^2; V_{bias} = -872 mV; I_t = 717 pA and (B) scan size 5 x 5 nm^2; V_{bias} = -872 mV; I_t = 717 pA.

Adsorption of molecular systems on surfaces often reveals pronounced stereochemical effects and STM is an effective tool for

studying these arrangements with submolecular resolution.[45] The most obvious case is when a chiral molecule adsorbs on surface and transfers its chirality to adsorption system. On the other hand for highly symmetric adsorbate, surface chirality arises, if they adsorb in such a way that the molecule-surface system in combination does not have any mirror symmetry elements. These molecules are achiral in the gas phase however exhibits a chiral arrangement once adsorbed on to surfaces. This effect originates from the confinement of molecules in two dimension which removes mirror symmetry in the plane of the substrate. Such molecules are said to be prochiral and their adsorption on surface can in principle lead to equal amounts of mirror-image surface enantiomers. It has been believed that the confinement on the surface would be sufficiently strong to render the chiral sense of an individual prochiral molecule upon adsorption. The phase separation has been ascribed to the lateral mass transport in combination with intermolecular chiral recognition at domain boundaries.[46,47]

In order to investigate these aspects different possibilities of interaction of phenyleneethynylene on surface were analyzed. The molecular modeling calculations, in combination with STM data indicate that the alkoxy side chains prefer an extended conformation. The molecule in this conformation has a highly symmetric planar structure with point

group (C_2h) and symmetry elements (S_2, C_2, C_s, C_i). In the present case, the two faces of the achiral molecule are interchangeable only by the actions of symmetry plane, center of symmetry or the alternating axis of symmetry but not by any of the simple symmetry axis. Hence, the two phases of the molecule are enantiotopic and the molecule is said to be prochiral.[48,49] Usually when an achiral reagent either complexes or reacts with one of the enantiotopic groups, it destroys the symmetry element and creates a racemic product mixture. Resolution of racemates into pure enantiomers is a challenging problem and requires additional chiral elements. Conglomerate formation, that is, the spontaneous resolution of racemic mixtures into equal amounts of enantiomerically pure crystals is a very potential and useful phenomenon but are reported only for few cases (About 5-10% of racemic organic compounds crystallize as conglomerates).[49] In such cases the additional chiral element that promotes resolution is the interaction of a second molecule of the same enantiomorph.

In the present case, the adsorption of the molecule **2** on to the planar HOPG substrate removes its centre of symmetry, mirror symmetry and the alternating axis of the symmetry. Hence the two modes of adsorption of molecule (with either faces) results in energetically similar but nonsuperimposable mirror images (Figures 4.16C,D). During the formation of '*a-strips*', the interaction of the second molecule with similar

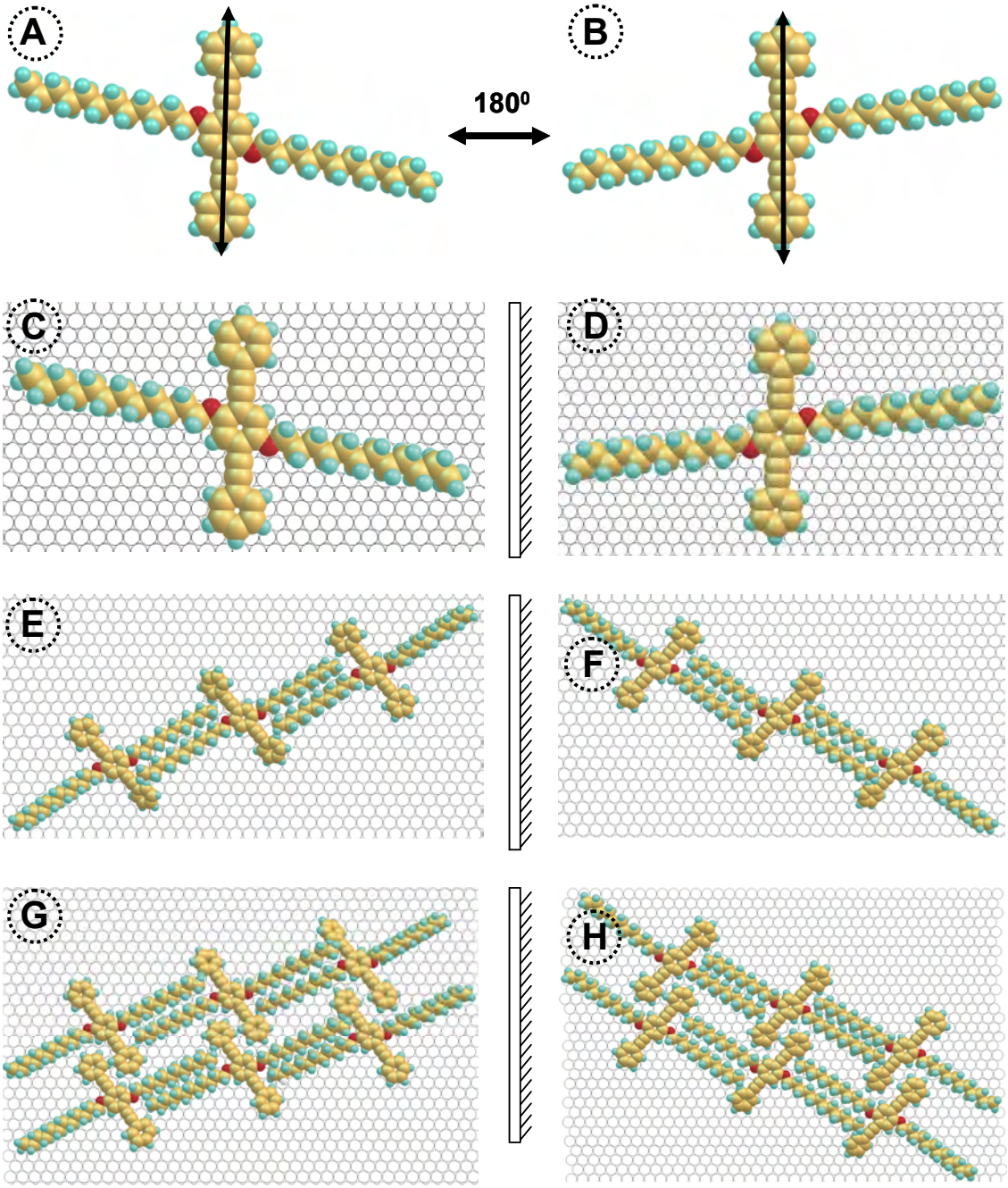

Figure 4.16. Various energy optimized geometries of **2** and their assemblies: (A,B) two enantiotopic faces of **2**, (C,D) adsorption of **2** on to the surface with the two faces resulting in the formation of enantiomeric systems, (E,F) formation of enantiomeric '*a-strips*' through the alkoxy interdigitation, (G,H) interlocking of '*a-strips*' into enantiomeric domains. (*optimized using Gaussian 03*[†])

enantiomorphic face is more thermodynamically favored. This results in an ordered and compact arrangement with relatively strong intermolecular interactions (Figures 4.16E,F). The enantiomeric '*a-strips*' thus formed further extends to 2D organization through interlocking of two similar enantiomophic '*a-strips*' which is thermodynamically favorable (Figure 4.16G,H). The images presented in Figures 4.15A,B has chiral molecular arrangements on surfaces and their corresponding geometry optimized structure are presented in Figures 4.16G,H respectively. Thus the adsorption of molecule with two faces results in enantiomeric 2D structures as observed in the STM images.

Effect of functional group: To control the self-assembly of molecules on surfaces, a phenyleneethynylene molecule bearing two hydroxyl groups at both ends (**3**) were synthesized. The samples for STM investigations were prepared by drop casting a 0.1 mM solution of **3** in 1,2,4-trichlorobenzene (75 μL) on to a freshly cleaved HOPG substrate. The solvent was removed by room temperature evaporation and imaged on a Multimode Scanning Probe Microscope (Nanoscope IV) controlled in the constant height mode. Figure 4.17A shows the large scan size (75 x 75 nm^2) STM current images of the self-assembled monolayers of **3** over HOPG. Similar to the previous cases, a number of the parallel wire-like structures, having a regular spacing of 1.3 nm, were observed. In the present case, the wire-like

structures (along 'b' axis) are found to be intermittent at regular intervals. A close analysis of the large scan size image showed the presence of two types of organizations (Figure 4.17 A) which were labeled as type I and type II (see the regions inside the encircled portions).

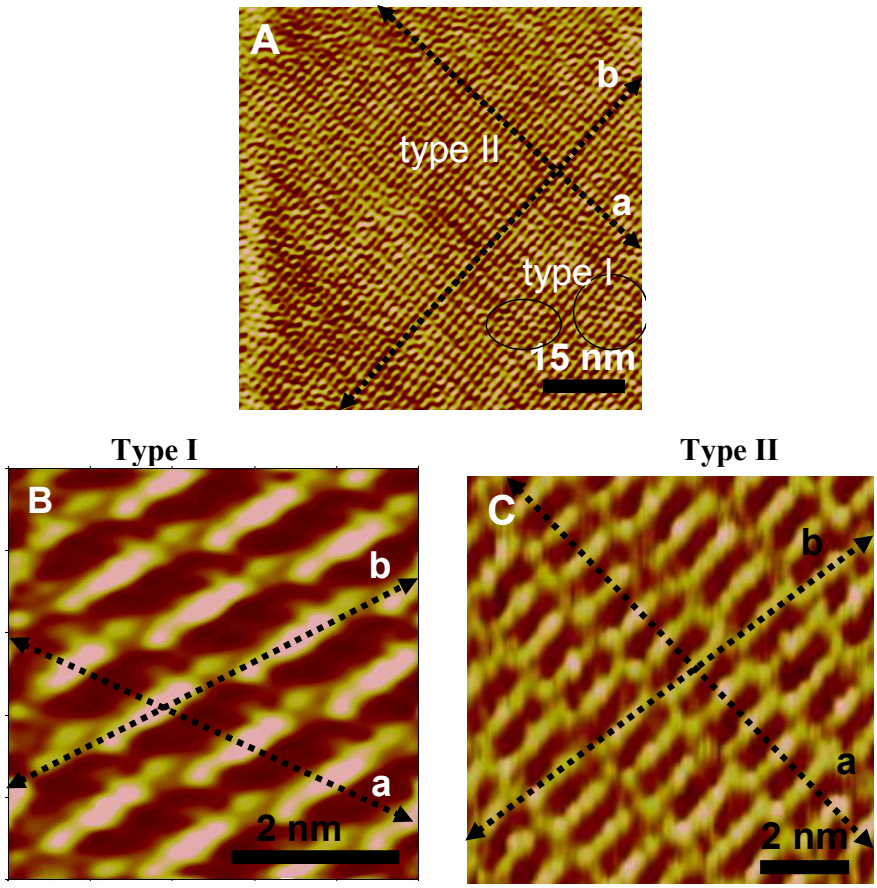

Figure 4.17. STM current images of **3** on HOPG substrate: (A) scan size 75 x 75 nm^2; V_{bias} = -1215 mV; I_t = 318 pA, (B) real time zoomed image of type I organization; scan size 5 x 5 nm^2; V_{bias} = -966 mV; I_t = 360 pA and (C) real time zoomed image of type II organization; scan size 10 x 10 nm^2; V_{bias} = -900 mV; I_t = 700 pA.

Real time zoomed images of the two regions showing different types of organization are presented in Figures 4.17 B,C. In both cases the bright rods assigned as phenyleneethynylenes which are arranged in an end to fashion along 'b' axis with a small gap between the molecules. The end to end organization is attributed to the hydrogen bonding interaction of the hydroxyl groups present at the terminal positions of the phenyleneethynylene. Molecule **3** possesses lower electron density at the terminal positions due to the presence of CH_2OH groups and hence less conducting. The hydrogen bonded regions appears less bright in STM images with slight steps between the molecules along 'b' axis. The molecules are arranged parallel along 'a' axis in both cases, however they are oriented ~60º in type I and ~85º in type II arrangement. From these results it is clear that the two organizations arise from the two possible modes of interdigitation of hexyloxy chains. These aspects were further investigated through molecular modeling experiments.

Molecular modeling experiments were performed by geometry optimization (AM1 level) with a pack of six molecules, corresponding to each assembly. A careful analysis of the geometry optimized structures presented in Figure 4.18 revealed that the major intermolecular interactions leading to type I assembly are (i) interdigitation of alkoxy chains and the resulting CH**...**O hydrogen bonding interaction between

terminal alky CH and hexyloxy oxygen and (ii) OH**...**OH hydrogen bonding interaction between CH_2OH groups. In contrast, the type II assembly is stabilized through (i) interdigitation of hexyloxy chains resulting in CH**...**π hydrogen bonding interaction between terminal alkyl CH and acetylenic π electron cloud and (ii) OH**...**OH hydrogen bonding interaction between CH_2OH groups. This was further supported by the fact that, with respect to the 'a' axis, phenyleneethynylene core makes an angle 61º in type I and 85º in type II assembly which is in good agreement with the observed values in Figure 4.17B,C.

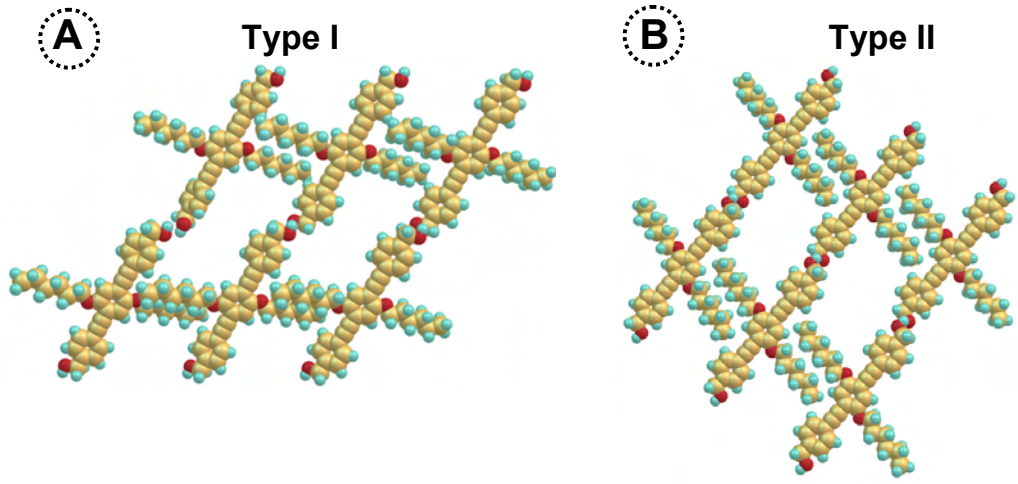

Figure 4.18. Geometry optimized structures type I and II assemblies formed through (A) *ortho* and (B) *meta* interactions of hexyloxy chains and the hydrogen bonding between the terminal hydroxyl groups. (*optimized using Gaussian 03*[†])

Bis-fullerene with phenyleneethynylene spacer: Fullerenes form a class of spherical molecules with nanoscale dimensions having interesting optical and electrical properties. Following to the discovery of fullerene-(C_{60}),

research have been directed towards the development of fullerene based hybrid materials. Bis as well as tris fullerene derivatives linked through flexible (alkyl chains) and rigid (phenyleneethynylene) spacer groups were earlier synthesized in our group at NIIST and their photophysical properties were investigated.[40,50] Tour and coworkers have extensively investigated the use of phenyleneethynylenes as a mechanical bridge between fullerene units and constructed nanoscale vehicles such nanocars and nanobikes (a representative example is shown in Figure 4.19).[51]

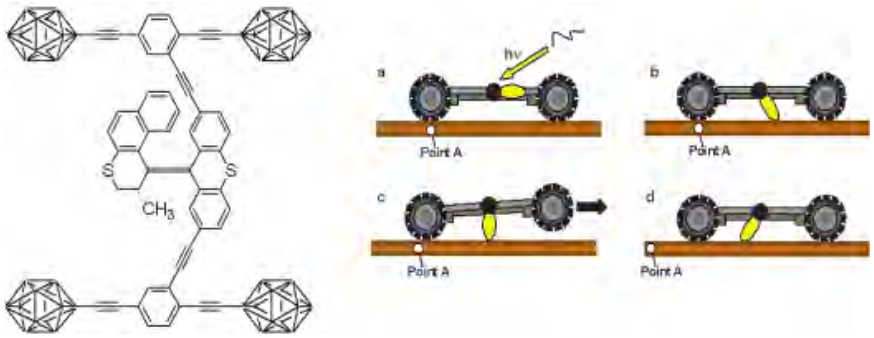

Figure 4.19. Schematic representation of photo-active motorized nanocars reported by Tour and coworkers. (*adapted from reference 51*)

Fullerenes form optically transparent clusters. These clusters are excellent acceptors of electrons and the transferred electrons survive for several hundred microseconds in the clustered network, compared to isolated molecules. This was attributed to the hopping of electrons between the fullerene molecules in the cluster network. More recently, a dumbbell shaped fullerene molecule was synthesized in our group by linking two **C_{60}**

using a phenyleneethynylene rigid molecule and investigated their clustering using AFM studies.[40] In order to obtain a better understanding on the basic interaction between the fullerene units in bisfullerene possessing phenyleneethynylene (**4**), STM studies were performed.

In the present study, lower concentrations of **4** were used in order to avoid the possibility of clustering. The samples for STM images were prepared by drop casting a 0.1 mM solution of **4** in 1,2-dichlorobenze on to a freshly cleaved HOPG substrate. The samples were allowed to dry in air at room temperature and imaged on a multimode scanning probe microscope (Nanoscope IV controller, Veeco instruments) in the constant height mode. Figure 4.20 shows the STM current images of **4** recorded at different scan sizes. When imaged over larger scan area, long wire like features of several micrometers length were observed at specific locations on the substrate (note that step heights are also observed). To further characterize, a portion of this image was zoomed in real time and is presented in Figure 4.20B. A number of bright spots, arranged in a one dimensional fashion were observed. Figure 4.20C represent the typical section analysis (variation of tunneling current) along the chain of the bright spots which clearly indicate that the bright spots corresponds to regions of high tunneling current and the average size of each spot is estimated to be <1 nm which is in accordance with the size of $\mathbf{C_{60}}$ molecule.[52]

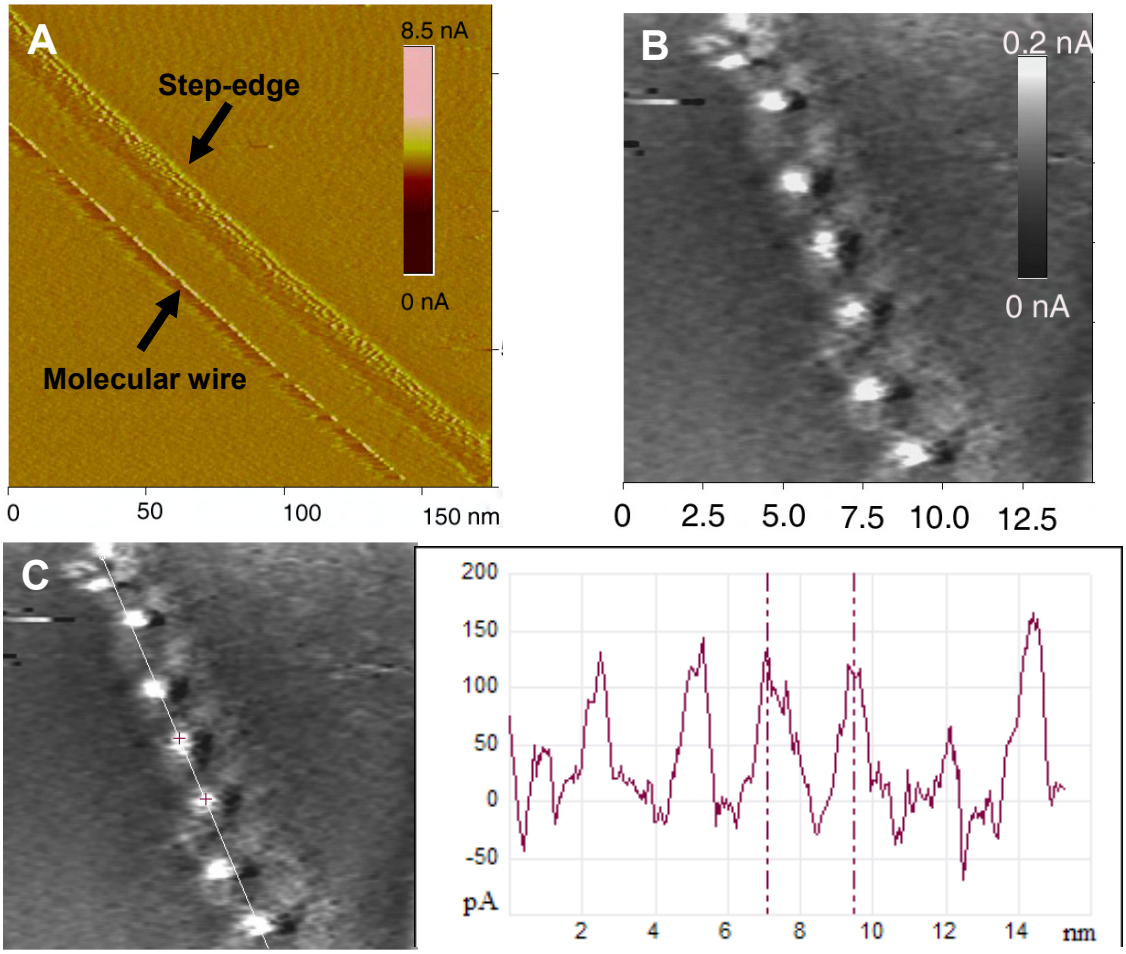

Figure 4.20. STM current images of **4** deposited on HOPG substrate recorded at different scan sizes (A) 175 x 175 nm^2 V_{bias} = 200 mV; I_t = 0.5 nA, (B) 15 x 15 nm^2 V_{bias} = 500 mV; I_t 1.0 nA and (C) cross sectional analysis.

To have a better understanding on organization of molecules leading to the 1D arrangement, STM images were compared with geometry optimized structure of **4**. Figure 4.21 shows the AM1 level optimized minimum energy conformation of **4** and various intramolecular distances are also represented. The molecule possesses a length of 3.14 nm along the major axis and the inner distance between the two fullerene units with in the

molecule is 1.75 nm. A detailed cross sectional analysis of the STM image revealed that the inner and outer distances of the alternate pairs of bright spots has the close resemblance with this value.

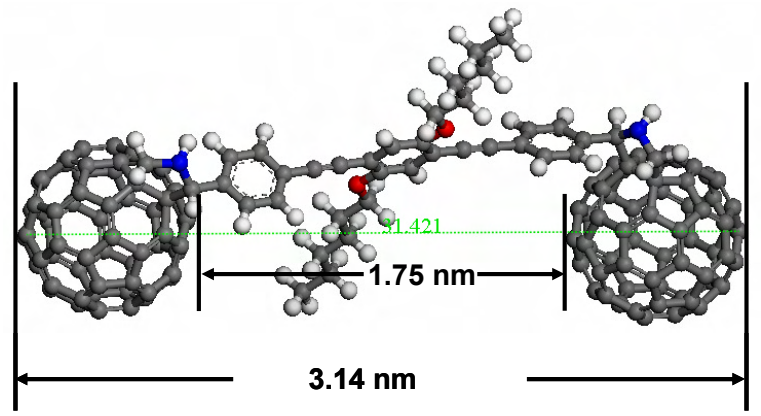

Figure 4.21. AM1 level optimized structure of **4** showing various intramolecular distances. (*optimized using MS modeling software, Accelrys*)

Organization of molecules on surfaces was further analyzed by superimposing the energy minimized structure over the STM image so that bright spots overlap with the $\mathbf{C_{60}}$ molecule (Figure 4.22). A careful analysis of this arrangement suggests that the intermolecular distance between two bis-fullerenes is greater than 1 nm. These results clearly indicate that the 1D organization is not as a result of intermolecular interactions between the $\mathbf{C_{60}}$ group, and surface interaction of the $\mathbf{C_{60}}$ molecule play an important role. A careful analysis of the large scan size image (Figure 4.20A) shows that the one 1D organization of molecule is observed only near the step edge of the surface and arranged along its direction. It has been recently reported that

the areas of the substrate near the step edge possess higher potential and molecules preferentially adsorb at these sites.[53-55] The 1D organization of bisfullerene observed in the present case may be attributed to the adsorption of molecules near the step edge possessing high surface potential.

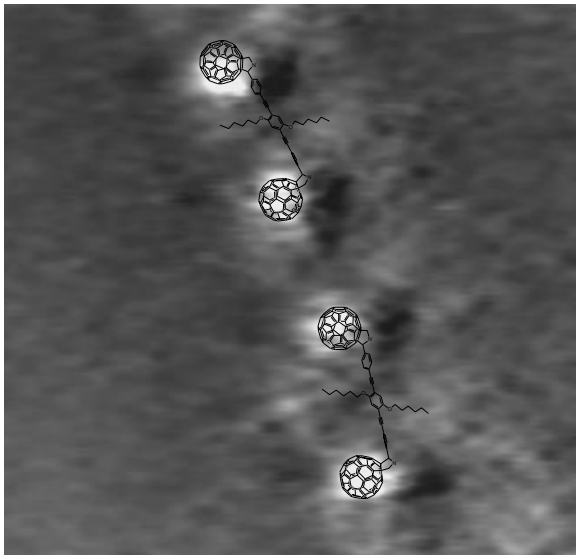

Figure 4.22. Representation of the 1D organization of **4** created by super imposing the energy minimized structure of **4** above the STM image.

4.5. Conclusion

The model phenyleneethynylene **1**, the basic building block of many molecular systems, forms well organized assemblies on surfaces through weak intermolecular interactions (acetylenic π-alkyl CH, acetylenic π-aromatic CH and alkoxy oxygen-aromatic CH). High resolution STM images revealed that the molecules are arranged in a skewed 1D fashion.

Based on the STM and molecular modeling studies, it is concluded that the molecular organization results from the interdigitation of alkoxy chains and the weak hydrogen bonding between alkyl CH (of the terminal CH_3 group) and the acetylenic π-electron/alkoxy oxygen which maintains a constant distance of 1.3 nm between the wires. The distance between the molecular wires was further varied by increasing the length of the alkoxy group. Phenyleneethynylene molecule having hydroxyl groups at the terminal positions (**3**) resulted in an end to end organization which is attributed to the hydrogen bonding of the hydroxyl groups. These results clearly indicate that the self-organization of phenyleneethynylnes on surfaces can be modulated by introducing proper functional groups. An in-depth understanding of various interactions is essential for the fabrication of optoelectronic devices and such studies on the formation of molecular assemblies on surface may pave way in the design of next generation photonic devices.

4.6. References

1. Koch, N., *ChemPhysChem* **2007,** *8*, 1438 - 1455.
2. Menard, E.; Meitl, M. A.; Sun, Y.; Park, J. U.; Shir, D. J. L.; Nam, Y. S.; Jeon, S.; Rogers, J. A., *Chem. Rev.* **2007,** *107*, 1117-1160.
3. Shirota, Y.; Kageyama, H., *Chem. Rev.* **2007,** *107*, 953-1010.
4. Facchetti, A.; Yoon, M.-H.; Marks, T. J., *Adv. Mater.* **2005,** *17*, 1705-1725.

5. Plass, K. E.; Grzesiak, A. L.; Matzger, A. J., *Acc. Chem. Res.* **2007,** *40*, 287-293.
6. Barth, J. V.; Costantini, G.; Kern, K., *Nature* **2005,** *437*, 671-679.
7. Armaroli, N.; Accorsi, G.; Holler, M.; Moudam, O.; Nierengarten, J. F.; Zhou, Z.; Wegh, R. T.; Welter, R., *Adv. Mater.* **2006,** *18*, 1313-1316.
8. Schmidt, R.; Göttling, S.; Leusser, D.; Stalke, D.; Krause, A.-M.; Würthner, F., *J. Mater. Chem.* **2006,** *16*, 3708-3714.
9. Palermo, V.; Liscio, A.; Palma, M.; Surin, M.; Lazzaroni, R.; Samorì, P., *Chem. Commun.* **2007**, 3326-3337.
10. Maruccio, G.; Cingolani, R.; Rinaldi, R., *J. Mater. Chem.* **2004,** *14*, 542-554.
11. Tour, J. M., *Acc. Chem. Res.* **2000,** *33*, 791-804.
12. Nierengarten, J. F.; Zhang, S.; Gegout, A.; Urbani, M.; Armaroli, N.; Marconi, G.; Rio, Y., *J. Org. Chem.* **2005,** *70*, 7550-7557.
13. Schenning, A. P. H. J.; Meijer, E. W., *Chem. Commun.* **2005**, 3245-3258.
14. Wan, L. J., *Acc. Chem. Res.* **2006,** *39*, 334-342.
15. Hermann, B. A.; Scherer, L. J.; Housecroft, C. E.; Constable, E. C., *Adv. Funct. Mater.* **2006,** *16*, 221-235.
16. Pawin, G.; Wong, K. L.; Kwon, K.-Y.; Bartels, L., *Science* **2006,** *313*, 961-962.
17. Giancarlo, L. C.; Flynn, G. W., *Acc. Chem. Res.* **2000,** *33*, 491-501.
18. Jackson, A. M.; Hu, Y.; Silva, P. J.; Stellacci, F., *J. Am. Chem. Soc.* **2006,** *128*, 11135-11149.
19. Tahara, K.; Furukawa, S.; Uji-i, H.; Uchino, T.; Ichikawa, T.; Zhang, J.; Mamdouh, W.; Sonoda, M.; De Schryver, F. C.; De Feyter, S.; Tobe, Y., *J. Am. Chem. Soc.* **2006,** *128*, 16613-16625.
20. De Feyter, S.; De Schryver, F. C., *J. Phys. Chem. B* **2005,** *109*, 4290-4302.
21. De Feyter, S.; De Schryver, F. C., *Chem. Soc. Rev.* **2003,** *32*, 139-150.

22. Surin, M.; Samorì, P., *Small* **2007,** *3*, 190-194.
23. Samori, P.; Francke, V.; Enkelmann, V.; Mullen, K.; Rabe, J. P., *Chem. Mater.* **2003,** *15*, 1032-1039.
24. Samorí, P.; Francke, V.; Müllen, K.; Rabe, J. P., *Chem. Eur. J.* **1999,** *5*, 2312-2317.
25. Lazzaroni, R.; Calderone, A.; Bredas, J. L.; Rabe, J. P., *J. Chem. Phys.* **1997,** *107*, 99-105.
26. Binning, G.; Rohrer, H.; Gerber, C.; Weibel, E., *Phys. Rev. Lett.* **1982,** *49*, 57-61.
27. Binnig, G.; Rohrer, H.; Gerber, C.; Weibel, E., *Phys. Rev. Lett.* **1983,** *50*, 120-123.
28. Samori, P. Self-assembly of conjugated (macro)molecules: nanostructures for molecular electronics (Doctoral dissertation, Humboldt University, Berlin), **2000**.
29. Shirai, Y.; Morin, J.-F.; Sasaki, T.; Guerrero, J. M.; Tour, J. M., *Chem. Soc. Rev.* **2006,** *35*, 1043-1055.
30. Sudeep, P. K.; James, P. V.; Thomas, K. G.; Kamat, P. V., *J. Phys. Chem. A* **2006,** *110*, 5642-5649.
31. James, P. V.; Sudeep, P. K.; Suresh, C. H.; Thomas, K. G., *J. Phys. Chem. A* **2006,** *110*, 4329-4337.
32. James, D. K.; Tour, J. M., *Top. Curr. Chem.* **2005,** *257*, 33-62.
33. Zhang, W.; Moore, J. S., *Angew. Chem. Int. Ed.* **2006,** *45*, 4416-4439.
34. Kim, I. B.; Phillips, R.; Bunz, U. H. F., *Macromolecules* **2007,** *40*, 814-817.
35. Breen, C. A.; Tischler, J. R.; Bulovic, V.; Swager, T. M., *Adv. Mater.* **2005,** *17*, 1981-1985.
36. Zhao, X.; Pinto, M. R.; Hardison, L. M.; Mwaura, J.; Muller, J.; Jiang, H.; Witker, D.; Kleiman, V. D.; Reynolds, J. R.; Schanze, K. S., *Macromolecules* **2006,** *39*, 6355-6366.

37. Li, H.; Powell, D. R.; Hayashi, R. K.; West, R., *Macromolecules* **1998,** *31*, 52-58.
38. Li, H.; West, R., *Macromolecules* **1998,** *31*, 2866-2871.
39. Fan, F.-R. F.; Yao, Y.; Cai, L.; Cheng, L.; Tour, J. M.; Bard, A. J., *J. Am. Chem. Soc.* **2004,** *126*, 4035-4042.
40. Sudeep, P. K.; James, P. V.; Thomas, K. G.; George, M. V.; Kamat, P. V., *Proc. Indian Acad. Sci. (Chem. Sci.)* **2003,** *115*, 321-332.
41. Guo, H. M.; Liu, H. W.; Wang, Y. L.; Gao, H. J.; Shang, H. X.; Liu, Z. W.; Xie, H. M.; Dai, F. L., *Nanotechnology* **2004,** *15*, 991-995.
42. Hembacher, S.; Giessibl, F. J.; Mannhart, J.; Quate, C. F., *Proc. Natl. Acad. Sci.U.S.A.* **2003,** *100*, 12539-12542.
43. Tománek, D.; Louie, S. G., *Phys. Rev. B* **1988,** *37*, 8327-8336.
44. Mizes, H. A.; Park, S.-i.; Harrison, W. A., *Phys. Rev. B* **1987,** *36*, 4491-4494.
45. Busse, C.; Weigelt, S.; Petersen, L.; Lagsgaard, E.; Besenbacher, F.; Linderoth, T. R.; Thomsen, A. H.; Nielsen, M.; Gothelf, K. V., *J. Phys. Chem. B* **2007,** *111*, 5850-5860.
46. Huang, T.; Hu, Z.; Wang, B.; Chen, L.; Zhao, A.; Wang, H.; Hou, J. G., *J. Phys. Chem. B* **2007,** *111*, 6973-6977.
47. Lingenfelder, M.; Tomba, G.; Costantini, G.; Ciacchi, L. C.; De Vita, A.; Kern, K., *Angew. Chem. Int. Ed.* **2007,** *46*, 4492-4495.
48. Eliel, E. L.; Wilen, S. H., *Stereochemistry of Organic Compounds*. Wiley-Interscience: New York, 1994; p 159.
49. Wei, Y.; Kannappan, K.; Flynn, G. W.; Zimmt, M. B., *J. Am. Chem. Soc.* **2004,** *126*, 5318-5322.
50. Biju, V.; Sudeep, P. K.; Thomas, K. G.; George, M. V.; Barazzouk, S.; Kamat, P. V., *Langmuir* **2002,** *18*, 1831-1839.
51. Morin, J. F.; Shirai, Y.; Tour, J. M., *Org. Lett.* **2006,** *8*, 1713-1716.

52. Goel, A.; Howard, J. B.; Sande, J. B. V., *Carbon* **2004,** *42*, 1907-1915.

53. Feng, M.; Lee, J.; Zhao, J.; Yates, J. T.; Petek, H., *J. Am. Chem. Soc.* **2007**, *129*, 12394-12395.

54. Xiao, W.; Ruffieux, P.; Aït-Mansour, K.; Gröning, O.; Palotas, K.; Hofer, W. A.; Gröning, P.; Fasel, R., *J. Phys. Chem. B* **2006**,*110*, 21394-21398.

55. Zhao, X.; Perry, S. S.; Horvath, J. D.; Gellman, A. J., *Surf. Sci.* **2004**, *563*, 217-224.

†. Gaussian 03, Version 6.1, Frisch, M. J.; Trucks, G. W.; Schlegel, H. B.; Scuseria, G. E.; Robb, M. A.; Cheeseman, J. R.; Montgomery, Jr. J. A.; Vreven, T.; Kudin, K. N.; Burant, J. C.; Millam, J. M.; Iyengar, S. S.; Tomasi, J.; Barone, V.; Mennucci, B.; Cossi, M.; Scalmani, G.; Rega, N.; Petersson, G. A.; Nakatsuji, H.; Hada, M.; Ehara, M.; Toyota, K.; Fukuda, R.; Hasegawa, J.; Ishida, M.; Nakajima, T.; Honda, Y.; Kitao, O.; Nakai, H.; Klene, M.; Li, X.; Knox, J. E.; Hratchian,H. P.; Cross,J. B.; Adamo, C.; Jaramillo, J.; Gomperts, R.; Stratmann, R. E.; Yazyev, O.; Austin, A. J.; Cammi, R.; Pomelli, C.; Ochterski, J. W.; Ayala, P. Y.; Morokuma, K.; Voth, G. A.; Salvador, P.; Dannenberg, J. J.; Zakrzewski,V. G.; Dapprich, S.; Daniels, A. D.; Strain, M. C.; Farkas, O.; Malick, D. K.; Rabuck, A. D.; Raghavachari, K.; Foresman, J. B.; Ortiz, J. V.; Cui, Q.; Baboul, A. G.; Clifford, S.; Cioslowski, J.; Stefanov, B. B.; Liu, G.; Liashenko, A.; Piskorz, P. ; Komaromi, I.; Martin, R. L.; Fox, D. J.; Keith, T.; Al-Laham, M. A.; Peng, C. Y.; Nanayakkara, A.; Challacombe, M.; Gill, P. M. W.; Johnson, B.; Chen, W.; Wong, M. W.; Gonzalez, C.; Pople, J. A., Gaussian, Inc., Pittsburgh PA, 2003.

List of Publications:

1. Self-Organization of Phenyleneethynylene into Wire-Like Materials on Surfaces,
   K. Yoosaf, P. V. James, A. R. Ramesh, C. H. Suresh and K. George Thomas
   J. Phys. Chem. C, **111**, 14933-14936 (**2007**) (with cover art).
2. In Situ Synthesis of Metal Nanoparticles and Selective Naked-Eye Detection of Lead Ions from Aqueous Media,
   K. Yoosaf, B. I. Ipe, C. H. Suresh and K. George Thomas,
   J. Phys. Chem. C, **111**, 12839-12847 (**2007**).
3. Functionalized Gold Nanoparticles as Phosphorescent Nanomaterials and Sensors,
   B. I. Ipe, **K. Yoosaf** and K. George Thomas,
   J. Am. Chem. Soc. **128**, 1907-1913 (**2006**).
4. Interfacial Properties of Hybrid Nanomaterials,
   B. I. Ipe**, K. Yoosaf** and K. George Thomas,
   Pramana -J. Phys., **65,** 909-915 **(2005)** (*Invited article in special issue*).

Posters Presented at Conferences:

1. Bipyridine Functionalized Gold Nanoparticles: Design of Nanophosphors, Superstructures and Allosteric sensors
   K. Yoosaf, Binil Itty Ipe and K. George Thomas
   In ***"3rd Trivandrum International Symposium on Recent Trends in Photochemical Sciences"*** held at Trivandrum, (India) January 5 –7, 2004**.**
2. Nanophosphors, Superstructures and Allosteric Recognition from Bipyridine Functionalized Gold Nanoparticles
   K. Yoosaf, Binil Itty Ipe, and K. George Thomas
   In *"Sixth National Symposium in Chemistry"* by CRSI held at Kanpur, (India) February 6-8, 2004.
3. Functional Nanomaterials for the Selective Detection of Metal ions
   K. Yoosaf, Binil Itty Ipe and K. George Thomas
   In the ***"7th CRSI National Symposium in Chemistry"* by CRSI** held at Culcutta, (India) February 4 – 6, 2005.

4. Functional Nanomaterials for the Selective Detection of Metal ions
   K. Yoosaf, Binil Itty Ipe and K. George Thomas
   In the **"*International Conference on Nanoscience and Technology, ICONSAT2006*"** held at New Delhi, India, March 16-18, 2006.

5. STM Investigations on the 2D-organization of Phenyleneethynylenes and their Molecular Conductivity
   K. Yoosaf, P. V. James, A. R. Ramesh and K. George Thomas
   In the "***Winter School on the Chemistry of Materials 2006*"** held at JNCASR, Bangalore, India, December 12-19, 2006

6. In Situ Synthesis of Metal Nanoparticles and Selective 'Naked-eye' Detection of Lead Ions from Aqueous Media
   K. Yoosaf, Binil Itty Ipe and K. George Thomas
   In the **"*International Conference on Materials for the Millennium (MatCon2007)*"** held at the CUSAT, Kochi, India, March 1-3, 2007.